Study of Azobenzene Derivatives in Water & their Application in DNA Nanotechnology

Shayne Gracious

Department of Chemistry, McGill University

Montreal, Quebec, Canada

A thesis submitted to McGill University in partial fulfillment of the requirements for the degree of Master of Science

September 2021

Abstract

Azobenzene is a widespread photo-switch that has been used extensively in many fields. However, there are a number of nuances that have deterred researchers from implementing it into aqueous systems; namely its inherent hydrophobic character and its abnormal isomerization behaviour in water. This has drastically hindered progress towards its application in biological settings. In this work, the subtle intricacies of the photodynamics of azobenzenes derivates in water are stringently analyzed. Using experimental data and computational methods, viable strategies to predict the photo-isomerization characteristics of azobenzene derivatives in water are presented. As a proof of principle, one of the derivatives was also implemented into DNA-based supramolecular fibres. By meticulously altering the placement and orient of the azobenzene motif on the DNA strand, its influence on the self-assembly process of the material could be divulged. This sheds light on the influence organic and photochromic molecules can have on self-assembly process and the resulting soft-bonded materials.

Resume

L'azobenzène est un photocommutateur répandu qui a été largement utilisé dans de nombreux domaines. Cependant, il existe un certain nombre de nuances qui ont dissuadé les chercheurs de l'implémenter dans des systèmes aqueux; à savoir son caractère hydrophobe inhérent et son comportement d'isomérisation anormal dans l'eau. Cela a considérablement entravé les progrès vers son application dans les milieux biologiques. Dans ce travail, les subtilités de la photodynamique des dérivés d'azobenzène dans l'eau sont rigoureusement analysées. À l'aide de données expérimentales et de méthodes de calcul, des stratégies viables pour prédire les caractéristiques de photo-isomérisation des dérivés d'azobenzène dans l'eau sont présentées. Comme preuve de principe, l'un des dérivés a également été implémenté dans des fibres supramoléculaires à base d'ADN. En modifiant méticuleusement le placement et l'orientation du motif azobenzène sur le brin d'ADN, son influence sur le processus d'auto-assemblage du matériau pourrait être divulguée. Cela met en lumière l'influence que les molécules organiques et photochromiques peuvent avoir sur le processus d'autoassemblage et les matériaux à liaison souple qui en résultent.

Acknowledgments

Firstly, I would like to acknowledge my supervisors, for their guidance and support. Dr. Barrett, your enthusiasm in my work was unprecedented, and helped me stay motivated throughout my degree. I am also very grateful for your understanding & patience throughout the COVID-19 pandemic. Dr. Sleiman, although I was not technically one of your students, you treated me as one. Our regular meetings guided me to become a better researcher. Your perspectives & insights on my research were extremely helpful and taught me so much. I am very thankful for this.

I would also like to thank my family: my mother, my father & Yulia. Your emotional support throughout this process was fundamental, despite the long distance between us.

Thank you for taking the time to come visit, giving me a place to visit, & for the Saturday phone calls in between.

Lastly, a big thanks goes out to my friends and colleagues. In particular, Dr. Tristan Borchers, Dr. Casey Platnich & Dr. Felix Rizzuto, three senior students whose guidance helped improve me as a scientist and person (I hope). Also, thank you to Javathan Asohan & Qventin Kerb, two dear friends who made my time in Montreal more memorable and enjoyable.

Table of Contents

Abstract	ii
Resume	iii
Acknowledgments	iv
List of Figures	viii
List of Tables	xi
List of Equations	xii
List of Acronyms	xiii
Chapter 1. Introduc	etion
	Photodynamics of Azobenzene2
1.1.2	Azobenzene in Aqueous Media7
1.1.3	Pump-Probe Spectroscopy11
1.1.4	Computations of Azobenzene13

1.2	DNA Na	notechnology & Supramolecular Polymer	.17
	1.2.1	DNA Origami & DNA Nanostructures	.17
	1.2.2	Supramolecular Polymers	.21
	1.2.3	DNA based Supramolecular Polymer	.24
	1.2.4	Azobenzene in DNA	.27
1.3	Scope of	Thesis	
	1.3.1	Thesis Overview & Objectives	.33
Chapter 2.	Methods	s, Results, & Discussion	
2.1	Synthesis	& Self-Assembly	.36
	2.1.1	Organic Synthesis	.37
	2.1.2 \$	Solid-Phase DNA Synthesis	.43
	2.1.3 1	Fibre Formation	.44
2.2	Spectroso	сору	.45
	2.2.1 \	UV-Vis & Kinetic Experiments	.45
	2.2.2]	Pump-Probe Spectroscopy	.45
	2.2.3	Circular Dichroism & Melting Temperature Analysis	.47
	2.2.4	Atomic Force Microscopy	.47
2.3	Computa	tional Methods	.48
	2.3.1	Optimized Ground State Structures	.48
	2.3.2 \$	Simulated UV-Vis Spectra	49
	2.3.3	Transition State Structures	.50
2.4	Results &	z Discussion	52

	2.4.1 Synthesis of Water Soluble Azobenzenes	52
	2.4.2 Effect of Substituents on Photo-dynamics	
	2.4.3 Rationalization of Substituent Effects through Computations	
	2.4.4 Self-Assembly of Azo-PolyA Systems	71
Chapter 3. C	Conclusions & Future Work	77
	3.1 Summary	77
	3.2 Future Work	79
Chapter 4. References		83
Chanter 6 A	Annendix	93

List of Figures

- **Figure 1.1.** Photo-isomerization of azobenzene with the proposed transition states. The rotational mechanism is shown on the top and inversion on the bottom. Authors have suggested that in some aqueous systems the isomerization process may be cyclic, opposed to a reversible linear process.
- **Figure 1.2.** The various types of azobenzenes and their classifications. In the literature, 3 common types are typically discussed: azobenzene, amino, and pseudostilbenes. Recently, a fourth category of ortho-substituted azos has been developed.
- **Figure 1.3**. Mechanism of the catalytic rotational cis-to-trans isomerization (top) and examples of substrates that can facilitate this process (bottom). The effect and magnitude of these interactions varies based on the azo derivative.
- **Figure 1.4.** Example of an optical setup for pump-probe spectroscopy. Here two laser sources are used to independently instigate the pump and probe beams.
- **Figure 1.5.** Reduced representation showing cross sections of the crossover points in a DNA helical lattice. As shown, the first three crossovers to adjacent helices are possible at 0 (330°), 7 (90°), and 14 (210°). These crossovers are also available again after the addition of 21 base pairs.
- **Figure 1.6.** An example of a supramolecular system that can have induced photo-actuation. (a) The assembled supramolecular polymer and its photo-actuation. (b) the isomerization process of the photochrome. Here the molecule switch has similar properties to azobenzene: isomerization of the molecule leads to a metastable secondary phase, which subsequently undergoes a thermal relaxation to thermodynamically stable state.
- **Figure 1.7**. Binding motif of the polyA:cyanuric acid fibres (a) and experimental AFM results (b & c).¹ Based on the number of polyA unites elongated (polyA₁₅, (b) or contracted fibres (polyA₁₅ (c), may be observed.
- **Figure 1.8.** The two predominant approaches to insert azobenzene into DNA. On the left, the azo motif is perpendicular to the DNA strand and bound through a L-threoninol linker. On the right, the azo elongates the phosphate backbone. Note azo:DNA size is not to scale.
- **Figure 2.1.** Optical setup used for the pump-probe spectroscopy experiments.
- **Figure 2.2**. Final structures of the synthesized azo derivatives and their yields.
- Figure 2.3. UV-Vis spectra of the parent compound (Azo1) in DMSO (red) and water (blue).

- Figure 2.4. UV-Vis spectra of the amino-type derivatives (Azo2-3) in DMSO and water.
- **Figure 2.5.** UV-Vis spectra of the *ortho*-substituted derivatives (Azo4-5) in DMSO and water. Here the sample is assumed to be composed predominately of the tr5ns isomer.
- **Figure 2.6.** Photo-isomerization of azo1 in distilled water after irradiation for 2 minutes with 365 nm light.
- **Figure 2.7.** Photo-isomerization of azo5 in distilled water after irradiation for 10 minutes with 532 nm light. Clear splitting of the n- π^* is observed.
- **Figure 2.8.** Typical thermal relaxation of *cis* azobenzene monitored by UV-Vis and the extrapolation of the change in absorption when fit to first order kinetics (inset). The irradiated sample is shown in red and is composed predominately of the *cis* isomer. Over time the sample relaxes back to the *trans* isomer (pink) as shown by the arrow. This specific data is from Azo2 in DCM.
- **Figure 2.9.** Typical data acquired from pump-probe spectroscopy. Irradiation at ~ 0.6 seconds induces a decrease in the transmission at 455 nm due to the *tran*-to-*cis* isomerization. Transmission subsequently returns to the initial state following 1st order kinetics.
- **Figure 2.10.** Arrhenius plots obtained for the thermal isomerization process for the azos monitored through UV-Vis. Plots yield a slope equal to $-E_a/R$ and y-intercept equal to $\ln A$, as per equation 4).
- **Figure 2.11.** The effect of the basis set on predicting the π - π * transition in water using the PBE0 functional with a PCM model. Here, the error can be up to 20 nm. Despite this, the PBE0 functional with a cc-pvtz basis set was used in future work as a comparison.
- **Figure 2.12.** The effect of the basis set on predicting the π - π * transition in water using the CAM-B3LYP functional with a PCM model. Based on these results, the CAM-B3LYP functional with a 63311+(2d,p) was used in future work.
- **Figure 2.13.** Typical optimized structures acquire using the CAM-B3LYP/6311+(2d,p) level of theory, showing the parent *trans* (left) & *cis* (middle) isomer and a fluorinated trans isomer (right).
- **Figure 2.14.** Schematic of the scan angles used to analyze the thermal relaxation of cis azobenzene (top left) and the energy landscapes obtained from the scans. These images provide rough ideas of the energy cost associated with conformational changes of the molecule. Following the y (ϕ) & x-axes (θ) yield the energy changes associated with the rotation and inversion pathways, respectively. A concerted pathway would be any path between the two.

Figure 2.15. Typical CD spectrum acquired with the formed fibres (blue) and when the fibres do not form (red). The strong negative peaks at 252 nm & 212 are indicative of the chiral fibres.

Figure 2.16. Melting curves of the DNA-azo fibres. The majority of strands displayed a single asymptotic curve indicative of one phase transition. However, the Azopoly A_{14} Azo strand displays two (purple).

Figure 2.17. AFM images of the fibre forming Azo-DNA strands: (a) PolyA₉Azo (b) PolyA₁₄Azo (c) PolyA₁₄Azo₂ & (d) AzoPolyA₁₄Azo.

List of Tables

- **Table 2.1.** List of the synthesized DNA strands.
- **Table 2.2**. Experimental thermodynamics & kinetics of the thermal *cis*-to-*trans* relaxation for the azo derivatives in water.
- **Table 2.3.** Computed excitation energies for the *trans* isomer using the CAM-B3LYP/6311+(2d,p) & PBE0/cc-pvtz methods.
- **Table 2.4.** Computed excitation energies for the *cis* isomer using the CAM-B3LYP/6311+(2d,p) & PBE0/cc-pvtz methods.
- **Table 2.5.** Computed activation energies using the QST3 method compared to experimental results.
- **Table 2.6.** Classification of the synthesized strands and their melting temperatures.

List of Equations

- 1) Normalized percentage of the cis azo in solution
- 2) First-order kinetics equation
- 3) Half-life equation
- 4) Linearized Arrhenius equation

List of Acronyms

1D: 1-dimensional

2D: 2-dimensional

3D: 3-dimensional

AFM: atomic force microscopy

Azo: azobenzene

CA: cyanuric acid

CD: circular dichroism

DCM: dichloromethane

DFT: density functional theory

DMSO: dimethyl sulfoxide

DMT: dimethoxyl trityl

DNA: deoxyribonucleic acid

dsDNA: double stranded deoxyribonucleic acid

dsRNA: double stranded ribonucleic acid

HCl: Hydrochloric acid

OD: optical density

polyA: polyadenine

QM/MM: quantum mechanical/molecular mechanics

QST3: quasi-newton synchronous transit-guided

siRNA: Small interfering ribonucleic acid

ssDNA: single stranded deoxyribonucleic acid

ssRNA: single stranded ribonucleic acid

TD-DFT: time-dependent density functional theory

THF: Tetrahydrofuran

UV: Ultraviolet

UV-Vis: Ultraviolet-Visible

 $\tau_{1/2}$: Half-life

λ: Wavelength

Chapter 1: Introduction

Evolution has proved that the best materials are those that adapt to their surroundings and not those that are confined to the characteristics of their initial creation. ¹⁻³ With this in mind, materials scientists are currently striving to develop devices that accommodate societies' needs while simultaneously adjusting to their daily habits or mishaps. These so-called "smart-materials" are materials that respond to external stimuli and give rise to a subsequent state and, consequently, enable dual functionality. These newage materials can be responsive to a multitude of environmental conditions, such as pH, heat, electric fields, or even light. ⁴⁻⁶

Amidst the development of these new materials, researchers must be wary of a new necessity in material science: green chemistry. In today's society state-of-the-art materials are those that exploit renewable resources and make use of greener processing techniques. Supramolecular chemistry is an elegant tool to develop green materials through the process of self-assembly, as the final products are not covalently bound. This allows the formation and degradation of the material via low energy processes. Additionally, the lack of covalent bonds makes these sophisticated systems extremely sensitive to external stimuli – some notable examples include: supramolecular polymers, molecular machines, and induced dissipative states. Water is an ideal green solvent for these systems, as it promotes fundamental thermodynamic phenomena (such as the hydrophobic effect) and can facilitate the formation of soft-bonded systems through noncovalent interactions (such as hydrogen bonding). Furthermore, an inherent advantage to aqueous-based systems is that it improves the biocompatibility and recyclability of the

material.^{5,8} In this context, light is an attractive stimulus for these devices because – in addition to many other advantageous properties – it is an inherently green source of energy. In the field of supramolecular chemistry, light induced isomerizations have an added advantage of being fully reversible.^{10,11} These photo-isomerization processes promote changes in the conformation, dipole, or even acidity, of the building blocks of self-assembly processes, drastically impacting the overall product; for example, a common feature is light induced self-assembly or disassembly. Additionally, when implemented into the final product of these systems, materials arise with fascinating properties, such as light induced birefringence¹² or actuation.¹³

1.1 Azobenzene

1.1.1 Photodynamics of Azobenzene

Azobenzene (azo) is the most exhaustively studied photo-switch to date and for good reason: it offers near-quantitative isomerization and can be cycled thousands of times with degradation. ^{13,14} Irradiating *trans* azobenzene with light (365 nm for an unsubstituted azo) yields the less stable *cis* isomer (Figure 1.1). The isomerization process invokes a change in the structural geometry of the molecule and, additionally, a change in its dipole moment. The *trans* isomer can then be re-obtained by a subsequent irradiation from of a different wavelength, or *via* a thermal relaxation process. This thermal isomerization process follows first order kinetics and is therefore quantified with a half-life. ¹³⁻¹⁵

More specifically, *trans* azobenzene displays a lambda max at about 330 nm (depending on the solvent) associated with the π - π * transition. It also displays a significant

absorption at about 440 nm (again solvent dependent) which can be attributed to the $n-\pi^*$ transition. On the other hand, cis azobenzene has strong absorption energies at ~290 nm $(\pi - \pi^*)$ and ~425 nm $(n - \pi^*)$. The fact that the $\pi - \pi^*$ transitions of the two isomers are not degenerate in energy is the key to the isomerization process for azobenzene. Irradiation with ~330 nm UV light shifts the equilibrium towards the *cis* isomer, as excited electrons can relax to either the *cis* or *trans* state. Should the electrons relax to the *cis* state, they will be locked in this metastable position and are less likely to interact with the incoming light. Contrarily, if the electrons relax back to the original *trans* state, they will be excited again by the irradiation and the cycle repeats. Thus, the equilibrium shifts towards the *cis* isomer. Subsequent removal of light will re-initiate the *trans* form *via* the thermal relaxation process.¹⁴

The exact mechanism of the isomerization process can be quite elusive and varies from system to system. For example, in some aqueous systems the mechanism of the isomerization process is hypothesized to be cyclical: such that the *trans*-to-*cis* isomerization involves a rotational mechanism, whereas the *cis*-to-*trans* thermal relaxation involves an inversion (or concerted rotational-inversion) mechanism (Figure 1.1). Other authors have shown evidence that the process may be occurring through a protonated species, such as the case of acid catalyzed *cis-trans* isomerization. As such, the pathway for the isomerization process can be highly dependent on the solvent, azobenzene derivative, or even the local environment of the photochrome. It should be noted that the optimal mechanism of the *cis*-to-*trans* isomerization process is directly related to the energy landscape associated with the configurations of the *cis* molecule and conversely,

largely influences the thermal relaxation process (or half-life) associated with the molecule.

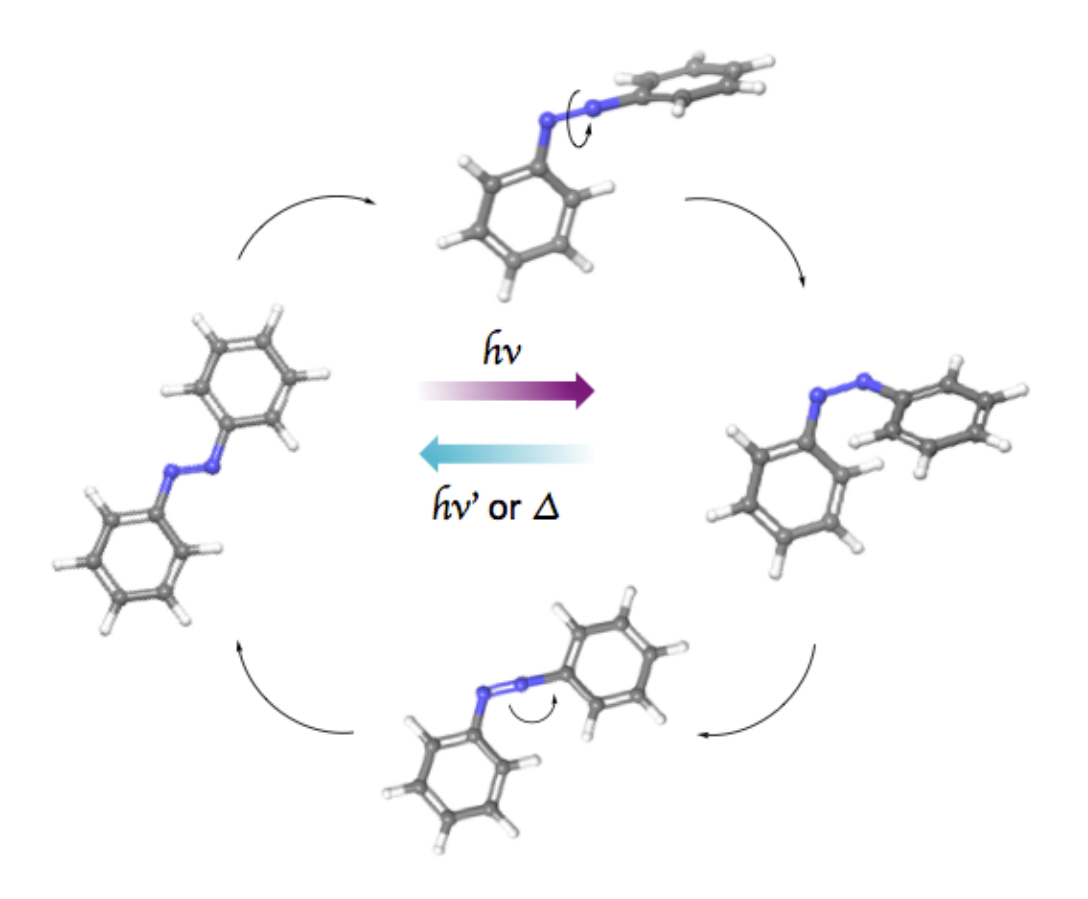


Figure 1.1. Photo-isomerization of azobenzene with the proposed transition states. The rotational mechanism is shown on the top and inversion on the bottom. Authors have suggested that in some aqueous systems the isomerization process may be cyclic, opposed to a reversible linear process.

One of the most important aspects when working with azos is the rational design of the photochrome. By altering the substituents around the phenyl ring the photo-dynamics of molecule can be drastically tuned. For convenience, azobenzene derivatives are typically categorized into three types: azobenzene type, amino-azobenzenes, and pseudostilbenes (Figure 1.2). Azobenzene type azos have mildly influencing substituents, such as alkyl groups. As such, the characteristics of these azos are very similar to that of the parent azobenzene compound. A strongly influencing electronic group in the para position, such

as an amino or nitro group, characterizes amino-azobenzenes. Note that they are also sometimes referred to as "nitro-azobenzenes". These amino-azos typically have red-shifted absorption spectra and have an intermediate half-life. Pseudostilbene azos are also referred to as "push-pull" azobenzenes. These azos have an electron-donating group on one end and an electron-withdrawing group on the other end. This leads to a very red-shifted absorption spectrum. Contrary to azobenzene type azos, the addition of these substituent groups typically enhances the water solubility of these compounds. However, it has been noted that the half-life of these molecules is also drastically decreased, especially in polar solvents.

Over the past decade, many groups have explored the synthesis of a new class of azobenzenes: *ortho*-substituted azos. In particular, the groups of Dr. Andrew Wooley & Dr. Stefan Hecht have designed di-*ortho* and tetra-*ortho* substituted azobenzene with half-lives that span the range of months to years. 19,20 Of these, the most studied are tetra-halogenated azobenzenes because they are less prone to photo-bleaching and their syntheses are less complex. The Barrett group has also synthesized a fully fluorinated azobenzene *via* a one step synthesis that displays similar properties. Regardless, substituents in the *ortho* position all appear to stabilize the *cis* isomer and subsequently increase the half-life of the molecule. It is believed the added bulk associated with these groups retards the isomerization process through steric hindrance. Many groups have validated this *via* computational methods. These derivatives also drastically red-shift the isomerization process as the n-orbital of the *cis* and *trans* isomer are no longer degenerate in energy; the halogen groups are believed to stabilize the n orbital through an inductive effect when in the *trans* configuration. This allows the isomerization process to

occur with visible light by probing the n- π^* transition. Additionally, the steric bulk that is introduced also leads to more accessible volume in the isomerization process, allowing these photochromes to isomerize in environments that may inhibit the process. ^{21,22} For example, the aforementioned fully fluorinated azobenzene designed by Barrett and coworkers can isomerize in the solid state when crystals of the *cis* isomer are irradiated. This is a strategy that could be exploited in solution when macromolecules inhibit the isomerization process of the azobenzene.

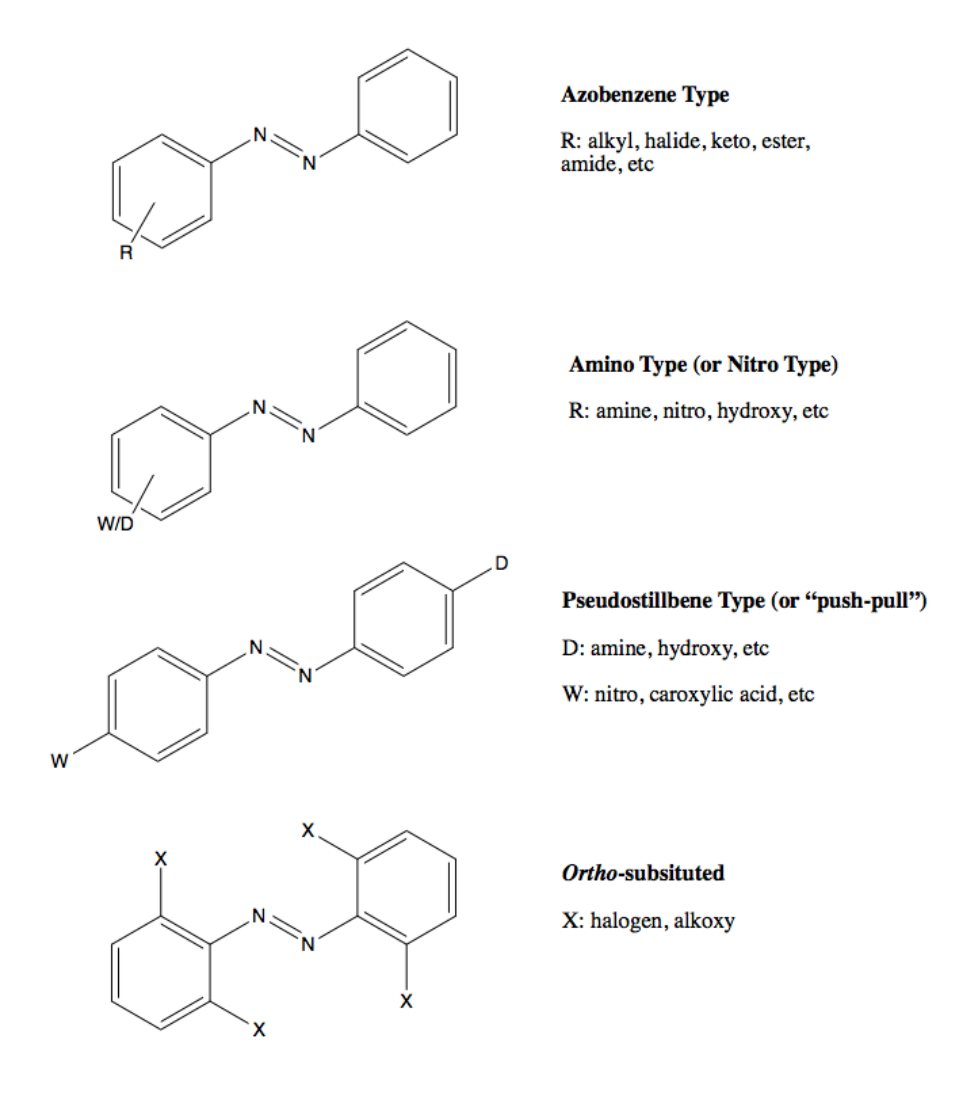


Figure 1.2. The various types of azobenzenes and their classifications. In the literature, 3 common types are typically discussed: azobenzene, amino, and pseudostilbenes. Recently, a fourth category of ortho-substituted azos has been developed.

1.1.2 Azobenzene In Aqueous Media

Despite its formidable potential traits, the use of azobenzene in aqueous media has been hindered. This can mainly be attributed to two main features: inherent solubility issues that arise from the azo core structure, and the abnormal photo-switching behaviour that is observed when working in aqueous environments - specifically, the drastic decrease in the half-life of the *cis* isomer. In aqueous media, an anomaly compared to other solvents is the rapid thermal re-isomerization of the *cis* isomer. Indeed, the effect is so large it leads to the discussion of whether certain azos are even capable of isomerizing in water. Recent experiments with ultrafast pump-probe absorption spectroscopy have shown they do, and display half-lives on the hard-to-observe ultra-fast picosecond time scale. As such, this decreased stability has often deterred the application of azo in many aqueous based devices, whether they are for medicinal or environmental purposes.

Another aspect that must be considered when working in aqueous systems is the *p*H and counterions in the system. It has been known for a long time that highly nucleophilic and electrophilic molecules can catalyze the thermal relaxation process. ^{17,25,26} More recently, groups have re-evaluated the notion of salt-based catalysis and how this intertwines with the acid catalysis mechanism. From these works, it is evident that the pH of a solution and the counter-ions in solution can significantly affect the half-life of the *cis* isomer, decreasing the activation energy by as much as 25 kJ/mol. ^{16,18,27} However, this change can also be highly specific to the azobenzene derivative in solution. ^{28,29} For the most part, it is speculated that this catalytic process can be attributed to the formation of a *cis*-azonium cation, which undergoes a rapid thermal relaxation to the *trans* form *via* a rotation mechanism.

Figure 1.3 presents the proposed mechanism for the acid catalyzed thermal relaxation process. As shown, protons (or other counter-ions) can form an azonium cation, which decreases the double bond character between the nitrogen atoms and facilitates the rotation to the *trans* state. As shown in Figure 1.3, intramolecular proton exchanges are also quite prominent in these species and, as a result, azobenzenes with strong electron donating groups are prone to acid catalysis. ^{16,18} A subtle characteristic that adds to the catalytic process is the fact that the *trans* azonium ion typically has a lower *p*Ka than the *cis* azonium ion; thus, enabling the rapid deprotonation of the *trans* isomer. For example, for 2-hydroxy-5-methylazobenzene the *p*Ka of the *cis*-cation and *trans*-cation are 2.9 and -1.5, respectively. ³⁰ Conversely, it has been demonstrated that the presence of hydroxide ions can decrease the isomerization rate by inhibiting the aforementioned protonation of the *cis* isomer. ²⁵ However, some substituents can also promote a base-catalyzed isomerization process as these functional groups stabilize "quinoid-like" structures that also decrease the double bond character. ¹⁶

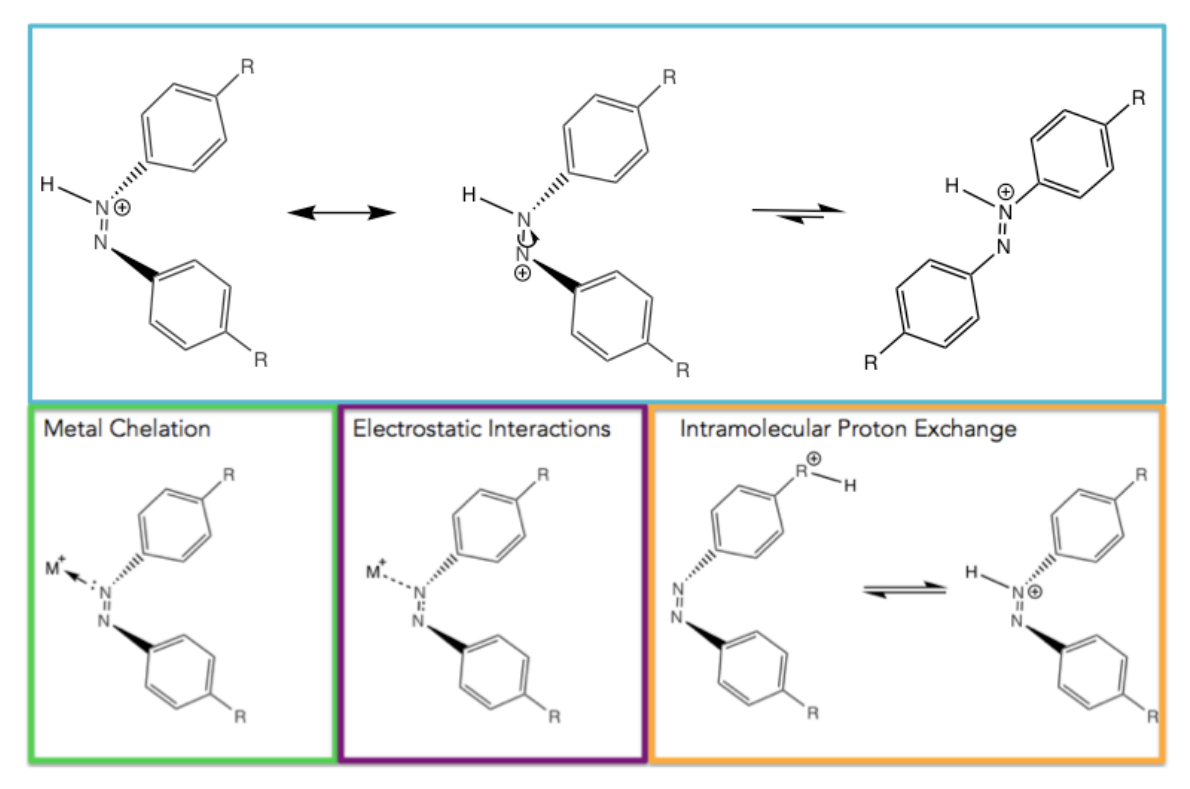


Figure 1.3. Mechanism of the catalytic rotational *cis*-to-*trans* isomerization (top) and examples of substrates that can facilitate this process (bottom). The effect and magnitude of these interactions varies based on the azo derivative.

Similarly, metal ions have been noted to catalyze the isomerization process, however, sometimes *via* a different mechanism. Cu²⁺ has notably demonstrated catalytic activity through a chelation mechanism similar to that of acid catalysis. ²⁶ Recently, certain azo dyes – the commonly used methyl orange and methyl yellow – have shown catalytic activity in the presence of alkali salts. ²⁸ From this work, the authors have deduced the following: 1) Cations can sufficiently decrease the double bond character of the azo group *via* electrostatic interactions 2) Solvation of the ions effects these interactions: larger cations are better catalysts due to a decreased solvation, whereas anions can decrease catalysis through ion pair association 3) Weakly acidic anions can inhibit the catalysis by decreasing the H⁺ concentration. Despite all these finding, more work in this regime to fully elucidate

the mechanism behind salts effect is needed, as discrepancies between azobenzene derivatives are not fully understood.^{26, 28}

Another aspect that researchers must be wary of is the irreversible degradation of azobenzene in reducing environments. Many reducing agents, such as hydrazine hydrate and sodium dithionate, are known to irreversibly cleave the azo double bond yielding aniline.¹⁷ Of these, sodium dithionate is by far these most commonly used and many authors have conducted studies to optimize the structure of azobenzene for this process.^{31,32} In short, these findings conclude that cleavage of the N=N bond is more favourable in azos with electron donating groups. Although typically viewed as an unwanted reaction, recently, many researchers in the field of bioorthogonal chemistry have exploited this reaction to design hypoxia-stimulated materials. By targeting the hypoxic microenvironments of cancer cells Fang et al. designed cleavable azobenzenes that are activated *in vivo*, creating new materials for cancer diagnostics.³³ However, because these microenvironments are difficult to replicate, the mechanism for the hypoxia-mediated reduction of azobenzene is still unclear.

Despite these shortcomings, many research groups have devised elegant strategies to overcome the obstacles associated with aqueous azobenzene systems. Another strategy involves coupling the photochrome with other water-soluble macromolecules, which conveniently alleviates issues associated with the water solubility of the molecule. More interestingly, implementing azos into these systems has a distinct effect on the molecules local environment, altering its photodynamic behaviour. This strategy will be discussed further in section 1.2.4.

1.1.3. Pump-Probe Spectroscopy

As noted previously, one of the most challenging issues when working with azobenzenes in aqueous systems is the fast thermal relaxation rate. That is, the *cis* isomer is so short-lived that its presence cannot be verified by typical linear spectroscopic methods. Therefore, for extremely fast-switching azos non-linear spectroscopic methods are necessary to observes the *cis* isomer and quantify the thermal relaxation rate. One example, is pump-probe spectroscopy.

A typical pump-probe optical set up is shown in Figure 1.4.

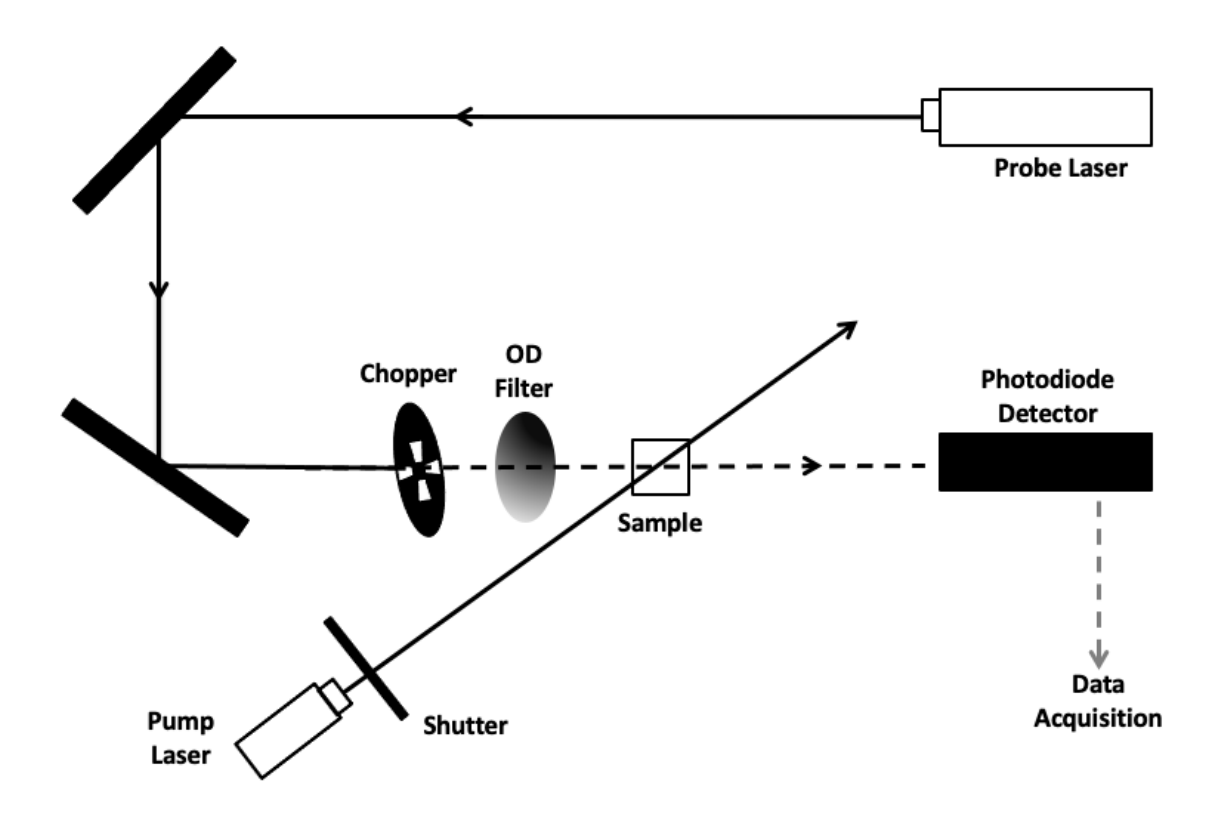


Figure 1.4. Example of a minimalistic optical setup for pump-probe spectroscopy. Here two laser sources are used to independently instigate the pump and probe beams.

By using two different optical sources samples can be simultaneously excited (pump) and monitored (probe). The above technique can be used to quantify the half-lives up to the

microsecond timescale. However, it should be noted that the time constant between the pump and probe could also be determined by altering the path length of two sources of light. In these optical setups species can be observed on the femtosecond timescale.²⁴

For azobenzene, a key criterion is to have a strong pump source, such that a sufficient portion of the molecules isomerizes. For example, Dunn et al. estimate that an optical setup with a 355 nm laser with an output energy of 3 mJ/pulse when operating at 1 Hz can isomerize approximately 10% of the molecules. Increasing the pulse time or the power of the laser would conversely increase this percentage. However, over irradiating the sample may also lead to photo-bleaching or thermal heating. Increasing the controlled by tuning the pulse time or by using a variable neutral density filter to alter the light intensity. Regardless, the key role of the pump laser is to excite the system into a secondary state. Simultaneously, a probe laser must be monitoring the system. For many systems, this can be done by continuously monitoring the sample at a specific wavelength. In the case of azobenzene, it is particularly important to keep the intensity of this laser low, to inhibit the formation of a photo-stationary state. Also, monitoring at a wavelength associated with an absorption peak can be advantageous to ascertain a greater change in the signal and a better signal-to-noise ratio.

1.1.4 Computational Predictions of Azobenzenes

Computational predictions of azobenzene derivatives typically aid in the rational design of photochromes with regards to two fronts: predicting the excitation spectrum of the molecule or determining the thermodynamics associated with the isomerization process. Accurate prediction of the absorption spectra of the derivative enables researchers to determine which wavelengths of light would be suitable to instigate the photo-isomerization process. Additionally, gaining insight into the energetics of the photo-isomerization can help determine the half-life of the *cis* isomer and elucidate the mechanism of the isomerization process.

The first step in these methods is to determine the ground state energy of the *trans* and *cis* isomer.³⁴ By using *ab initio* methods the optimal geometry of the orbitals and atoms can be determined. One of the most standard approaches is through the use of density functional theory (DFT). Here, the nuclei of the molecule are fixed and the energy of the system can be modeled using a time-independent Schrodinger equation. The total energy of the system is evaluated as a functional of the electron density, a simple function of three coordinates.

Ground state DFT calculations immediately give researchers insight towards the energy and geometry differences between the *cis* and *trans* isomers, and subsequently an idea of the half-life, differences in excitation energies, and other metastable configurations. However, it should be noted that many factors can influence the thermal relaxation and, ultimately, the energy of a proposed transition state is optimal to estimate the experimental half-life. This will be discussed further later. Nevertheless, ground state energy calculations help to build the energy landscape of the azobenzene and have had particular merits in

developing azo derivatives. Indeed, some of the first synthesized *ortho*-substituted were guided by computational techniques. ^{19, 23} In many computational studies it has been noted that *ortho*-substituents instigate a non-planar structure in the trans isomer, which drastically effects the energy and quantum yield of the n- π * transition. ¹⁹ Similarly, it has been noted that many *ortho*-substituents can decrease the energy of the *cis* isomer, which should theoretically increase the thermal stability of the molecule. ²³

Once the ground state geometries have been determined, many authors have used time dependent-DFT (TD-DFT) to predict the wavelengths associated with the π - π * and n- π^* transitions in organic solvents.^{34,35} For example, Konrad et al. were able to accurately predict the splitting of the $n-\pi^*$ transition energies in the cis and trans isomer of novel ortho-substituted azobenzenes.²² Thus, they were able to accurately design novel azobenzene derivatives that could be applicable in biological settings due to their ability to isomerize with deeply red-shifted light. In a fairly recent review, Adamo and Jacquemin provide a very thorough explanation of TD-DFT and its underlying principles.³⁵ One particular aspect that should noted is the exact energy that is calculated from these TD-DFT calculations. As shown in the Jablonksi diagram in Figure 1.5, there are many methods to measure the energy differences between a ground state and an excited state. For example, E^{adia} relates to the true energy difference between the ground state and excited state in a system that is not influence by any heat transfer (hence adiabatic). However, in practice the energy of electrons in a molecule follow a distribution, due to thermal fluctuations, and are not confined to a single energy. For this reason, the energy difference shown in blue in Figure 1.5 (E^{vert-abso}) is typically used to approximate the λ_{max} of a given transition. E^{vert-abso} is termed the idealized (or vertical) absorption energy and relates to the difference between the ground state and an excited electronic vibrational state. It is so named because the transition is purely vertical, in that the electron would transition 'straight up' in the diagram to a vibrational state with sufficient orbital overlap. However, experimental processes are not typically purely vertical and for this reason, the idealized absorption energy is an estimation of the λ_{max} . Nevertheless, the accuracy of this approach has proven to be adequate for many systems.^{19, 41}

In these calculations, special consideration is also taken into the effects of solvents. As noted previously, in many systems solvent-solute interactions can drastically influence the excitation energy of electronic transitions. As such, TD-DFT methods have been developed to account for these differences. The most common, and simplest, approach is to use an implicit solvent model. In this model, the solvent is treated as a continuum and estimated with a dielectric constant. While this method is convenient it fails to represent subtle solvent-solute interactions that may be occurring on the atomic scale. Thus, explicit models that implement individual water molecules have seen increasing interest despite the added computational requirements.³⁵

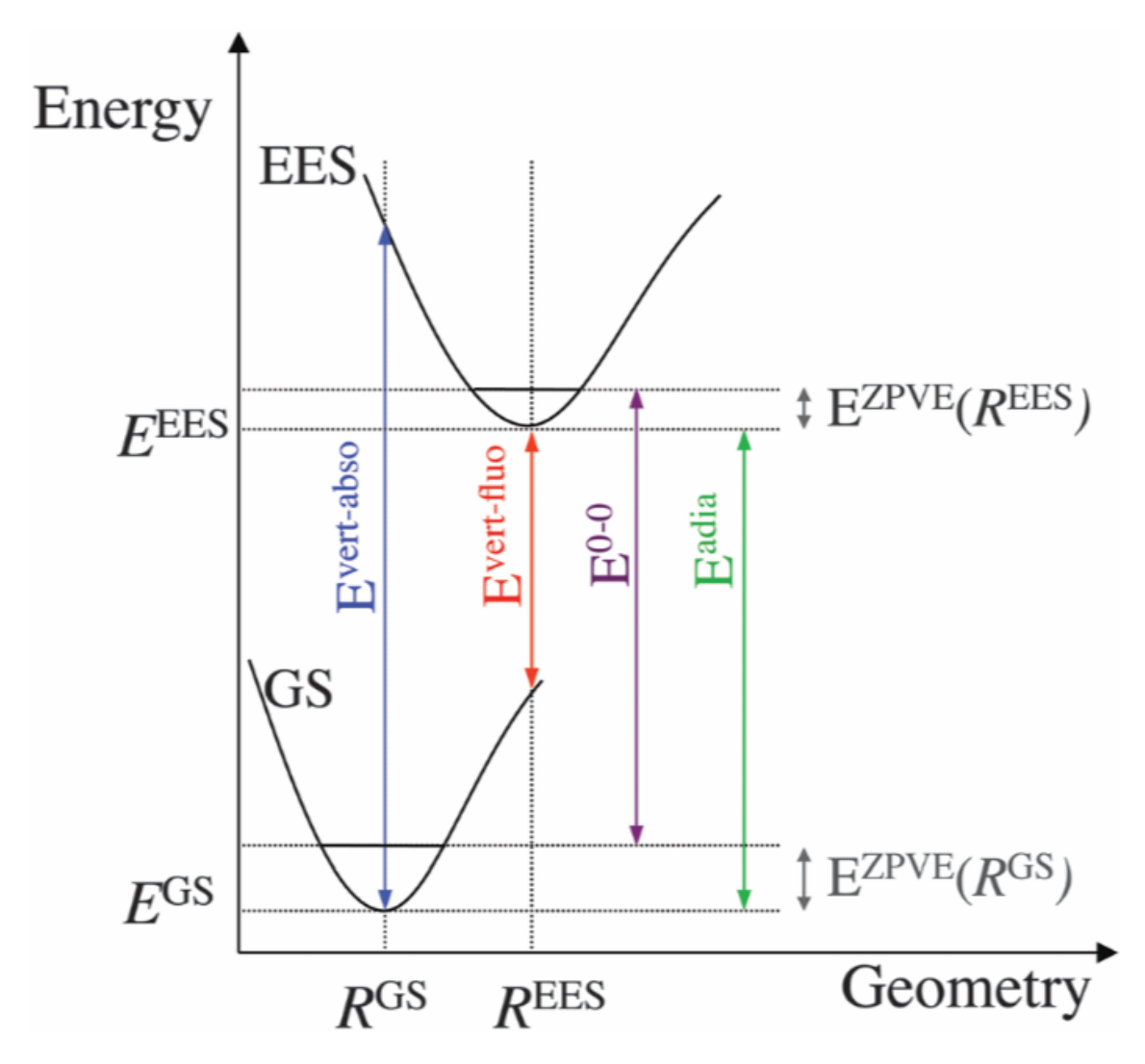


Figure 1.5. Jablonski diagram of the excitation of electrons from the ground state to an excited state. It can be shown that multiple methods can be used to measure the energy difference between the two states.³⁵

As mentioned previously, the exact mechanism of isomerization process can be quite elusive, however, has a large impact on the thermal half-life of the *cis* isomer. *Ab initio* quantum mechanic calculations enables authors to build the energy landscape associated with potential *cis* and *trans* azobenzene derivatives. This gives insight into the exact energy differences associated with the *cis* and *trans* isomers and, also, other hypothetical molecular configurations that may also be occurring. ^{37,38} However, these *ab initio* methods

are limited to determining the ground states of the molecules. Therefore, additional methods that implement transition state energy optimizations can provide even more insight into the system. For example, the Quasi-Newton Synchronous Transit-Guided (QST3) method developed by H.B. Schlegel and co-workers helps accurately determine the free-energy associated with the transition state and, conversely, the activation energy of the reaction. In this way, a hypothetical half-life of the *cis* isomer is determined.³⁹⁻⁴¹

Although the results of these computational experiments are promising, little work has been done to implement these calculations in aqueous systems. While authors have noted the stark differences in computational (and experimental) results in organic solvents, water is typically not compared.^{34,42,43} The necessity to validate theoretical results with experimental results presents a large barrier as determining the photodynamics of azos in water is not always straightforward. Still, there is great potential for this work as many biological applications that could implement azobenzene are based on aqueous systems.

1.2 DNA Nanotechnology & Supramolecular Polymers

1.2.1 DNA Origami & DNA Nanostructures

The advent of automated oligonucleotide syntheses has ushered in a whole new ensemble of technologies.⁴⁴ The automated DNA synthesis process revolves around synthesizing a DNA base that has a 4-4'-dimethoxytrityl (DMT) protected oxygen on one end and a phosphoramidite derivative on the other. This allows for fully automated control of the single stranded DNA (ssDNA) sequence. Not only does this allow researchers to mimic the sequences produce by biological systems, it also enables them to create novel

sequences that can be implemented into complex structures with a high degree of specificity. One key example is DNA origami. 45,46

A large effort has go into understanding and controlling the geometry of DNA strands.^{47,48} The infamous "photo 51" first eluted the helical nature of DNA. While this intricate geometry gives rise to many fascinating properties, such as chirality, it also poses a complex framework for creating basic Euclidian shapes, such as cubes or tetrahedrons. Strict attention must be paid to the turning of DNA base pairs in order to properly control DNA helices. For example, a full 360° helical turn incorporates approximately 10.5 base pairs.⁴⁵ This gives rise to the formality of working with base pairs in multiples of 21, or two helical turns. In a lattice where the helices are arranged in a hexagonal lattice, the first three crossover points to the neighbouring helices would be achievable at 0, 7, and 14 base pairs (Figure 1.5).

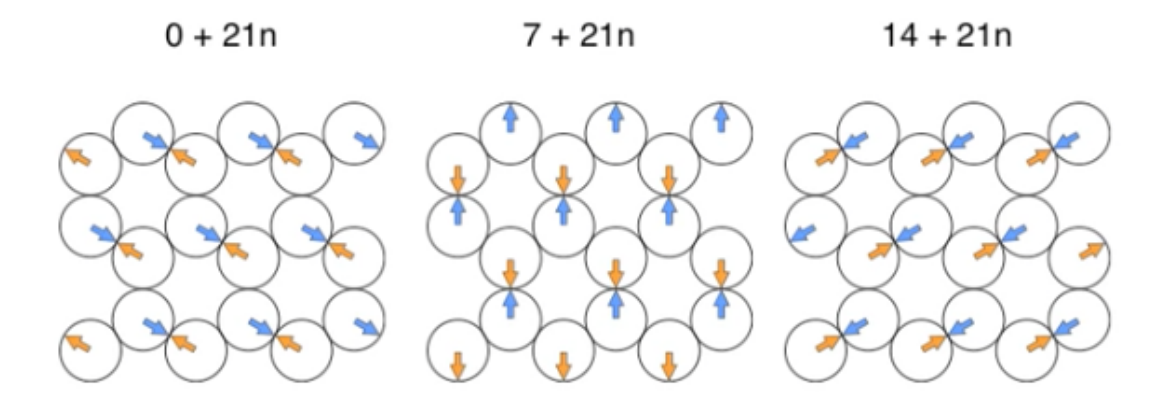


Figure 1.6. Reduced representation showing cross sections of the crossover points in a DNA helical lattice. As shown, the first three crossovers to adjacent helices are possible at $0 (330^{\circ})$, $7 (90^{\circ})$, and $14 (210^{\circ})$. These crossovers are also available again after the addition of 21 base pairs.

This stems the bases for DNA origami, however other lattice types have also been explored.^{49,50} By accounting for the natural turns occurring in these structures favourable

geometries can be hypothesized. This allows for a controlled self-assembly of 2 and 3 dimensional shapes by tuning the number of base pairs in a single strand of DNA. ^{49,50}

In more detail, DNA origami incorporates designing DNA 'staple' strands to fold ssDNA sequences into specific geometries. Specifically, one long strand of DNA backbone is obtained either from bacteria or some synthetic process. Staple strands are then designed that are complementary to two locations of the DNA backbone. This enables the DNA backbone to fold on itself and create a two-dimensional structure. Through this concept a wide variety of 2- dimensional (2D) and 3-dimensional (3D) nanostructures have been formed.⁵¹ Note that this process relies on the principle of selfassembly: the components on the system arrange themselves to optimize the energetics associated with the conformations of the molecules and non-covalent interactions.⁴⁴ As hydrogen bonding and the hydrophobic effect are large contributors in DNA duplex formation, the same factors are crucial in DNA nanostructure formation. Indeed, specific control of the structures formed can be obtained, however, they are typically susceptible to thermal degradation at relatively low temperatures.⁵² Some other drawbacks to existing DNA origami systems are that they require a large number of nucleotides and have poor yields, making them inadequate for industrial use.⁴⁴ Homogeneity in these systems is also hard to control, due to defects easily formed in the structures.⁵³

One strategy to improve the viability of DNA nanostructures is the incorporation of synthetic organic molecules units into the ssDNA.^{54,55} In this strategy a small organic molecule is used instead of a DNA base pair in the automated synthesis process. As such, this analogously revolves around synthesizing a diol molecule that has a DMT protected oxygen on one end and a phosphoramidite derivative on the other. This has proved to

promote the self-assembly of these nanostructures, leading to higher yields and a decrease of defects. It also decreases the number of nucleotide bases needed in these systems, giving rise to more efficient 'minimalistic structures'. 56 The choice of the polymeric unit has a large effect. Rigid organic linkers, through the use of rings or conjugated systems, provide more strict conformations then flexible systems. Furthermore, the placement and geometry of the organic linker will have a profound effect on the 2D structure that is obtained.^{54,55} This is a direct consequence of the fact that DNA base pairs turn in a helical fashion oppose to being linear. This however can be taken advantage of to acquire a wide variety of 2D shapes, with varying numbers of DNA strands. The simple modification of the organic linker's placement - or the number of base pairs - in a DNA strand can yield squares, circles or linear aggregates, which consist of dimers, trimers, or polymers.⁵⁴ The majority of examples show organic linkers inserted directly into the DNA backbone. This results in no overall change in the orientation of the DNA base pairs. That is, they are all aligned in the same orientation, 3' to 5', or 5' to 3'. Methods have been proposed that would insert an organic linker at only the 5' ends of DNA strands, resulting in an asymmetric linear molecule. Similarly, insertion of organic linkers at the 3' ends of DNA is also possible.⁵⁷ The formation of DNA duplexes is orientation dependent such that single strands oriented in a 5' to 3' fashion will only hydrogen bond to a complementary strand oriented in a 5' to 3' fashion. 45 This selective supramolecular bonding gives rise to a whole new arsenal of DNA self-assembly products.

1.2.2 Supramolecular Polymers

A further step to optimize the self-assembly of DNA nanostructures is to move away from the concept of DNA origami itself. Many authors have demonstrated that supramolecular polymers are an efficient method to build higher ordered nanostructures. In these systems, monomers are designed to interact with themselves through non-covalent interactions to promote aggregation. ⁵⁸⁻⁶¹

A complex issue with supramolecular polymers is the unique thermodynamics that arise in these systems.⁶² It has been suggested that the chemical instability of these systems is due to the lack of enthalpic gain.^{62,63} A consequence of this is a system that thermodynamically dominated by entropic effects. Supramolecular polymers display a unique elongation temperature, above which depolymerization of these materials occurs. These temperatures are specific to the system at hand and have a large dependence on not only the types of interactions between monomers however, in addition, the solvent. For example, a supramolecular polymer that utilizes hydrogen bonding to bind monomers would see an even lower enthalpic gain in aqueous systems due to the competitive hydrogen bonding occurring with water molecules.⁶¹ Similarly, the hydrophobic effect also plays a large role in these systems and will vary based on the size of aggregates formed, ions in solution, and solvent choice. All these specifications lead to materials that require fragile conditions for synthesis.

A distinct contrast from covalent polymers is the concept of a fluxional monomer.⁶³ Due to the weak bonding interactions occurring between monomers the polymers formed present a higher degree of instability and fluidity. This leads to a more dynamic system with pathway complexity in the polymerization process. Pathway complexity also presents

issues in covalently-bound polymers as well. This underlines commonly addressed imperfections such as polydispersity or tacticity.⁶¹ The difference in supramolecular systems is that these changes are no longer permanent. Thus, the polymerization process can exhibit self-correcting behaviour leading to fewer variations in the final product.⁶⁴ This fluxional monomer also leads to a polymerization mechanism that is sensitive to external forces such as changes in pH, temperature, or even solvent.⁶⁵ Indeed, due to their labile interactions, supramolecular polymers provide a unique platform for stimuli responsive materials. By using monomers that are responsive to external stimuli, systems have been developed that respond to light, heat, and even pH. 66-68 Contrary to typical covalently bound polymers, these materials have the added advantage that they can easy assemble or disassemble with lower amounts of energy. As such, many systems have been designed that spontaneously aggregate or degrade when probed with external stimuli.⁶⁹ Furthermore, the materials formed typically also display a relatively low Young's modulus. Therefore, actuation or other deformations can be easier to implement in these systems. In particular, many authors have displayed the concept of photo-actuation in these systems by implementing photo-responsive molecules. ^{67,68} A primary example is shown in Figure 1.6 below.

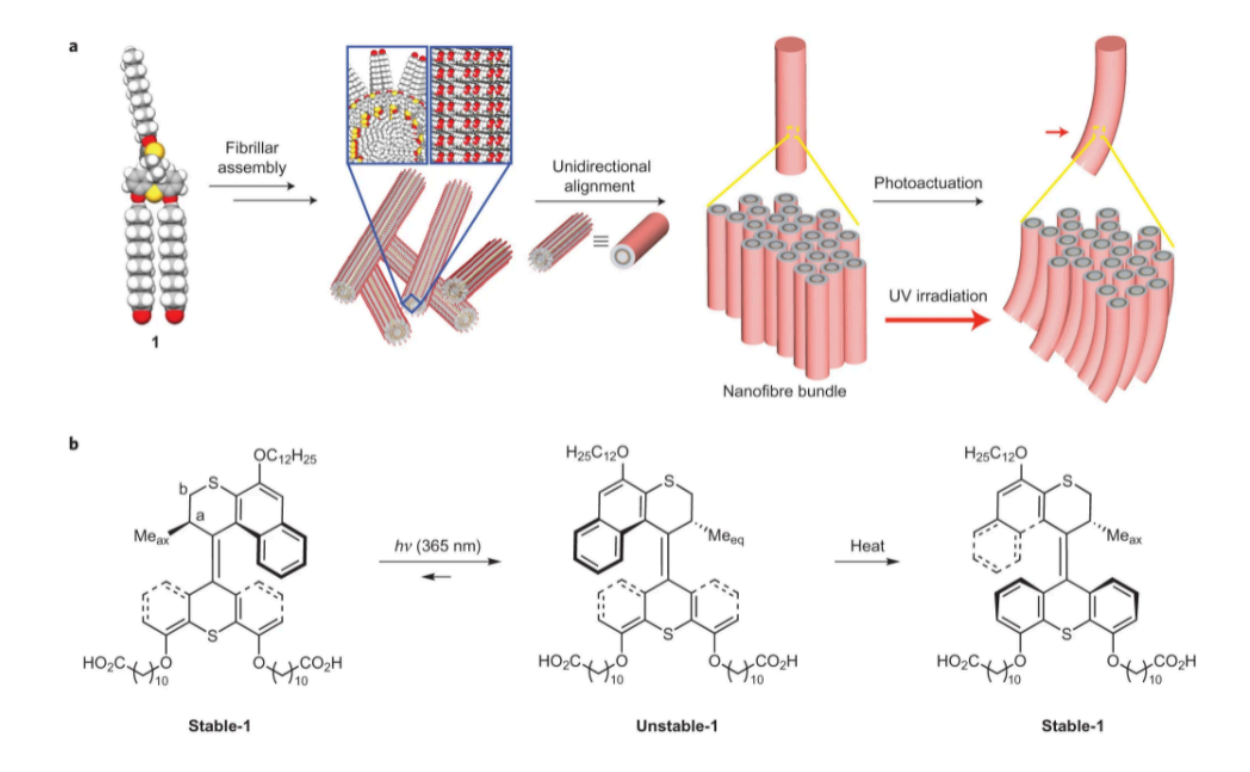


Figure 1.7. An example of a supramolecular system that can have induced photo-actuation. (a) The assembled supramolecular polymer and its photo-actuation. (b) the isomerization process of the photochrome. Here the molecule switch has similar properties to azobenzene: isomerization of the molecule leads to a metastable secondary phase, which subsequently undergoes a thermal relaxation to thermodynamically stable state.

Here, a molecule is designed that will naturally assemble onto itself in aqueous media due to the hydrophobic effect. By implementing a photochromic motif into the molecules core the product of the self-assembly process displays photo-responsive attributes. In this case, irradiation leads to macroscopic actuation of the material due to the concerted rotary motion of the monomers.

Despite their rigorous specifications, supramolecular polymers are an abundant material in our everyday lives. Nature commonly employs these materials and takes advantage of the vast properties they exhibit. 60,67,69 Many biological processes in our body rely on the self-organization of these molecules. 70 How do these systems overcome the

fragile nature of self-assembly? Can these examples contribute to synthesizing more robust supramolecular polymers? DNA is an example of such a material and offers a versatile platform for designing novel supramolecular polymers and studying their properties.

1.2.3 DNA-based Supramolecular Polymers

The Craig group reported a wide variety of ssDNA monomers that self-assemble into linear supramolecular polymers in the early 2000's. 71,72 This was done by creating monomers that were self-complementary to each other. Many of these examples also incorporate organic linkers into the DNA monomer backbone. While the target structures for many of these systems were linear supramolecular polymers, they often speculated that cyclic DNA structures were also being formed. Indeed, this can most likely be attributed to many of the aforementioned factors such as, the use of flexible organic linkers, the location of the organic linker, and the number of base pairs used. 54 Despite this, the group was still able to obtain reversible supramolecular polymers that display many physical properties similar to covalent polymers. Given the recent advances in self-assembling DNA materials there is no doubt that these materials could be obtained today with even higher yields and lower defects.

Other methods revolve around monomers aggregating based on the synthetic portion of the molecule, leaving the DNA portion exposed. This is the case with amphiphilic DNA molecules.^{73,74} Similar to other amphiphilic molecules theses monomers will aggregate in aqueous conditions to form spherical micelles. However, by tuning the ratio of hydrophilic to hydrophobic components, or the molecules themselves, 1D rods and 2D sheets can also be formed.⁷⁵ In this way, DNA can be implemented into micelle

structures.^{76,77} The high specificity of DNA base pairings allows for a fine control of the overall structure obtained and, furthermore, enables secondary interactions with the exposed DNA strands. For example, with spherical nucleic acids, the amphiphilic DNA monomers assemble through the hydrophobic effect presented by the synthetic hydrophobic portion leaving the ssDNA portion free to interact with complementary DNA sequences.⁷⁸ This is an important concept that should be highlighted when discussing DNA based supramolecular polymers: not only does working with DNA improve the specificity of the materials obtained; it also creates opportunities to explore different functionalities.⁷⁹

Another distinct example that intertwines the areas of DNA nanotechnology and supramolecular polymers is the work of polyadenine (polyA) rosettes, pioneered by Sleiman and co-workers. This system differs from the aforementioned ones because it relies on a secondary molecule to form. That is, there are two different types of monomers. In the presence of cyanuric acid (CA) the polyA strands spontaneously form a rosette structure. As demonstrated in Figure 1.7 cyanuric acid presents three faces that can hydrogen bond complementarily to adenine. In this fashion, it is hypothesized that the CA can interact with two sides of the adenine moiety to create a six membered binding motif. As the adenine units are connected through phosphate backbones these motifs can readily stack upon each other to give rise to rod like structures. Additionally, the chiral nature of the DNA structure is imposed on the structures yielding chiral fibres. Atomic force microscopy (AFM) images verify fibres that are microns in length and morphologies that are dependent on the polyA length (Figure 1.7, b and c). It should be noted that these fibres only form under slightly acidic conditions, as protonation of the cyanuric acid is essential in promoting cyanuric acid-adenine interaction. Furthermore, recent theoretical studies

have suggested that the fibres are actually elongated duplexes and not the hypothesized rosette structures, however, sufficient experimental evidence to verify these claims have not been conducted.⁸⁰

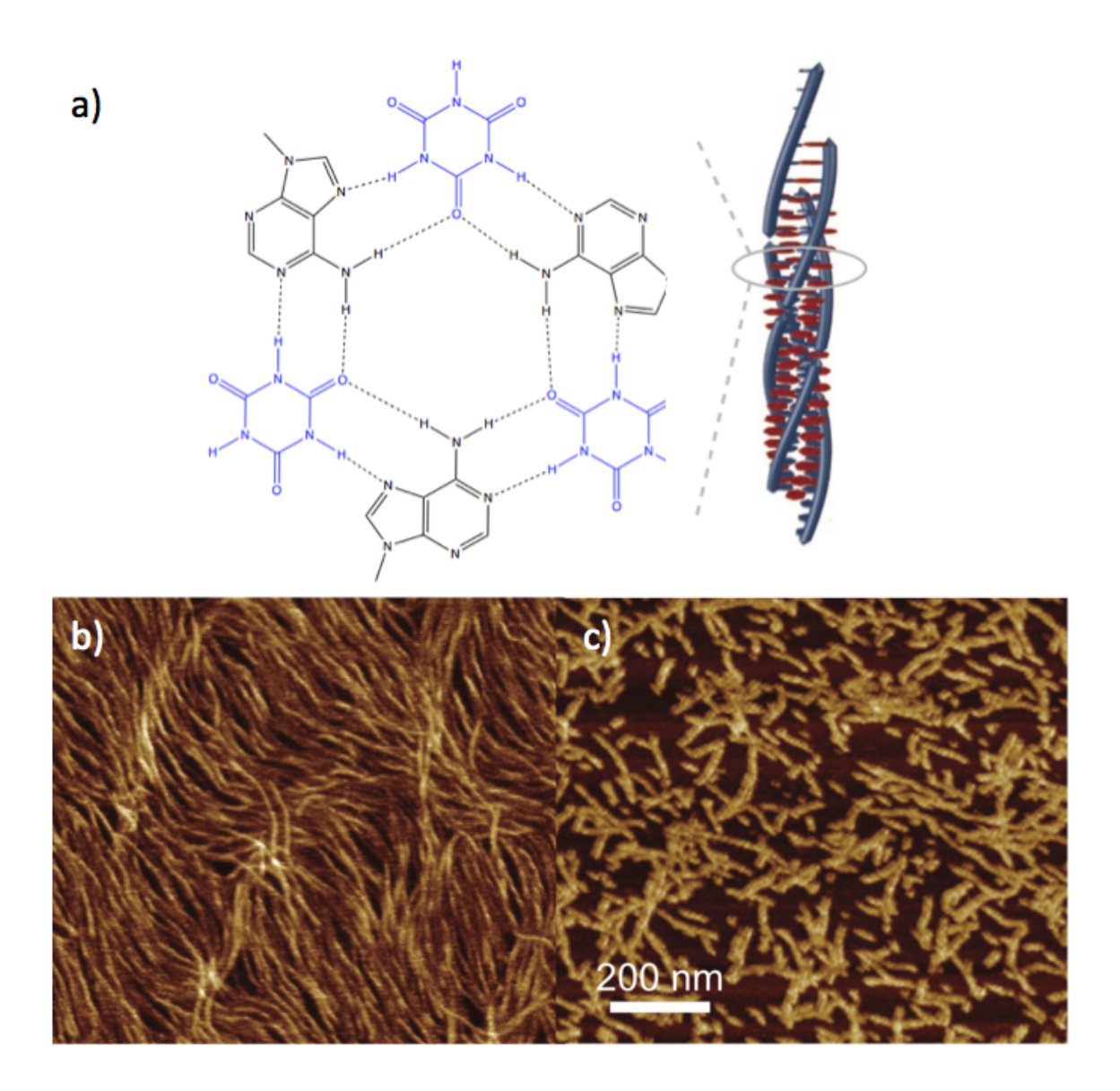


Figure 1.8. Binding motif of the polyA:cyanuric acid fibres (a) and experimental AFM results (b & c). Based on the number of polyA unites elongated (polyA₁₅, (b) or contracted fibres polyA₁₅ (c), may be observed.

1.2.4 Azobenzene in DNA

The incorporation of organic linkers into a DNA backbone provides an apt opportunity for molecular control over DNA based materials. Introducing functional groups into the organic linkers that are sensitive to orthogonal interactions, for example, pH, temperature, electric fields, or even light, can easily produce a stimuli responsive material. With the case of azobenzene, this could present materials that exhibit substantial property changes as a response to light or temperature.⁸¹ Azobenzene readily undergoes a trans-to-cis isomerization upon π - π * excitations when exposed to irradiation (~320 nm). It will also undergo thermal isomerization back to the more stable trans isomer under dark conditions. 14 This conformation change can lead to a change in the dipole moment of up to 3 Debye and a large conformational change in end-to-end length of up to 3.5 angstroms.⁸² When incorporated into covalently bonded polymeric materials with sufficient amounts of azobenzene, these conformational changes can be observed on the macroscale. These interesting features have given rise to a whole new range of materials that can bend, contract, or even oscillate upon the exposure of light.^{81,83} Therefore, embedding these molecules into DNA nanostructures that are soft bonded is extremely intriguing, as these supramolecular systems should be even more susceptible to change than their covalent counterparts. However, to integrate these appealing characteristics into DNA nanostructures many parameters must be considered. Fortunately, other groups have already briefly explored this field and provided insight into the nature of these materials.

The most common method to integrate azobenzene into ssDNA is as an intercalating unit. 84,85 In this method, the *trans* azobenzene moiety lies parallel to the DNA base pairs as it participates in π - π stacking between two base pairs (Figure 1.8). Essentially,

it can be visualized as another base pair. This has been noted to increase the melting temperature on the DNA duplex as the added π - π interaction adds to the enthalpic gain and hydrophobicity as the azobenzene moiety promotes the hydrophobic effect. However, upon UV irradiation the azo isomerizes to the *cis* form, which is non-planar and more polar. Now the π - π interaction is lost and the moiety is more susceptible to interact with the solvent, which destabilizes the DNA duplex. By implementing only two azobenzene unites into a DNA strand with eight base pairs, a difference in melting temperature of up to 21.5°C can be obtained.⁸⁶ Thus, these systems are convenient to mediate the photo-disassembly of systems.

It should be noted that a stark difference was seen when altering the stereocenter of the azo moiety. Specifically, the azo was introduced *via* a threoninol linker as either L-threoninol (S,S) or D-threoninol (R,R). When enantiomerically pure L-threoninol was introduced into the DNA a melting temperature of only 4°C degrees was observed. Conversely, when enantiomerically pure D-threoninol was introduced into the same system a melting temperature of 14°C degrees was observed. Using molecular modelling, it can be rationalized that the D enantiomer orients the azobenzene residue in a more preferable fashion, such that it can easily intercalate between the base pairs. This sheds light on the enatioselective nature of the system and a key factor that must be considered when working with these chiral DNA-based systems.

One interesting irregularity in these systems is the differences in the photodynamics of azobenzene. Samai et al performed an in depth study analyzing the quantum yields of azobenzene when implemented into DNA.⁸⁸ Interestingly, there is large decrease in the quantum efficiency when azobenzene is in DNA; longer irradiation times are required in

order to sufficiently isomerize trans azobenzene. This hindrance to the isomerization process was further amplified when applied to systems with double stranded DNA, suggesting a high dependence on the local environment. In fact, the efficiency of the photo-isomerization was even found to be sequence dependent, as different neighbouring base pairs affected the rate of isomerization. Contrarily, the thermal relaxation process was unaffected by these changes and remained constant regardless of the induced local environment. These findings led the authors to hypothesize that the initial photo-isomerization process proceeds through a rotation pathway, which is dependent on the free volume surrounding the azo moiety. Thus, when the azo is sterically constrained, as is would be in double stranded DNA systems, the isomerization process is hindered and requires longer irradiation times. Notably, at higher temperatures the differences in the photo-isomerization were negligible, further indicating the importance of the local environment and spatial freedom.

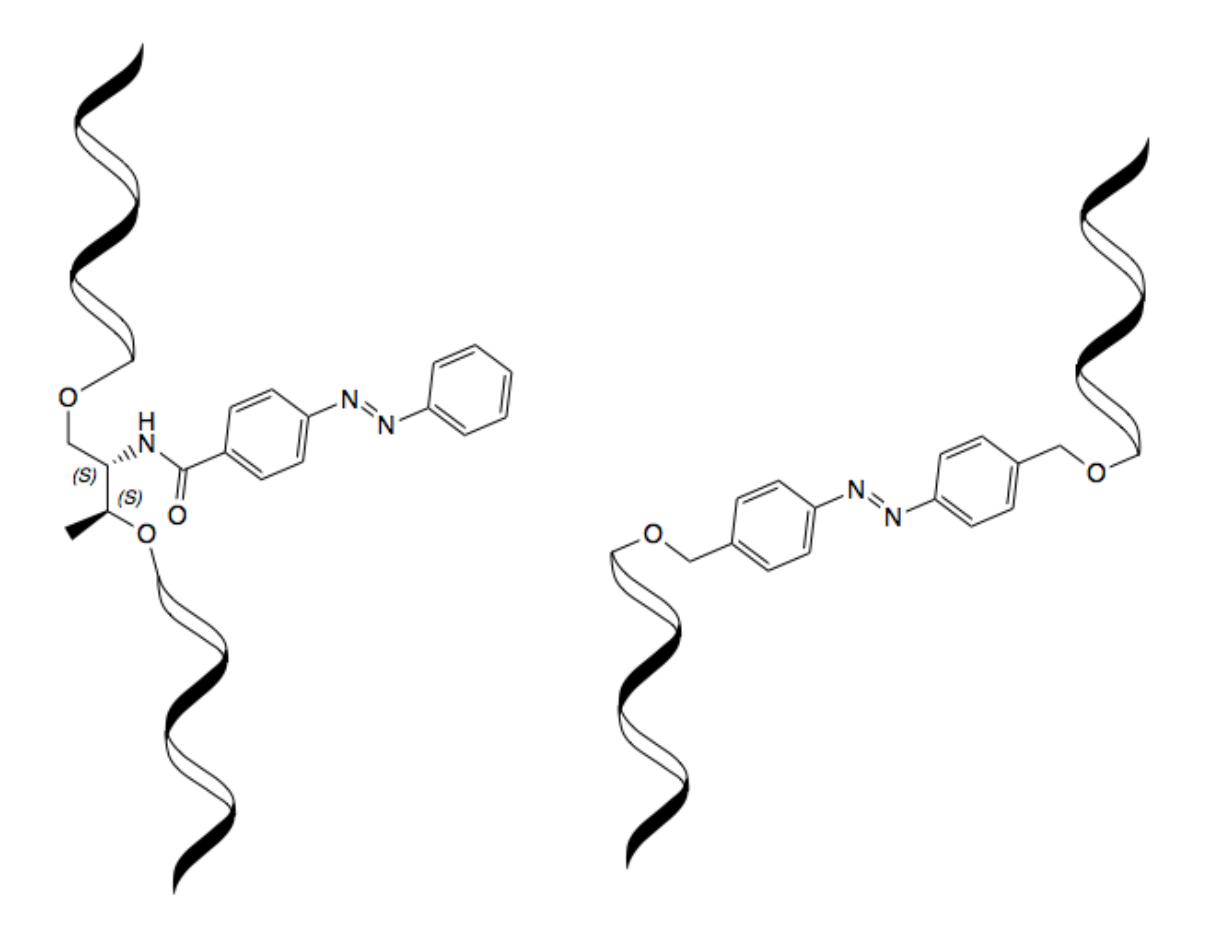


Figure 1.8. The two predominant approaches to insert azobenzene into DNA. On the left, the azo motif is perpendicular to the DNA strand and bound through a L-threoninol linker. On the right, the azo elongates the phosphate backbone. Note azo:DNA size is not to scale.

Another method to integrate azobenzene into DNA is as a backbone linker where the azo moiety sits perpendicular to the base pairs (Figure 1.8).⁸⁵ In this position, the azobenzene can no longer interact with the base pairs through π - π interactions; however, it now offers the opportunity for more dynamic control over the conformation of the DNA. In the *trans* conformation the azobenzene is linear and aids in the elongation of the DNA strands. Conversely, upon the irradiation, the *cis* azo moiety adopts a bent structure and can assist in the contraction of the DNA strand. It should be noted that the persistence length of ssDNA ranges from 0.6 to 6 nm, while that of double stranded DNA can surpass

35 nm.^{44,46} Thus, it can be hypothesized that such conformation rearrangements would be more suitable in double stranded DNA systems. Nevertheless, proper experiments to elucidate the behaviour of azobenzene in these positions still need to be conducted, as these systems have been far less studied.

One method to confirm the contraction of ssDNA is by designing azo-DNA molecules as hairpin loops. ⁸⁹ This guides the ssDNA to adopt a contracted structure that has folded onto itself. By inserting azobenzene into the loop portion of the molecule a change in the denaturation temperature of the hairpin is observed depending on which conformation the photoswitch is in. Specifically, irradiation initiates a *trans*-to-*cis* isomerization, which results in a highly conformationally strained hairpin loop. ⁹⁰ Thus, the denaturation temperature of the hairpin is lower than when in this conformation. The change in the denaturation temperature is dependent on the DNA bases used. However, in these systems the contraction of the ssDNA is assisted by the self-complementary nature of the ssDNA due to the hairpin design. Furthermore, it contrarily suggests that a *trans* isomer is likely to allow ssDNA to fold on itself despite the wormlike nature of ssDNA. Indeed, in these structures the *trans* isomer is more likely to yield a contracted DNA stranded whereas the *cis* isomer is more likely to yield an elongated structure, however, this is due to the specific design of the ssDNA sequence.

Another system that explores the conformational changes that arise in these azooligonucleotide molecules is in the field of small interfering RNA (siRNA).^{91,92} In this work, azobenzene is introduced into systems that are dependent on dsRNA structures. The authors hypothesize that in the trans conformation the ssRNA is able to adequately bind to the complementary RNA strand, yielding a dsRNA complex. This dsRNA RNA can then act as a substrate of the RNA-induced silencing (RISC) complex and participate in the gene-silencing pathway. However, in the *cis* conformation, the RNA is no longer a true dsRNA entity and can no longer be recognized. Thus, the system can invoke light mediated gene silencing.

In the aforementioned studies, little work has gone into validating the hypothesized structures obtained. Carefully designed experiments are necessary to reveal the exact structures that are obtained in solution. For example, quantifying the change in the end-to-end distance of the ssDNA upon irradiation would be extremely beneficial. Similarly, analyzing how the polarity or chirality of the molecule changes would provide great insight for future work. Furthermore, the photodynamics of these systems has not been analyzed to ascertain information pertaining to the mechanism of the photo-isomerization and thermal relaxation processes.

1.3 Scope of Thesis

1.3.1 Overview of Thesis & Objectives

As outlined previously, stimuli-responsive materials are becoming highly intriguing candidates for many applications. In particular, DNA-based supramolecular polymers are very viable smart materials for many biological systems. This can primarily be attributed to their ability to initiate secondary interactions with biological substrates through unbound ssDNA. Furthermore, the labile nature of these soft-bonded materials provide an apt opportunity to implement responsive properties through orthogonal stimuli. Due to the promising photodynamic characteristics of azobenzene, it is a good contender to instigate photo-responsive properties into these materials. However, the abnormal isomerization behaviour of azobenzene in water has hindered progress in this area. As such, this thesis can be separated into two parts: the first, where the photodynamic properties of different azo derivatives are analytically analyzed in aqueous systems and the second, where a promising azo derivative from part one is implemented into an existing DNA-based supramolecular system.

For the first portion, water—soluble azos are synthesized to yield a wide variety of azobenzene classes and photophysical properties. The photodynamics of these azos were then analyzed in organic solvents and water. In particular, special attention is paid to the kinetics surrounding the *cis*-to-*trans* thermal isomerization process and the required excitation wavelength to induce the *trans*-to-cis isomerization. To further rationalize the changes observed computational methods were used. In particular, the geometries of the derivatives were optimized with *ab initio* calculations and the excitation energies calculated through time-dependent density functional theory (TD-DFT). Lastly, the

transition states of the *cis*-to-*trans* thermal relaxation were also optimized to gain insight into the thermodynamics associated with this process.

In the second part of this work an azo derivative is implemented into a polyAcyanuric acid supramolecular system. This was done by first synthesizing an azobenzene derivative that was fully compatible with the automated DNA synthesis. By altering the position of the azo motif on the polyA strand its influence on the self-assembly process could be analyzed. Fibres of different morphologies were obtained and their characteristics were analyzed through circular dichroism (CD) spectroscopy and atomic force microscopy (AFM). Preliminary studies were also conducted to observe the effect of the photo-isomerization on these supramolecular systems.

The work in the first portion sheds light on the intricacies of dealing with azobenzene in water. The findings show how to easily rationalize the optimal type of azo derivative for a specified application. In particular, amino-azos are rationalized as a suitable photo-switch for applications that require fast isomerizations, for example optoelectronics. Contrarily, azobenzene-type derivatives and *ortho*-substituted azos are optimal for systems that seek to exhibit dual functionality. Due to their long half-life the molecules can act as a binary system that exists in the *cis* or *trans* state. However, with these derivatives researchers must be particularly wary of the inherent water-insolubility that exists due to the hydrophobic substituents. Furthermore, the computational results presented aid researchers in further optimizing the azo derivative. By employing in-silico methods researchers can easily acquire an understanding of the expected wavelength required for photo-isomerization and also an estimate of the half-life.

In the second portion, the subtle influences azobenzene has on the self-assemble processes were analyzed. Specifically, how the orientation and placement of the azo motif affects the macroscopic properties of a material can be stringently dissected. By combining the findings of both portions, this work demonstrates how transferring potential azobenzene derivatives into aqueous systems, such as supramolecular polymers, can be more straightforward. Particularly, the photodynamics azo derivatives can easily be rationalized through the works presented in the first portion. Based on these findings they can next be easily implemented into an existing self-assembly system. In addition, coupling the azo motif to an already existing building block of the supramolecular system could potentially alleviate the issues associated with its water insolubility. This enables researchers to easily classify and determine the implications of introducing photo-switches into supramolecular systems.

Chapter 2: Methods, Results, & Discussion

2.1 Synthesis & Self-Assembly

Five azobenzene derivatives were first synthesized to yield a series of different azobenzene classes. Specifically, one azobenzene-type azo, two amino-type azos, and two ortho-substituted azos were synthesized. Schemes for each azo derivative are shown below. Based on the experimental results the azobenzene-type azo (azo1) was used as a precursor to implement into the polyA-cyanuric acid systems. As such, an azobenzene phosphoramidite was synthesized as shown in Scheme 1. However, it can be noted that due to the hydroxyl substituent present on each derivative, any of the azos presented could theoretically have been covalently implemented into a DNA-based system. The two aminotype azos (Azo2 and Azo3) were synthesized through typical azobenzene coupling reactions.⁹³ The syntheses of these compounds were therefore quite straightforward and matched the experimental results of similar derivatives. On the other hand, the synthesis of the ortho-substituted azos (Azo4 and Azo5) was less straightforward and was guided by relatively recent studies. As shown in Scheme 4, the synthesis of Azo4 was particularly intensive and relied heavily on following the previous results of Bleger et al. However, for both Azo4 and Azo5 a novel LAH reduction was employed to reduce the carboxylic acid substituent to a hydroxyl group. A recently presented azo coupling was then further used in the final step to yield the respective azo.94 To aid future researchers, relevant NMR for each compound can be found in the Appendix.

2.1.1 Organic Synthesis

Scheme 1. Synthesis of Azol and its respective phosphoramidite derivative (Azolb).

Bis(hydroxymethyl)azobenzene (Azo1)

Azo1 was synthesized through a typical reductive coupling. 91,93 2.00 g (0.013 mol) of 4-nitrobenzyl alcohol was added to a round bottom flask with 50 mL 10% sodium hydroxide and sonicated for 30 min. To this solution 3 g (0.022 mol) of zinc powder was added slowly, over the course of 30 min while stirring rapidly. The solution was refluxed at 100°C overnight & filtered to yield orange crystals. The crude material first purified through soxhlet extraction (hexanes) and subsequently purified *via* recrystallization (methanol) or column chromatography (Hexanes/Ethyl Acetate). ¹H NMR (CDCl₃, 500

MHz) δ 7.86 (d, J = 7.49 Hz, 4H) 7.53 (d, J = 7.51 Hz, 4H) 5.35 (s, 2 H) 4.61 (d, J = 5.39 Hz, 4H) HRMS-ESI: m/z = 243.1129 (calcd: 243.1134).

4-hydroxymethyl-4'-O-(4,4'-dimethoxytrityl)-azobenzene (Azo1a)

2 mmol of azo1 was added to 10 mL of dry THF under an inert atmosphere and stirred until dissolved. The solution was then cooled to 5°C after which, a solution of 2.4 mmol of dimethoxytrityl chloride dissolved in 5 mL of dry THF was added dropwise. The solution was then stirred overnight at room temperature and subsequently evaporated. The crude product was then purified by column chromatography (Hexanes/Ethyl Acetate/Triethylamine). 1 H NMR (CDCl₃, 500 MHz) δ 7.93 (m, 4H), 7.55 (m, 6H), 7.44 (m, 4H), 7.32 (m, 3H), 6.88 (m, 4H), 4.83 (d, 2H 6.00 Hz), 4.28 (s, 2H), 3.82 (s, 6H) HRMS-ESI: m/z = 567.2238 (calcd: 567.2259, M + Na)

2-Cyanoethyl-4-O-{[4-hydroxymethyl-4'-O-(4,4'dimethoxytrityl)-O-methyl-diazenyl]kon}-N,N'-diisopropylaminophosphoramidite (Azo1b)

0.9 mmol of was dissolved in dry DCM under an inert atmosphere. 4 mmol of dry DIPEA and 0.9 mmol of DMAP were then added to the solution and stirred for 5 min. Using a syphon, 1.1 mmol of 2-cyanoethyl N,N-diisopropylchlorophosphoramidite under an inert atmosphere was then added drop-wise to the solution. The solution was stirred for 2 hrs after which it was evaporated. The solution was immediately dissolved in Hexanes/Ethyl Acetate/Tryethylamine (80:18:2) and purified through column chromatography under an inert atmosphere (Hexanes/Ethyl Acetate/Tryethylamine

80:18:2). ¹H NMR (CDCl₃, 500 MHz) δ 7.94 (m, 4H), 7.55 (m, 5H), 7.44 (m, 3H), 7.34 (m, 1H), 6.88 (m, 4H), 4.82 (s, 1H), 4.29 (s, 2H), 4.15 (m, 1H), 3.83-3.77 (m, 8H), 3.71-3.58 (m, 2H), 2.24 (m, 2H), 1.27 (m, 12). HRMS-ESI: m/z = 783.3083 (calcd: 783.8367, M+K)

Scheme 2. Synthesis of Azo2.

4-hydroxy-4'-hydroxymethylazobenzene (Azo2)

Azo2 was synthesized through a diazonium salt coupling.⁹³ 20 mmol of the respective 4-aminobenzyl alcohol was added to a 2.4 N hydrochloric acid (HCl) solution . The solution was cooled to 5°C and 24 mmol of sodium nitrite was added. The solution was stirred for 30 min and after was added drop-wise to a solution of 20 mmol phenol in 8 mL 20% sodium hydroxide cooled to 5°C. The pH was monitored throughout this process to ensure basic conditions. The reaction was allowed to stir for 24 hrs, after which the solution was neutralized with HCl & filtered. The precipitate was then purified through column chromatography (Hexanes/Ethyl Acetate). ¹H NMR (DMSO, 500 MHz) δ 10.26

(s, 1H), 7.79 (m, 2H), 7.49 (m, 2H), 7.33 (m, 2H), 6.94 (m, 2H), 4.58 (d, J = 6.12 Hz, 2H) HRMS-ESI: m/z = 229.0967 (calcd: 229.0977)

Scheme 3. Synthesis of Azo3

4-hydroxymethyl-4'-nitro-azobenzene (Azo3)

Azo3 was synthesized through an oxone coupling. 93 200 mg of 4-nitroanaline was dissolved in 5 mL of DCM under an inert atmosphere. To this solution was added 1.79 g Oxone® dissolved in 20 mL water. The biphasic reaction was stirred for 6 hrs and monitored *via* TLC to ensure completion. After which, the solution was separated and the aqueous phase was washed with DCM twice. The organic fractions were collected and sequentially washed with 1 M HCl, saturated sodium bicarbonate solution, water, brine, and then dried over magnesium sulphate. The solution was then evaporated to dryness to yield the nitrosoarene intermediate. The compound was then redissolved in acetic acetic and 1.4 mmol of 4-aminobenzyl alcohol was added. The reaction was stirred over night after which it was diluted with water and extracted DCM (3x). The organic fractions were collected and sequentially washed with 1 M HCl, saturated sodium bicarbonate solution, water, brine, dried, and evaporated. The crude compound was purified through column chromatography

(Hexanes/Ethyl Acetate). 1 H NMR (DMSO, 500 MHz) δ 8.45 (m, 2H), 8.09 (m, 2H), 7.96 (m, 2H), 7.59 (m, 2H), 4.64 (d, J = 6.06 Hz, 2H), 4.34 (t, J = 5.15 Hz, 1H) HRMS-ESI: m/z = 258.0873 (calcd: 258.0878)

Scheme 4. Synthesis of Azo4.

4-amino-3,5-difluorobenzoic acid (4a-4c)

Compounds 4a-4c were synthesized as per the protocols described by Bleger et al.²⁰ Briefly, 2,6-difluoroaniline was reacted with NBS to yield 4b. 4b was further reacted with copper cyanide to yield 4c, which was subsequently oxidized in NaOH to yield 4d. NMR data as per reference. HRMS-ESI: 4a m/z = 207.9558 (calcd: 207.9573), 4b m/z = 155.0419 (calcd: 154.0421), 4c m/z = 174.0357 (calcd: 174.0366)

4-amino-3,5-difluorobenzyl alcohol & 4-amino-2,3,5,6-tetrafluorobenzyl alcohol (4d & 5a)

5 mmol of LiAlH₄ was dissolved in 5 mL of dry THF under inert atmosphere at 0°C. The solution was then added dropwise to a solution of 2.5 mmol of the respective aminofluorobenzoic acid dissolved in 5 mL dry THF (under N_2 , 0°C). The reaction was then stirred at room temperature overnight under an inert atmosphere. After monitoring *via* TLC, the reaction was cooled to 0°C and quenched with saturated sodium bicarbonate solution. It was then diluted with excess water and extracted into ethyl acetate (2x). The organic fractions were combined, dried over magnesium sulphate, and evaporated. The crude material was purified through column chromatography (Hexanes/Ethyl Acetate). ¹H NMR (CDCl₃, 500 MHz) of 4d δ 6.87 (m, 2H), 4.58 (s, 2H) HRMS-ESI: m/z = 160.0564 (calcd: 160.0574). ¹H NMR (CDCl₃, 500 MHz) of 5a δ 4.80 (d, J = 6.65 Hz,), 4.04 (s, 1H) HRMS-ESI: m/z = 194.0223 (calcd: 194.0229)

Scheme 5. Synthesis of Azo5.

bis(2,6-difluoro-4-hydroxymethyl)diazene & bis(2,3,5,6-tetrafluoro-4-hydroxymethyl) diazene (Azo4 & Azo5)

Azo4 & Azo4 were synthesized using N-chlorosuccinimide (NCS) and 1,8-Diazabicyclo[5.4.0]undec-7-ene (DBU). 94 1 mmol of the respective aniline was dissolved in 15 mL of DCM. 2 mmol of DBU was added and the reaction was stir for 10 min. The reaction was then cooled to -78°C and the 2 mmol of NCS was added and stirred for 30 min. The reaction was then quenched with saturated sodium bicarbonate. The solution was diluted with DCM then sequentially washed with 1 M HCl, water, dried over magnesium sulphate and evaporated. The crude material was purified through column chromatography (Hexanes/Methanol). 1 H NMR (CDCl₃, 500 MHz) of Azo4 δ 7.98 (m, 4H), 4.62 (s, 4H) HRMS-ESI: m/z = 315.0754 (calcd: 315.0756). 1 H NMR (CDCl₃, 500 MHz) of Azo5 δ 4.75 (s) HRMS-ESI: m/z = 387.0367 (calcd: 387.0379)

2.1.2 Solid-Phase DNA Synthesis

Automated solid-phase DNA synthesis was carried out using a MerMade 6 oligonucleotide synthesizer from Bioautomation. Once synthesized, the strands were immersion in ammonium hydroxide and heated at 60°C overnight to deprotect the bases and cleave the strands from the solid support. The solutions were subsequently evaporated and re-dissolved in water. The strands with azobenzene on the 5' end were then purified through high-performance liquid chromatography using an Agilent Infinity 1260. Strands with azobenzene in the interior were purified through gel-electrophoresis. The strands were

quantified using a NanoDrop Lite Spectrometer (Thermo Scientific). Target structures were confirmed through LC-MS. A full list of synthesized strands is shown in Table 2.1.

Table 2.1. List of the synthesized DNA strands.

Sample	Sequence (5'-3')
PolyA ₅ AzoA ₅	AAAAA-Azo-AAAAA
PolyA7AzoA7	AAAAAAA-Azo-AAAAAAA
PolyA ₉ Azo	Azo-AAAAAAAA
PolyA ₁₄ Azo	Azo-AAAAAAAAAAAA
PolyA ₁₄ Azo ₂	Azo-Azo-AAAAAAAAAAAAA
AzoPolyA ₁₄ Azo	Azo-AAAAAAAAAAAAAAAA

2.1.3 Fibre Formation

A solution was made containing 20 uM of DNA, 10 mM of cyanuric acid and 12.5 mM Tris-acetic acid buffer (pH = 6) with magnesium (TAMg). Specifically, a 20 mM cyanuric in 25 mM TAMg buffer was added to a 40 uM solution of the purified DNA sample in equal parts. Note that above 18 mM concentration cyanuric acid typically crashes out of solution due to its low solubility in water. As such, the solution was heated and sonicated prior to the DNA addition to ensure the total solubility. The samples were then annealed using an Eppendorf Master Cycler Thermocycler by heating at 90°C for 3 min,

followed by cooling to 5°C, at a rate of 0.5°C/min. After this point, it was critical to keep the samples in the dark to ensure no photo-isomerization had taken place. This was achieved by either running the samples immediately, or storing them in tinfoil in a dark and cold environment.

2.2 Spectroscopy

2.2.1 UV-Vis & Kinetic Experiments

All UV-Vis measurements were completed with an Agilent Cary 300 UV-Vis spectrometer. Concentrations were kept similar to yield an absorbance of <1. For the isomerization experiments, samples were irradiated with a 10 Watt 365 nm or 523nm LED light, for 5-10 min. The length of time depended on when a photostationary state was obtained, as confirmed by a constant UV-Vis spectrum. Measuring the absorption of the azobenzene at its λ_{max} over the necessary timeframe was then used to observe the thermal relaxation process. For azo1, sampling was conducted every 30 minutes. For the orthohalogenated compounds, sampling was conducted every hour.

2.2.2 Pump-Probe Spectroscopy

The exact optical setup is presented in Figure 2.1. Samples were first loaded into a 1 mm square cuvette. *Trans-cis* photochemical isomerization was induced in the samples by irradiating them with a 100 mW·cm⁻² laser operating at 375 nm. A pump cycle of 0.5 seconds was used: long enough to ensure a photo-stationary state, however, short enough

to inhibit heating of the sample. This was controlled with an optical shutter. The absorption of the samples was constantly monitored using a 455 nm light line from a Melles Griot Argon laser. This laser was first passed through a $\frac{1}{4}$ λ filter, an optical chopper and a variable neutral density to improve the signal-to-noise ratio and ensure the probe light was not isomerizing the sample. The $\frac{1}{4}$ λ filter acts to circularly polarize the light, as polarized light has been noted to align azos throughout isomerization cycles. The optical chopper operated at 1415 Hz. A broadband filter (425 – 465 nm) was also placed in front of the photodiode to filter background light. All data was collected using a Standford Research Systems SR830 lock-in amplifier, which was connected to the optical chopper. As the two were paired to the same frequency, this is how the signal-to-noise ratio was increase.

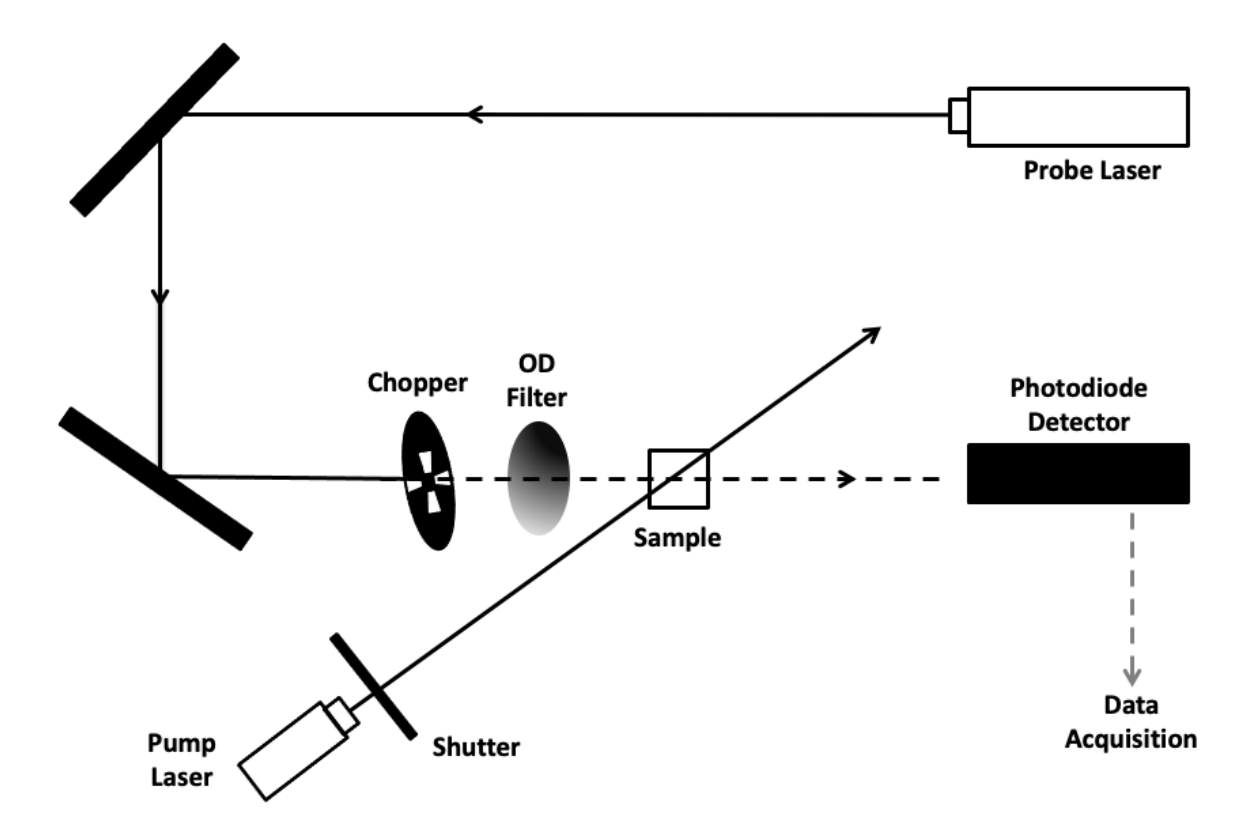


Figure 2.1. Optical setup used for the pump-probe spectroscopy experiments.

2.2.3 Circular Dichroism & Melting Temperature Analysis

All circular dichroism (CD) measurements were done on Jasco J-815 spectropolarimeter equipped with either a Xe (200 nm) or D₂ (230 nm) lamp. For isothermal spectra, scans were conducted from 400 nm to 200 nm using a Xe lamp. Thermal denaturation was simultaneously monitored by CD & UV-Vis by monitoring the samples at 252 nm (D2) while heating at a rate of 2°C/min. Samples were taken straight from the annealing chamber to avoid exposure to light and thermal denaturation.

2.2.4 Atomic Force Microscopy

Samples were prepared in a cold room (6°C) by depositing 5 uL of the annealed fibres onto mica. The samples were left for 30 seconds to deposit and then subsequently dried with filter paper (wicking method). This enabled the removal of some of the solvent while maintaining the structures of the samples. The samples were then air dried for 1 minute at room temperature and immediately transferred to a desiccator to dry overnight. The samples were analyzed the next day using a Multimode scanning probe microscope and Nanoscope IIIa controller (Digital Instruments) using ScanAsyst mode. An initial rough scan of 25 um x 25 um was done for all samples then focused in based on those results. All images were acquired in the tapping mode with silicon probes.

2.3 Computational Methods

All molecular computations were performed using the Guassian16 software package using Compute Canada's high performance cluster. Computations were run in parallel on nodes with 64 central processing units. In all cases, initial geometries of the ground state structure of each derivative were first obtained. The UV-Vis spectra were then analyzed by employing a TD-DFT method, also using the Gaussian16 package.

2.3.1 Optimized Ground State Structures

All structures were optimized using time-independent density functional theory (DFT). Initial structures were drawn in using the Avogadro software package and preliminarily optimized using the universal force field (UFF) package. This served as a good means to reduce the computational time by providing a rough estimate of the initial geometries. Molecular structures were then optimized in the gas phase with Gaussian16 using either a CAM-B3LYP/6311+G (2d,p) or PBE0/cc-pvtz level of theory. In some cases, it was beneficial to first optimize the structures with a more minimalistic basis set, for example cc-dvtz. This helped minimize the total computational time as later calculations with larger basis sets were expedited. In all cases the molecules were initially optimized in the gas phase. Once a reasonable structure was obtained through this method the molecules were further optimized with the incorporation of a solvent model. A reasonable structure was classified as a molecule with similar bond angles as reported in previous literature. In particular, special attention was paid to the angles θ and ϕ , as these are of particular interest with regards to the isomerization process. However, a more

quantitative method was to perform a vibrational analysis on the proposed molecules. By confirming the absence of any negative vibrational energies, the molecules could be confirmed as a minimum. For these studies the polarized continuum model (PCM) was used to replicate the effect of water. As mentioned previously, this is an implicit model that neglects any solute-solvent interactions however can replicate the bulk effects of the solvent. Vibrational analyses were also conducted on the solvated molecules to ensure the structure was a minimum. To gain insight into the thermal relaxation processes the transition structures of the *cis*-to-*trans* isomerization was also analyzed. Again, this was done with the Gaussian 16 package using a reaction coordinate scanning-based method.

2.3.2 Simulated UV-Vis Spectra

Electronic transitions were evaluated with time dependent density functional theory (TD-DFT) with single point calculations up to three transitions. For some initial studies single point calculations were conducted for up to 25 transitions to obtain a more exact simulated spectra of the corresponding molecules. However, as the π - π * and n- π * transitions were the first two transitions calculated, they were deemed sufficient for the purpose of this study. Indeed, the frequency factor of the transitions dropped significantly after the first two transitions, indicating that excitations not associated with the π - π * and n- π * transitions were improbable in an experimental setting. Depending on how the structure was optimized, either the CAM-B3LYP or PBE0 functional was used in the TD-DFT calculations. In a similar vein, the corresponding basis set used for the geometry optimization was also used for the TD-DFT calculations. However, an initial screening was performed on the parent compound (Azo1) to determine the effect of different basis sets.

From these results, the CAM-B3LYP/6311+G (2d,p) and PBE0/cc-pvtz level of theory in water using a PCM water model were deemed the most appropriate. This is because these two functional/basis set combinations offered accurate results with minimal computation time. As such, these methods were then applied to the other azobenzene derivatives synthesized: molecules were optimized with the CAM-B3LYP/6311+G (2d,p) and PBE0/cc-pvtz, and then the TD-DFT calculations were done with the same functional/basis set.

2.3.3 Transition State Structures

Initial transitions state predictions were obtained via an intrinsic reaction coordinate approach. Molecules were initially scanned over the -N=N-C- moiety to give a rough approximation of the energy landscape with respect to inversion or rotation. In particular, two scanning angles were used: the dihedral angle involving the C-N=N-C atoms to analyze the rotational freedom (referred to as ϕ) and the bond angle involving the C-N=N atoms for the inversion (θ). For ϕ , five scan steps of 25° were used to fully cover the rotation of the cis derivative to trans derivative. Similarly, for θ , four scan steps of 10° were conducted to cover the inversion mechanism. In the scan method presented in Gaussian16, structures are analyzed for each permutation available for the given variables. Thus, in this scenario, the energies of 20 (5x4) different conformational isomers were analyzed for each derivative. From these, the higher energy molecules were then used in a QST3 method to obtain accurate transition structures. In this method three structures are proposed, the initial starting molecule (here the cis isomer), the final molecule (the trans isomer) and a proposed transition structure molecule. As such, the higher energy molecules obtained through the

initially scanning process served as adequate guess for the transition state structures. Note that some higher energy conformations were not always successful and lead to inconclusive computational results. However, for each derivative there existed at least one adequate structure, which lead to conclusive results. For both the scan and QS3T process, all structures were calculated using the DFT method at the CAM-B3LYP/6311+G (2d,p) level of theory. Therefore, in the QST3 method the same level of theory was used for computing all three structures – the *cis* isomer, the *trans* isomer and the transition state structure – thus, the energies of the structures could be easily compared. Using this data, a theoretical activation energy could be extrapolated from the results by using the energy of the *cis* isomer and the energy of the proposed transition state structure.

2.4 Results & Discussion

2.4.1 Synthesis of Water Soluble Azobenzenes

The structures of the synthesized azobenzenes, along with their respective overall synthetic yields, are shown in Figure 2.2. Azos were designed to incorporate hydroxyl groups to increase their water solubility. Thus, Azo1 served as a parent compound for this study. We then envisioned other target structures that incorporate electron-donating, electron-withdrawing, & ortho halogenation to further study these effects on the photodynamics of the molecule. As shown, the azos presented cover all the various types of azobenzene molecules discussed early, except "push-pull" types. Specifically: Azo1 is an "azobenzene" type molecule, Azo2 & Azo3 are "amino-azobenzenes" and Azo4 and Azo5 are "ortho-substituted azobenzenes". "Push-pull" azos were not included, as the hypothesized fast isomerization rates would deem them unsuitable for this experimental setup.

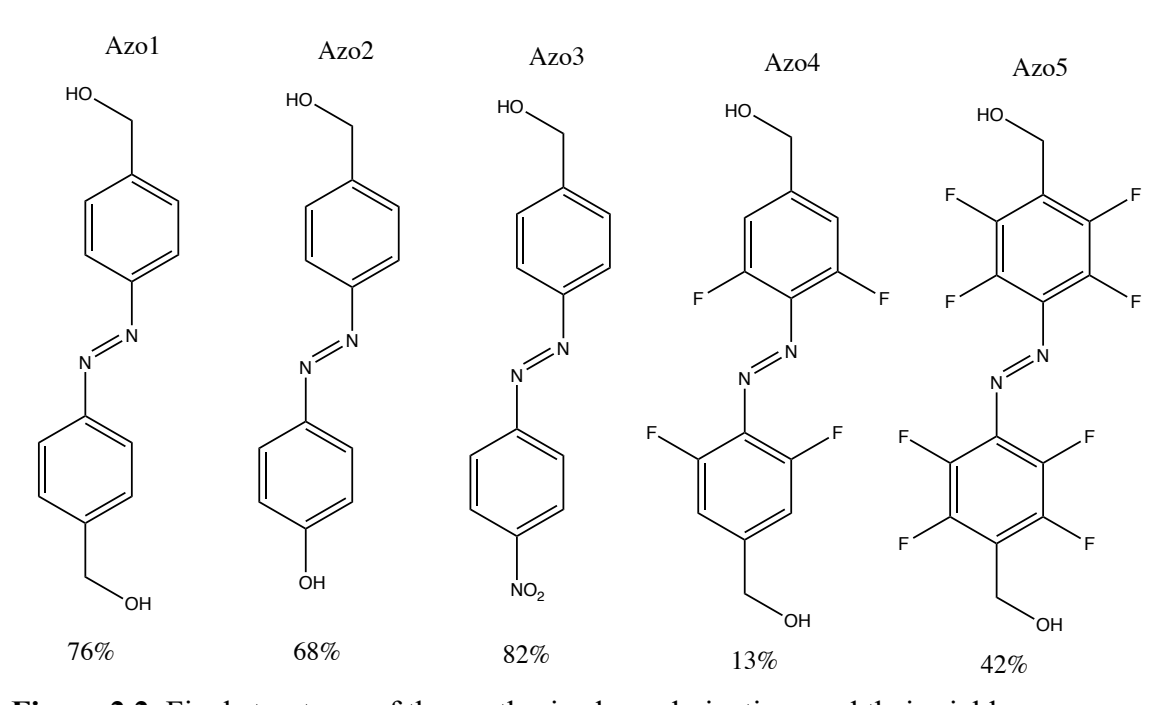


Figure 2.2. Final structures of the synthesized azo derivatives and their yields.

While Azo1-3 all have acceptable yields, the lower yields of Azo4-5 decrease their applicability. Furthermore, Azo1-3 can be acquired through single-step synthesizes, whereas Azo4-5 require multiple synthetic procedures. It has been noted that the introduction of halogens into the ortho position of azobenzene can be synthetically challenging, however, synthetic methods are continuously being developed to address this issue.94 In particular, coupling of ortho-halogenated amines to form the N=N azo bond remains a significant challenge. Nevertheless, authors are continuously developing strategies to overcome this obstacle, such as selectively halogenating azobenzene derivatives in the *ortho* positions in the final synthetic step. 92 As such, methods that further decrease the number of synthetic procedures or the costs associated with the required reagents will consequently increase the viability for these azo derivatives. As will be shown later, this is of the upmost importance as these azos also typically display the most viable characteristics for applications geared towards biological systems. Should they become less synthetically demanding, they will no doubt rise as suitable candidates for these systems.

2.4.2 Effect of Substituents on Photo-dynamics

The UV-Vis spectra of the azos in water and THF are shown in Figure 2.3-2.5. Specifically, these figures display a comparison of the synthesized azo derivatives UV-Vis spectra in water and DMSO. For clarity, the parent compound, amino type, and *ortho* substituted azos are each plotted in their own figure; Figure 2.3, Figure 2.4, and Figure 2.5, respectively.

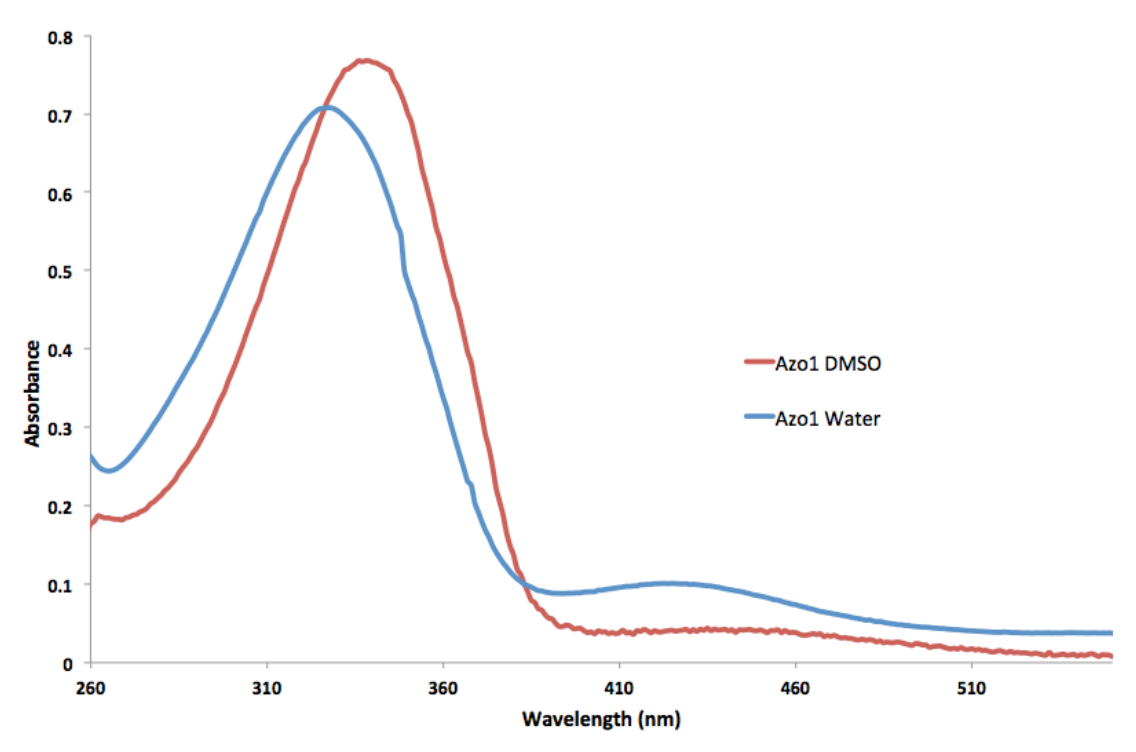


Figure 2.3. UV-Vis spectra of the parent compound (Azo1) in DMSO (red) and water (blue). Here, the samples are assumed to be composed predominately of the *trans* isomer.

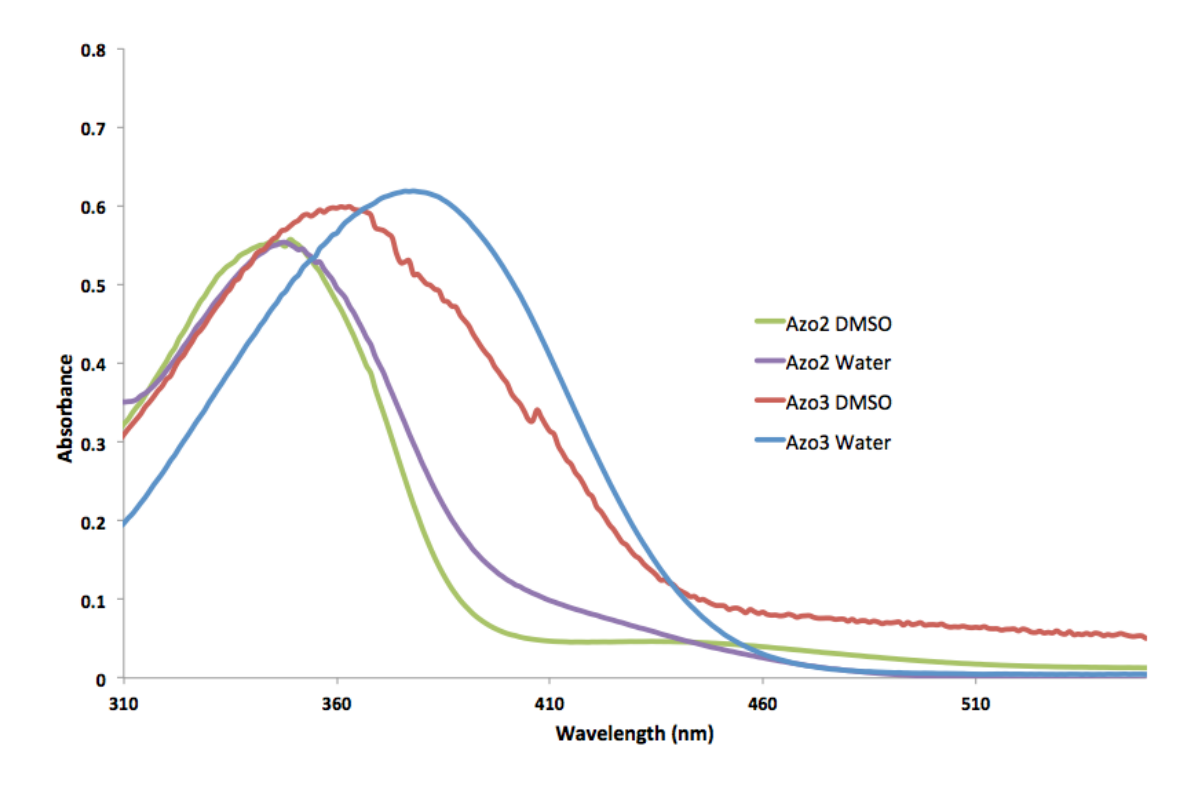


Figure 2.4. UV-Vis spectra of the amino-type derivatives (Azo2-3) in DMSO and water. Here, the samples are assumed to be composed predominately of the *trans* isomer.

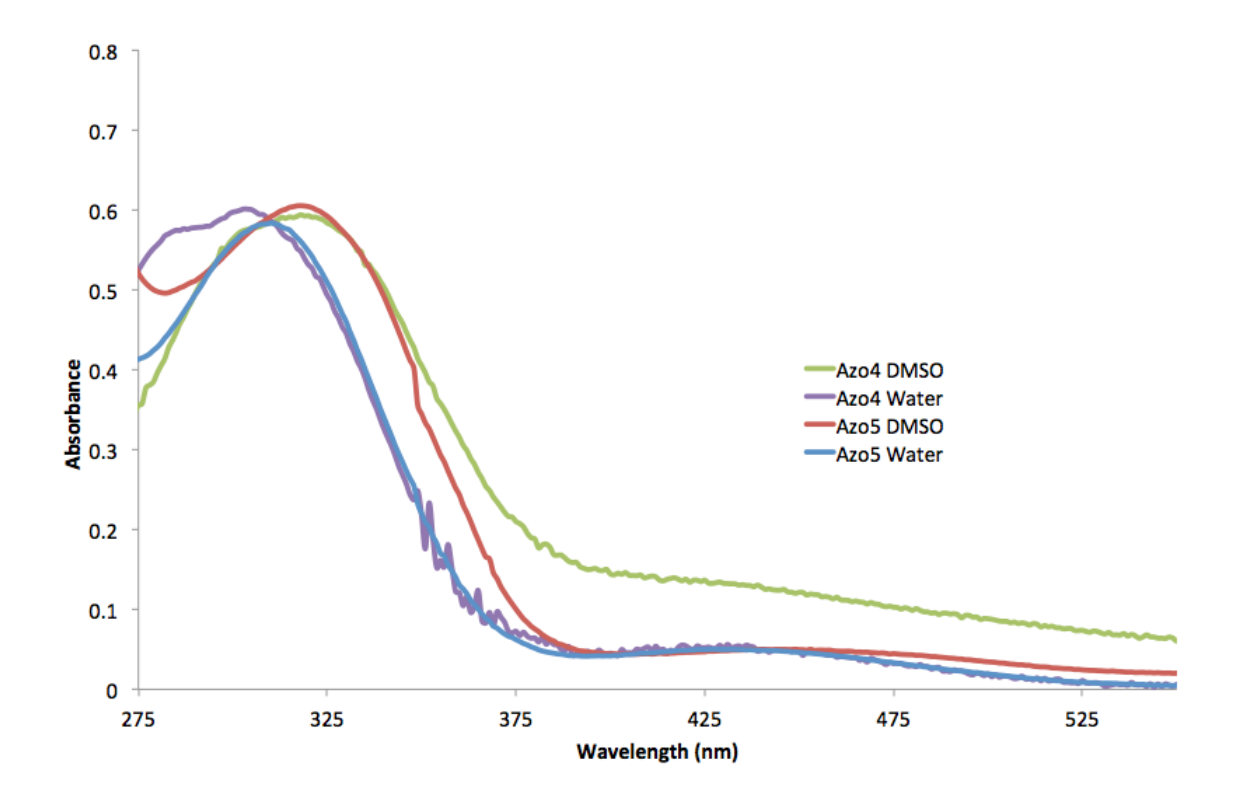


Figure 2.5. UV-Vis spectra of the *ortho*-substituted derivatives (Azo4-5) in DMSO and water. Here, the sample is assumed to be composed predominately of the *trans* isomer.

Notably, two distinct differences in the absorption spectra can typically be observed when the azos are dissolved in water: a shift of the π - π * transitions and, for some azos, a significant increase in intensity of the n- π * transition. The shift of the excitation energy for the π - π * transition can be attributed to an increase in the polarity of the solvent, which further increases the dielectric constant. The change could also be potentially linked to solvent-solute interactions, such as hydrogen bonding between the water and lone pairs of the nitrogen atoms. As a hydrogen belone pairs would increase the energy gap between the energy states and thus require a higher excitation energy, as observed with Azol and Azo4-5. Interestingly, this shift is not observed in the amino-type azos. Instead, the excitation energy for the π - π * transition stays constant (Azo2) or is red-shifted (Azo3). It

is possible that the strong electron withdrawing character of the nitro group in Azo3 may be more influential in the polar aprotic solvent, leading to a better stability of the lone pair electrons. The increase in the $n-\pi^*$ transition can most notably be observed in Azo1. As shown, in water Azo1 shows a clear peak at about 420 nm that is indicative of the $n-\pi^*$ transition; however, this peak is barely visible when the sample is measured in DMSO. This change could most likely be due to a decrease of symmetry when the molecule is dissolved in water, as the hydrogen bonding promotes a more asymmetrical dipolar structure. This would indeed increase the intensity of the transition as dictated by Laporte selection rules.³⁵

The typical photo-isomerization behaviour of the azos is shown in Figure 2.6 and Figure 2.7. The parent azo compound is shown in Figure 2.6 and an *ortho* substituted azo (azo5) is show in Figure 2.7. Upon irradiation with 365 or 523 nm light the π - π * transition blueshifts and its intensity decreases. For Azo1, the n- π * transition remains isoenergetic and the intensity of the transition increases. Whereas for the fluorinated azos, the n- π * is blueshifted, which can be attributed to the increased steric clash between lone pair electrons and *ortho* fluorine groups, as discussed previously. Indeed, these spectroscopic changes are indicative of the *cis* configuration in solution. Indeed, these spectroscopic changes to-*cis* photo-isomerization process for these azos is quite similar to what is observed in other organic solvents. Furthermore, the photo-dynamics associated with the *trans*-to-*cis* isomerization process remains constant in aqueous media.

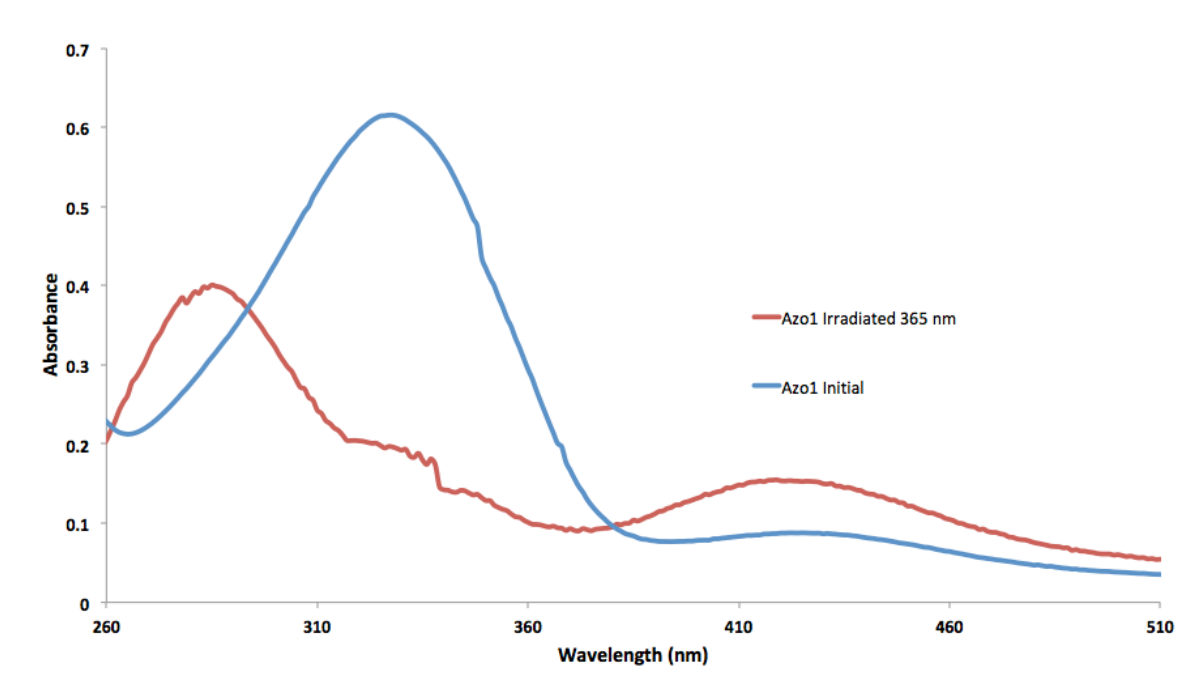


Figure 2.6. Photo-isomerization of azo1 in distilled water after irradiation for 2 minutes with 365 nm light. In blue is shown the initial azobenzene, composed predominately of the *trans* isomer. Upon irradiated the π - π * peak at ~323 nm decreases and shifts to ~285 nm, indicative of the *cis* isomer, as shown in red. Furthermore, the *n*- π * transition associated with the peak at ~425 nm also increases, as expected with the *cis* isomer.

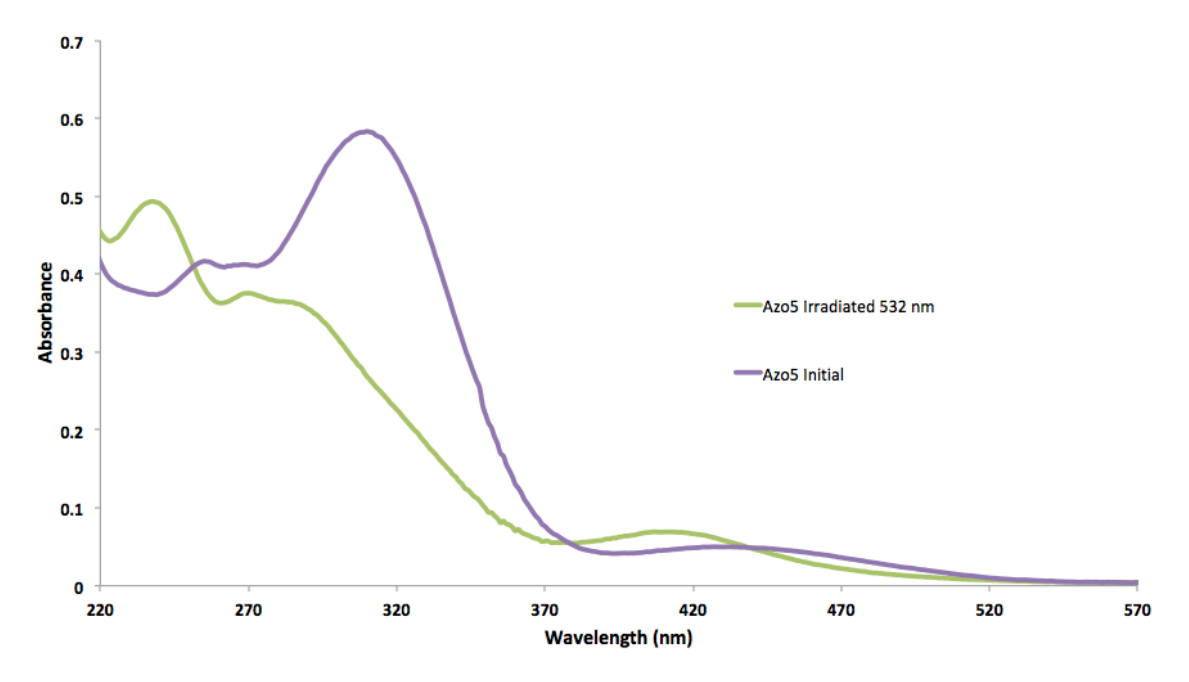


Figure 2.7. Photo-isomerization of azo5 in distilled water after irradiation for 10 minutes with 532 nm light. The initial *trans* azo is shown in purple. Upon irradiation, the intensity of the π - π * peak at ~318 decreases and the n- π * at ~435 nm increases. Both peaks also shift to new wavelengths indicative of the *cis* isomer, shown in green.

After irradiation, the azos can be monitored over time to observe the thermally induced *cis*-to-*trans* isomerization. Figure 2.8 shows this process. For Azos2-3 irradiation with 365 nm light yields no difference to the UV-Vis spectra in aqueous media. However, the isomerization process can be observed in organic solvents, such as in DCM (Figure 2.8). It can be deduced that the *cis*-to-*trans* isomerization is too fast to observe *via* UV-Vis spectroscopy, as expected for these amino-azobenzenes. ⁹⁶ Pump-probe spectroscopy was therefore used to analyze these samples. The typical results acquired from these experiments are shown in Figure 2.9.

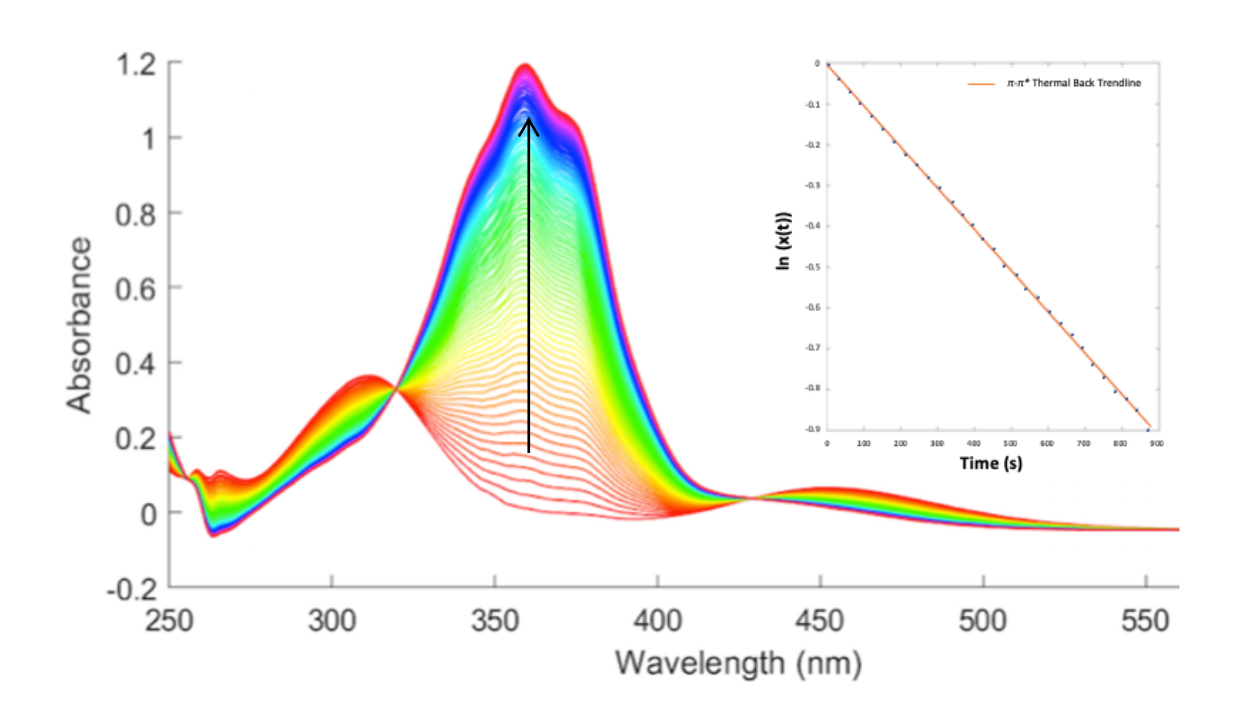


Figure 2.8. Typical thermal relaxation of *cis* azobenzene monitored by UV-Vis and the extrapolation of the change in absorption when fit to first order kinetics (inset). The irradiated sample is shown in red and is composed predominately of the *cis* isomer. Over time the sample relaxes back to the *trans* isomer (pink) as shown by the arrow. This specific data is from Azo2 in DCM.

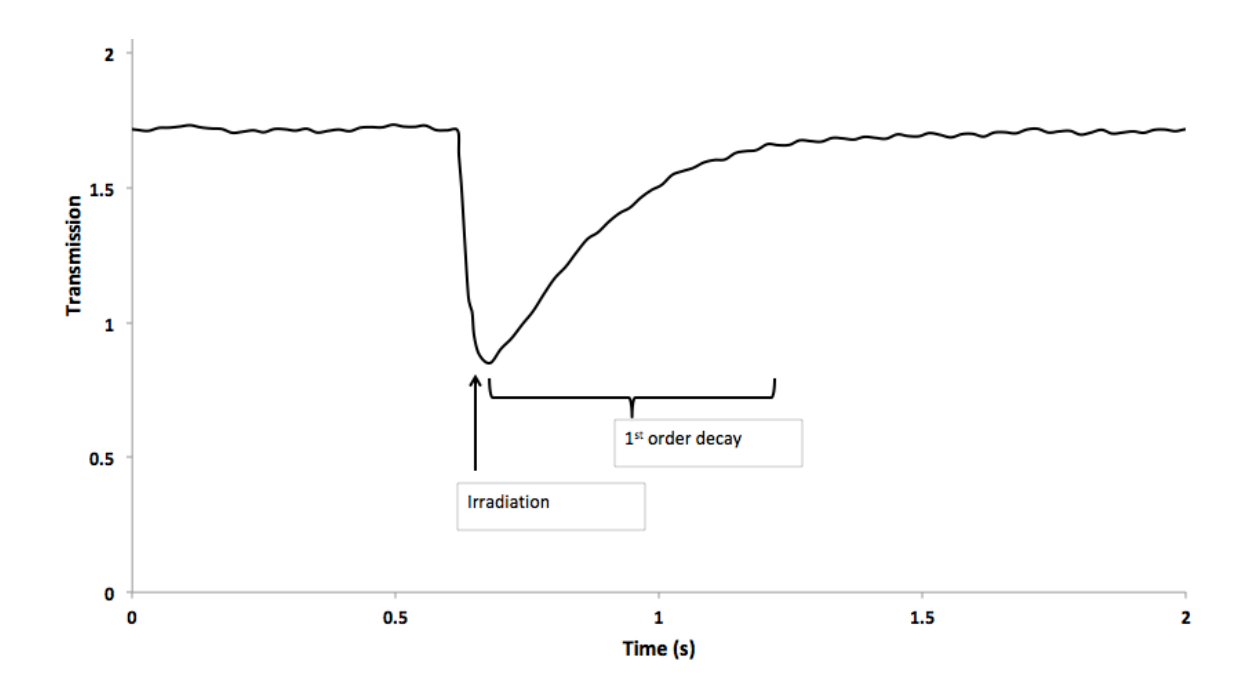


Figure 2.9. Typical data acquired from pump-probe spectroscopy. Irradiation at ~ 0.6 seconds induces a decrease in the transmission at 455 nm due to the *tran*-to-*cis* isomerization. Transmission subsequently returns to the initial state following 1st order kinetics. Note: Transmission raw data show are shown; kinetic analysis used Absorbance.

With both techniques, the absorption (or transmission) of the sample decays exponentially overtime, indicative of 1st order kinetics. The following 1st kinetic equations can then used to determine the half-life of the *cis* isomer:

$$x(t) = \frac{A_{trans} - A(t)}{A_{trans} - A_{cis}}$$

$$ln\left(x(t)\right) = x_o - kt \tag{2}$$

Where A(t), A_{trans} , and A_{cis} , are the measured absorbance of a mix of *trans* and *cis*, absorbance of the pure *trans* isomer, and the absorbance of the *cis* isomer, respectively. Thus, x(t) represents the normalized percentage of the *cis* isomer in solution. Following first order kinetics, a plot of $\ln(x(t))$ vs time should yield a linear line with a slope equal to

the reaction constant, k.⁹⁷ Such a plot is shown in the inset in Figure 2.8. These calculations are analogous to those used for pump-probe experiments; however, in those cases transmission was used opposed to absorbance. Once the reaction constant is calculated the half-life of the cis isomer can be determined through the following equation:

$$\tau_{1/2} = \frac{\ln\left(2\right)}{k} \tag{3}$$

By repeating these experiments at different temperatures, the thermodynamics associated with the thermal relaxation process can be acquired. Specifically, the rate determination of rate constants at different temperatures can be fit to the following equation:

$$\ln k = \ln A - \frac{E_a}{RT} \tag{4}$$

Thus, an Arrhenius plot of $\ln k$ vs 1/T yields a linear line with a slope equal to the activation energy, Ea, over the gas constant, R, and a y-intercept equal to natural log of the pre-exponential factor, A. This was done with for the azobenzenes monitored via UV-Vis and the results are shown below in Figure 2.10.

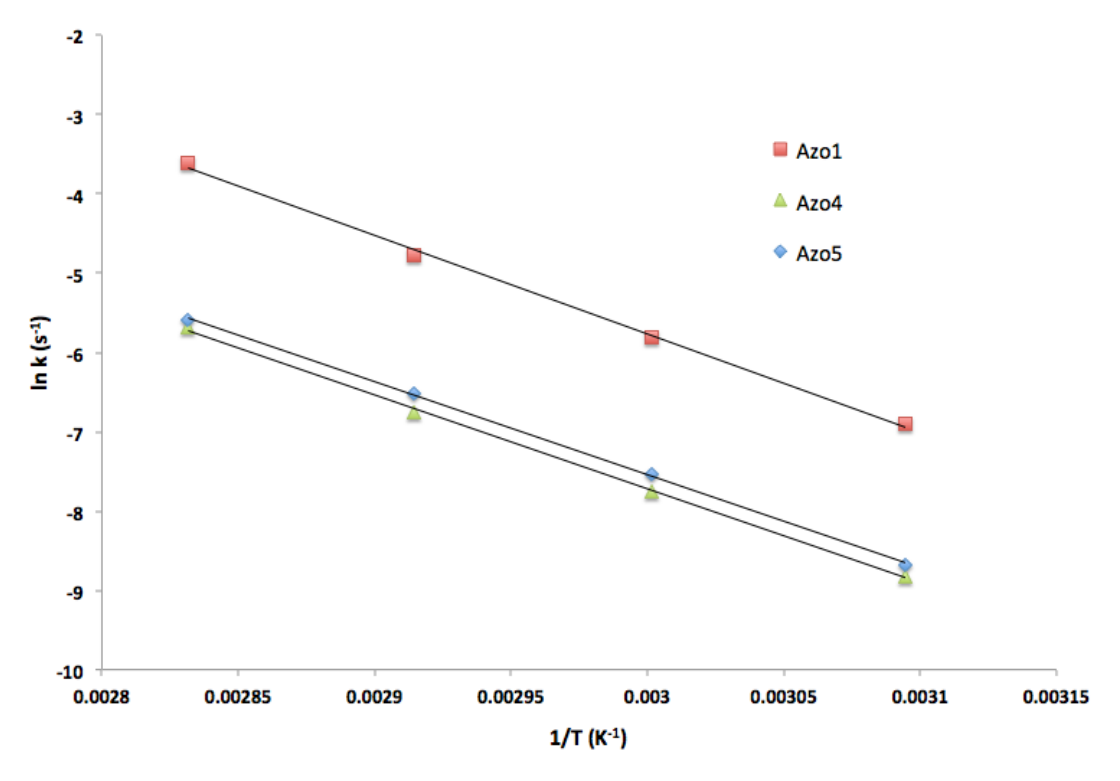


Figure 2.10. Arrhenius plots obtained for the thermal isomerization process for the azos monitored through UV-Vis. Plots yield a slope equal to $-E_a/R$ and y-intercept equal to $\ln A$, as per equation 4).

The key findings from the aforementioned *cis* thermal isomerization experiments are summarized in Table 2.2. Here, the computed values from the experimental spectroscopy methods are presented. For the azos with slower thermal relaxation processes (Azo1, Azo4, and Azo5) the thermodynamics and half-life associated with the *cis*-to-*trans* isomerization is presented. For the azos with faster isomerization processes, only the computed half-lives from pump-probe experiments are listed.

Table 2.2. Experimental thermodynamics & kinetics of the thermal *cis*-to-*trans* relaxation for the azo derivatives in water.

Sample	E _a (kJ)	A	τ _{1/2} at 25°C
Azo1	96.9	1.42E+13	3.21 days
Azo2	NA	NA	0.45 seconds
Azo3	NA	NA	0.34 seconds
Azo4	98.5	1.04E+12	57.85 days
Azo5	97.6	1.22E+12	72.13 days

Contrary to the *trans*-to-*cis* photo-isomerization process, the *cis*-to-*trans* isomerization is highly solvent dependent. Specifically, Azo2 and Azo3 show a challengingly short half-life of the *cis* isomer on the millisecond timescale. Other authors have associated these short half-lives to the stabilization of a planar dipolar transition state, ⁹⁸ however, interestingly when comparing the fluorinated azos to the parent compound the activation energy for the thermal relaxation process is quite similar, however, the pre-exponential factor changes significantly. This suggests that the transition states for these process is the same and the differences in the kinetics can be attributed to the solvent-solute interactions. ⁹⁷ One possible theory is the influence of hydrogen bonding with the nitrogen lone pairs of the azo. ⁴³ This could therefore be another mechanism contributing to the decreased half-life of the *cis* isomers for azo2-3: the presence of electron-donating or withdrawing groups could help facilitate this interaction and lead to a further decrease of the observed half-life.

2.4.3 Rationalization of Substituent Effects through Computations

To validate the use of this level of theory for the computations, different models were tested to evaluate their efficiency at predicting the π - π * transition of the parent compound in water. As mentioned previously, the CAM-B3LYP and PBE0 functionals are the most prominent theories used in the literature. Figures 2.11 and 2.12 show the accuracy of these theories at predicting the π - π * excitation wavelength when different basis sets are used.

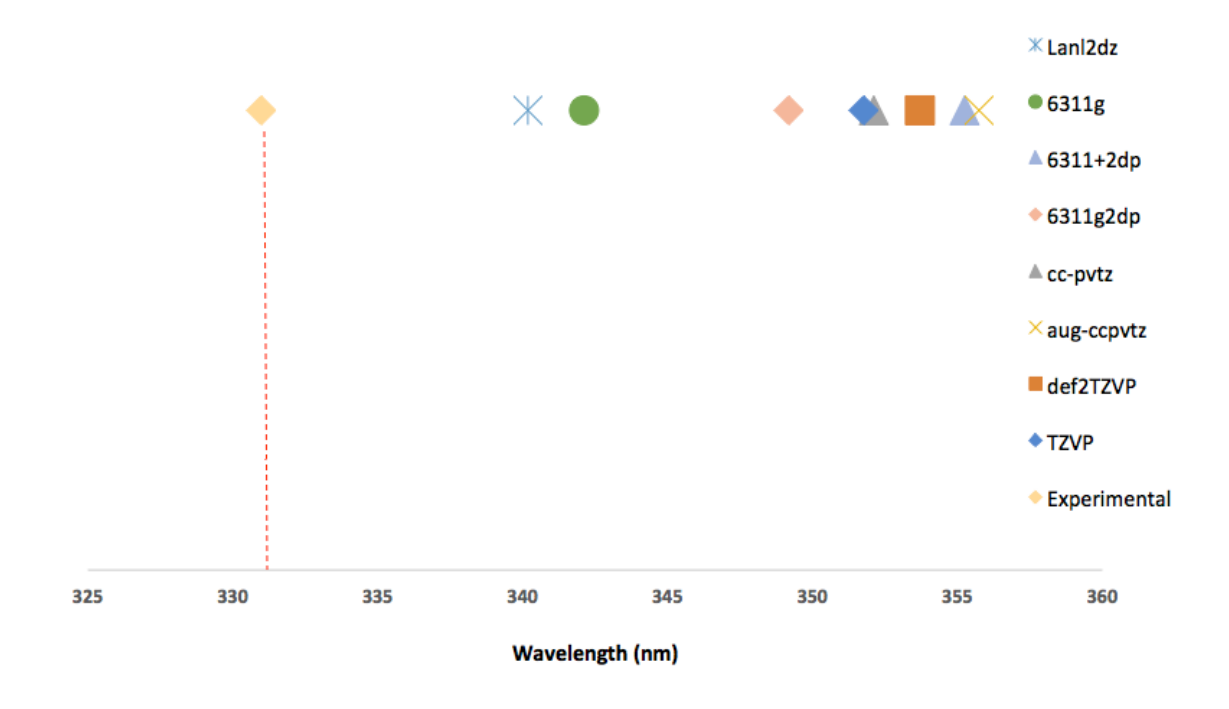


Figure 2.11. The effect of the basis set on predicting the π - π * transition in water using the PBE0 functional with a PCM model. Here, the error can be up to 20 nm. Despite this, the PBE0 functional with a cc-pvtz basis set was used in future work as a comparison.

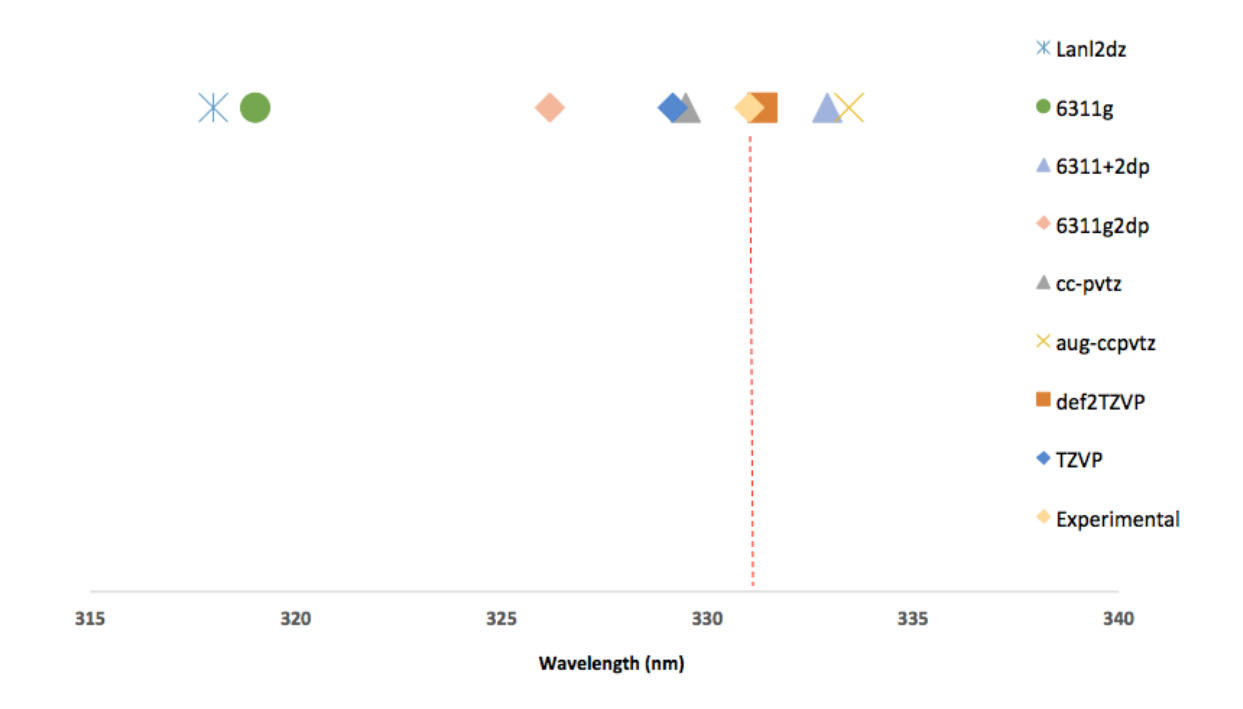


Figure 2.12. The effect of the basis set on predicting the π - π * transition in water using the CAM-B3LYP functional with a PCM model. Based on these results, the CAM-B3LYP functional with a 63311+(2d,p) was used in future work.

As shown, the PBE0 functional drastically underestimates the energy required to induce the π - π * transition. Although the PBE0/cc-PVTZ model has previously been used to predict these transitions in the literatures, here it is shown that this level of theory can be off by as much as 20 nm when working in aqueous media. ¹⁰⁰ Contrarily, the CAM-B3LYP functional behaves quite well regardless of the basis set used. One interesting note is that the trend is the exact same regardless of the functional. In other words, when working with the PBE0 functional similar results are obtained however with an increased error. This indicated that the CAM-B3LYP functional is superior for these systems. To minimize the computational time and correlate the results with previous work, the triple zeta 6311+(2d,p) basis set was used for the rest of the azos and future computations.

Figure 2.13 displays the breadth of optimized structures obtained using DFT. While all the *cis* isomers display similar geometric conformations, the *trans* isomers of the fluorinated azos differ from that of the other azos.

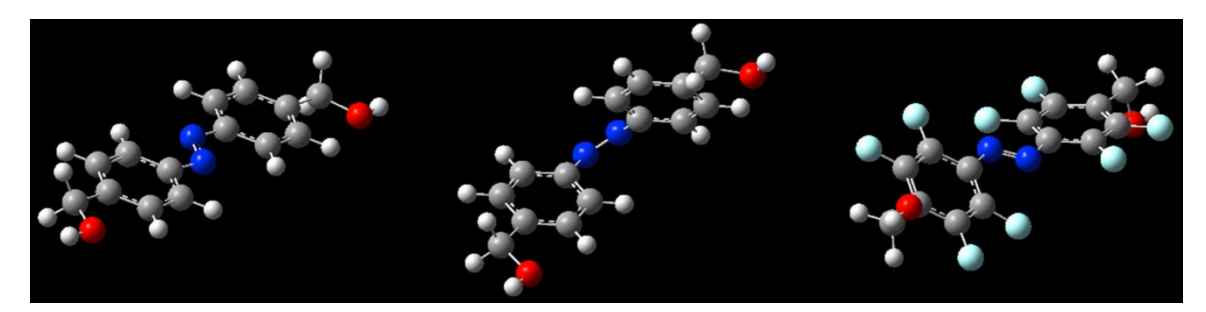


Figure 2.13. Typical optimized structures acquire using the CAM-B3LYP/6311+(2d,p) level of theory, showing the parent (Azo1) *trans* (left) & *cis* (middle) isomer and a fluorinated *trans* isomer (right).

Unlike Azo1-3, Azo4-5 trans isomers display a non-planar conformation that can be attributed to the steric clash between the *ortho*-substituted fluorines. These findings correlate with the observed UV-Vis spectra, as the decrease in the symmetry of the molecule would promote the n- π * as dictated by Laporte Selection Rules. This is observed in the UV-Vis spectra of these azos as the intensity of the peak associated with the n- π * transition is almost equivalent in both the *trans* and *cis* conformation. Whereas for Azo1, the intensity of the n- π * transition significantly increases when in the *cis* conformation.

Table 2.3 shows the computed n- π^* and π - π^* transition wavelengths and the experimentally observed values. As shown, the calculated π - π^* transition for the *trans* isomer is very close to what was observed experimentally (within 5 nm). Indeed, with regards to this transition, the CAM-B3LYP/6311+(2d,p) PCM model properly accommodates the substituent effects of the all the azobenzenes tested. Contrarily, the energy of the n- π^* is typically underestimated in this model. This can most likely be attributed to the fact that an implicit solvent model was used and thus neglects the

influences of specific solvent-solute interactions, such as hydrogen bonding. This is especially problematic for the fluorinated azos as this parameter is crucial for isomerizing the azos with visible light. In order to increase the viability of these molecules for biomedical devices they must use lower energy light, therefore, methods to more accurately predict this transition energy would be highly beneficial. Furthermore, the estimated transition energies associated with the cis isomer can also be improved. Again, this is crucial for the fluorinated azos as the separation of the n- π * transition of the *cis* and *trans* isomer is a fundamental requisite for obtaining a high percentage of the cis isomer when photo-isomerizing with green light. Interestingly, an idea of the UV-Vis spectra associated with cis Azo2 and Azo3 in aqueous media can also be obtained. However, as these systems could not be observed experimentally, the validity of the results cannot be confirmed. Nevertheless, the accuracy of the model with the other cis molecules supports these findings. For consistency, the transitions were also evaluated at the PBE/cc-pvtz level of theory, as this has been previously been used by other authors in organic solvents. However, here it is clearly demonstrated that the CAM-B3LYP/6311+(2d,p) is more appropriate for predicting these samples transition energies than the PBE/cc-pvtz method, especially with regards to the *trans* excitations (Table 2.3 & Table 2.4).

Table 2.3. Computed excitation energies for the *trans* isomer using the CAM-B3LYP/6311+(2d,p) & PBE0/cc-pvtz methods.

Derivative	Experimental π -π* & n-π*	Calculated (CAM-B3LYP)	Calculated (PBE0)
Azo1	331 & 419	332 & 440	352 & 469
Azo2	346 & NA	342 & 433	365 & 499
Azo3	380 & NA	387 & 508	402 & 515
Azo4	317 & 439	321 & 463	365 & 512
Azo5	311 & 443	309 & 476	356 & 509

Table 2.4. Computed excitation energies for the *cis* isomer using the CAM-B3LYP/6311+(2d,p) & PBE0/cc-pvtz methods.

Derivative	Experimental π - π * & n- π *	Calculated (CAM-B3LYP)	Calculated (PBE0)
Azo1	285 & 423	271 & 458	305 & 474
Azo2	NA	289 & 456	308 & 472
Azo3	NA	305 & 456	345 & 479
Azo4	374 & 421	289 & 451	317 & 465
Azo5	368 & 417	296 & 432	349 & 443

As shown in Table 2.3, the CAM-B3LYP/6311+(2d,p) method is superior in predicting both the π - π * and n- π * transitions for the *trans* isomer. Although the method is better at predicting the π - π * transition, the accuracy of the n- π * transition wavelength is still superior to that of the PBE0 method. With regards to predicting the *cis* excitation energies, both methods are less accurate. However, the CAM-B3LYP/6311+(2d,p) method does reasonably well at predicting the n- π * transition energies for the *ortho*-substituted azos. For these derivatives this excitation energy is of more important, as this directly affects the *cis:trans* ratio in solution upon irradiation.²³ Thus, the fact that the CAM-B3LYP/6311+(2d,p) method predicts this accurately is valuable, even if it comes at the cost of inaccurately predicting the π - π * transition.

To further elucidate the substantial acceleration of the thermal isomerization the potential energy surface about the nitrogen-nitrogen double bond was evaluated and from this optimized transition states were determined (Figure 2.14). This roughly approximates the change in energy when the bond is rotated and/or inverted.³⁷ It has been noted that the thermal isomerization of azobenzene can proceed through an inversion, rotation, or concerted rotation and inversion mechanism.⁴¹ From these energy landscapes it can be hypothesized that a concerted mechanism is the favourable pathway when working in aqueous media. Furthermore, Table 2.5 shows the activation energy associated with the transition state structures with regards to this pathway. As shown, the activation energy follows the trend displayed by the measured experimental half-lives. However, it should be noted that these computed values disregard the pre-exponential factor and therefore cannot accurately predict the thermal half-life to a reasonable degree. However, these

values do shed light on the trends associated with substituents when working in aqueous media.

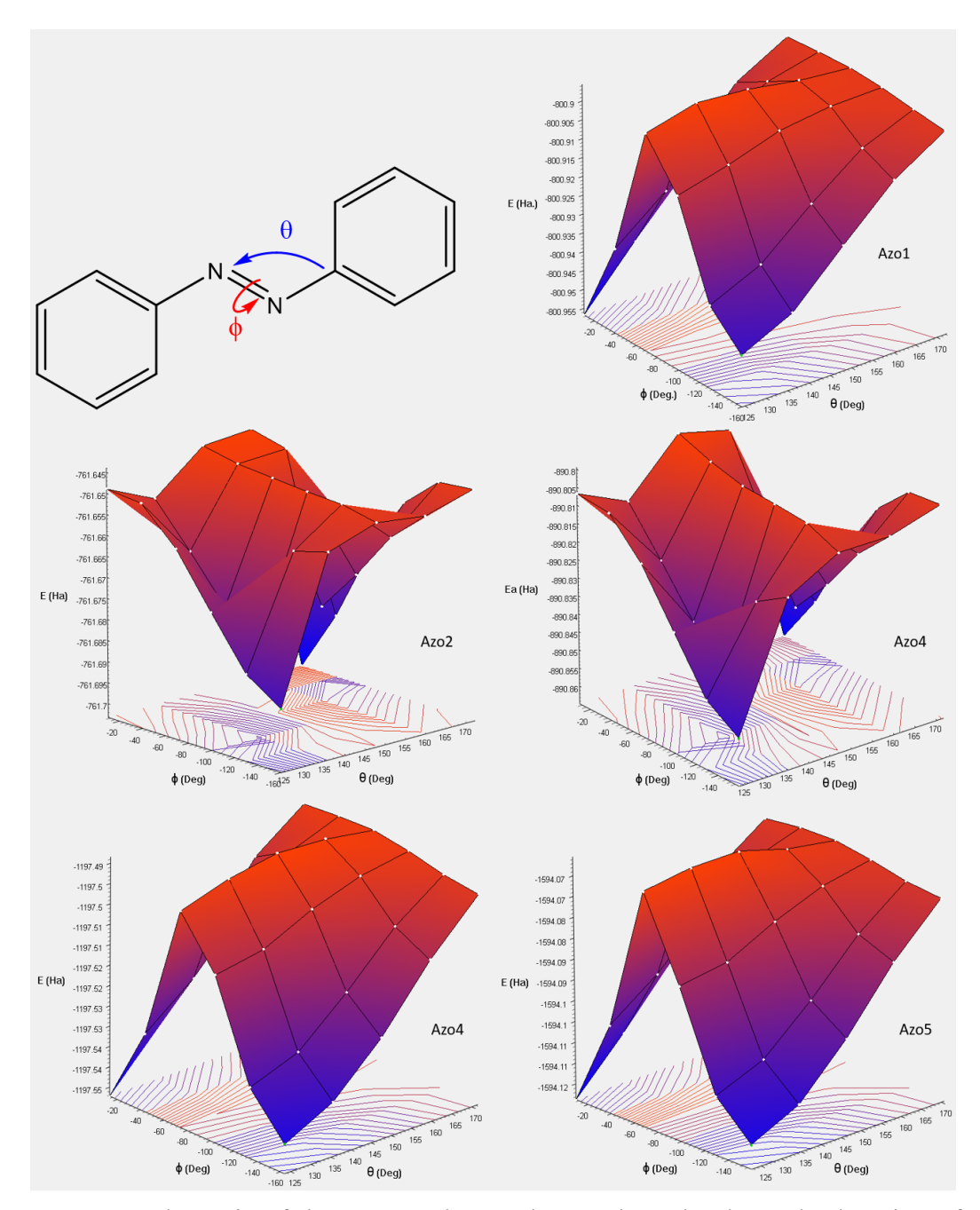


Figure 2.14. Schematic of the scan angles used to analyze the thermal relaxation of *cis* azobenzene (top left) and the energy landscapes obtained from the scans. These images provide rough ideas of the energy cost associated with conformational changes of the molecule. Following the y (ϕ) & x-axes (θ) yield the energy changes associated with the rotation and inversion pathways, respectively. A concerted pathway would be any path between the two.

Table 2.5. Computed activation energies using the QST3 method compared to experimental results.

Sample	Experiment E _a (kJ)	τ _{1/2} at 25°C	Calculated E _a (kJ)
Azo1	96.9	3.21 days	109.8
Azo2	NA	0.45 seconds	106.4
Azo3	NA	0.34 seconds	104.7
Azo4	98.5	57.85 days	114.3
Azo5	97.6	72.13 days	112.7

From the experimental and computational findings the azo derivatives can be grouped into two categories: fast and slow switches. The amino-type azos (Azo2 and Azo3) display significantly fast kinetics, and are affected by aqueous solvents. For this reason they would be appropriate for applications that require fast photo-switches, such as optoelectronics. However, in these applications other previously proposed derivatives would probably be more preferable.²⁴ More interesting are the slow switches: Azo1, Azo4, and Azo5. Here it can be noted that the aqueous solvent does not affect the isomerization process of azobenzene-type or *ortho*-fluorinated azos. These azos display sufficiently slow kinetics such that binary systems can be obtained. This is ideal for biological applications that must transfer smoothly between two states. This provides a rational basis for authors to design azo derivatives for aqueous systems moving forward.

2.4.4 Self-Assembly of Azo-PolyA Systems

The strands synthesized can be crudely characterized into two groups: fibre forming and fibre non-forming. The typical CD results for these strands when annealing with cyanuric acid are shown in Figure 2.15. As shown in blue, two distinct peaks at 212 nm and 252 nm can characterize the fibre forming strands. Contrarily, the unassembled strands have no peak at 212 nm; however, surprisingly, show a fairly strong band at 252 nm.

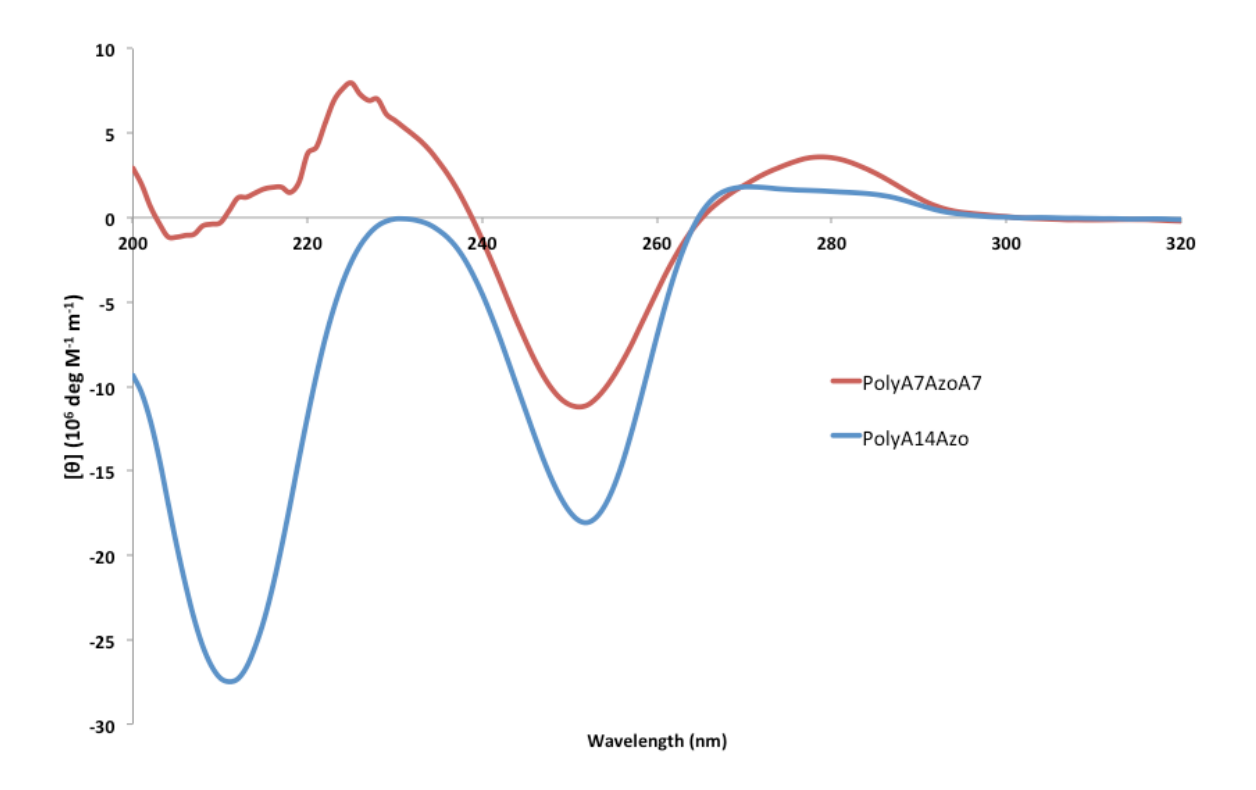


Figure 2.15. Typical CD spectrum acquired with the formed fibres (blue) and when the fibres do not form (red). The strong negative peaks at 252 nm & 212 are indicative of the chiral fibres.

Upon heating a sigmoidal curve can be obtained while monitoring the CD reading at 252 nm (Figure 2.16). This is indicative of a phase transition and can be attributed to the disassembly of the fibres.¹ Interestingly, the polyA strand with azobenzene on the 3' and 5' end undergoes two phase transitions when heated (Figure 2.16). Although the nature of

these transitions is unclear, such transitions have also been observed in other polyAcyanuric acid systems.¹ It is hypothesized that the AzoPolyA₁₄Azo system obtains a unique morphology at cooler temperatures. Specifically, the azo motifs in the 5' and 3' position can stabilize a phase between 5 to 20°C. After which, the sample transitions to a state similar to the other samples, that eventually melts ~35°C. This hypothesis will be further supported by the AFM images presented later.

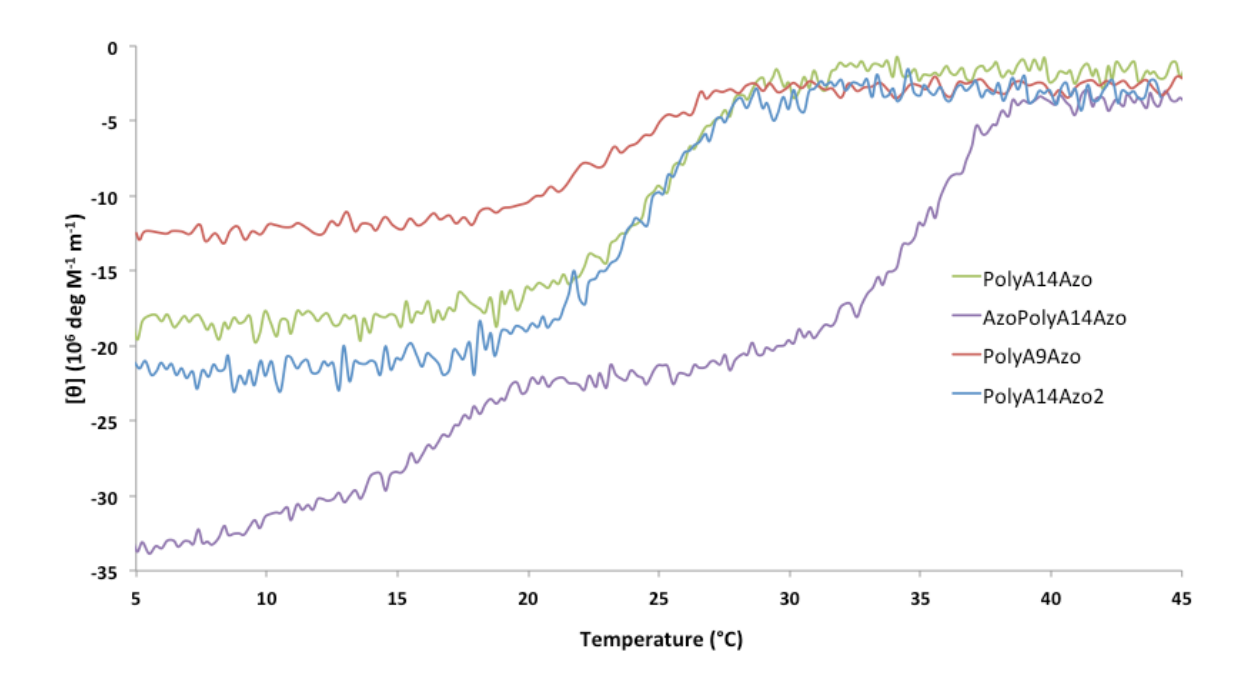


Figure 2.16. Melting curves of the DNA-azo fibres. The majority of strands displayed a single asymptotic curve indicative of one phase transition. However, the AzopolyA₁₄Azo strand displays two (purple).

Table 2.6 summarizes the results acquired from these experiments while classifying the strands synthesized. Interestingly, the placement of azobenzene into the interior of the strand seems to inhibit the fibre formation. Indeed, both strands with this design are unable to form fibres. However, the introduction of azobenzene into the exterior of the strand seems to stabilize the fibres. In particular, the melting temperature associated with polyA₉Azo is much higher than polyA₁₀ strands without the azobenzene (~5 °C).¹ This

can most likely be attributed to the intercalation of the azo between the adenine and cyanuric acid motifs as it has been demonstrated that intercalating molecules can stabilize DNA duplexes. 101,102

Table 2.6. Classification of the synthesized strands and their melting temperatures.

Sample	Sequence (5'-3')	Fibre Forming	T _m (°C)
PolyA ₅ AzoA ₅	AAAAA-Azo-AAAAA	No	NA
PolyA ₇ AzoA ₇	AAAAAAA-Azo-AAAAAAA	No	NA
PolyA ₉ Azo	Azo-AAAAAAAA	Yes	24.5
PolyA ₁₄ Azo	Azo-AAAAAAAAAAAAAA	Yes	23.9
PolyA ₁₄ Azo ₂	Azo-Azo-AAAAAAAAAAAAAA	Yes	24.2
AzoPolyA ₁₄ Azo	Azo-AAAAAAAAAAAAAAAA	Yes	13.3 & 35.4

These phase transitions can be better rationalized through AFM, as shown in Figure 2.17. As shown, the strands with azobenzene on the 5' end all show a similar morphology of intertwined fibres. While the height of each sample remains approximately constant, the morphologies do display slight differences. Notably, the AzoPolyA14Azo sample tends to have a shorter persistence length and does not appear to form networks as easily. On the other hand, the other samples all appear to have a high degree of crosslinking between strands. This indicates that the azo moiety could be inhibiting the elongation of the rosettes.

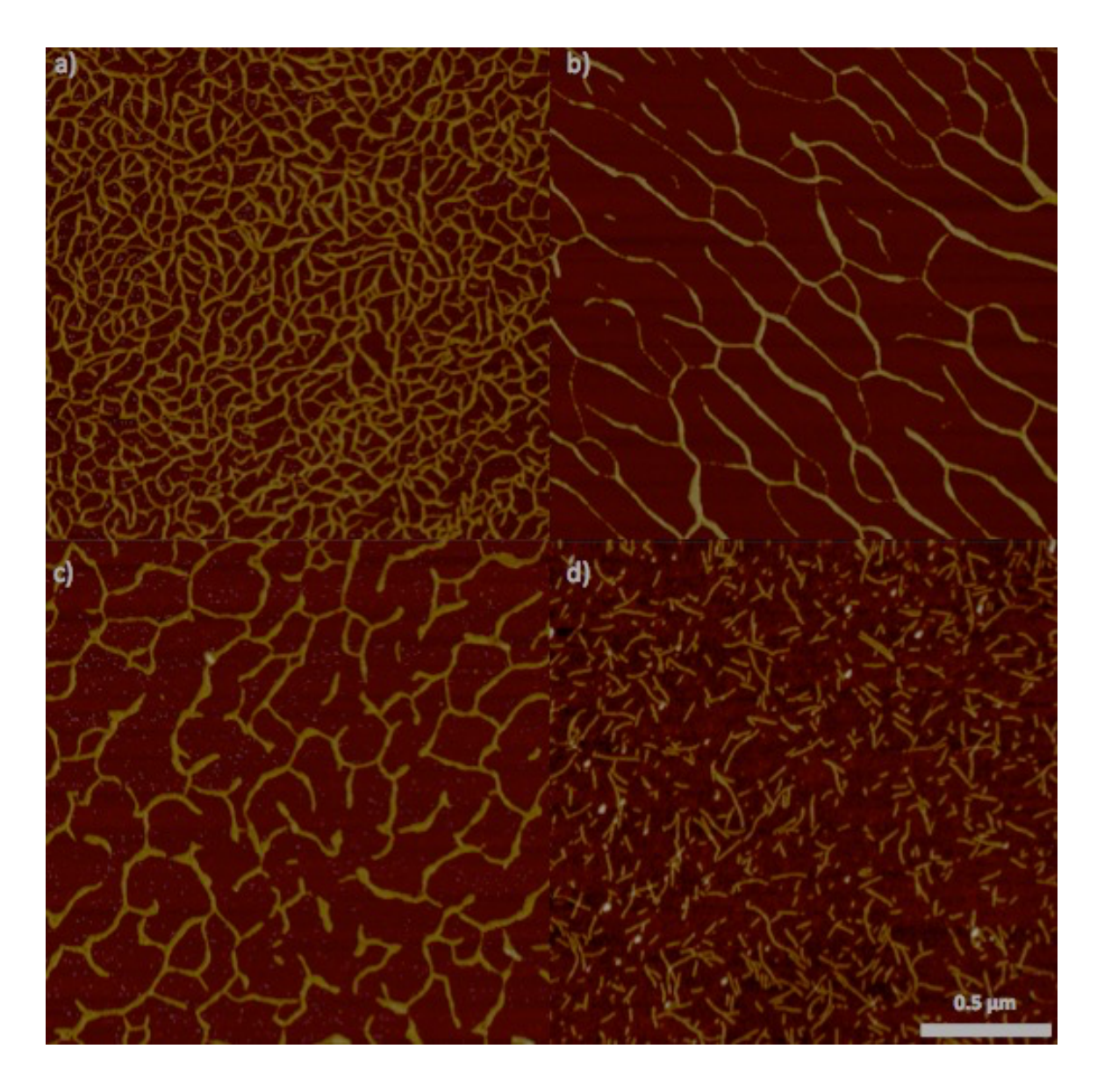


Figure 2.17. AFM images of the fibre forming Azo-DNA strands: (a) PolyA₉Azo (b) PolyA₁₄Azo (c) PolyA₁₄Azo₂ & (d) AzoPolyA₁₄Azo.

In accordance with the CD results, AFM images of strands with azobenzene in the middle of the strand were inconclusive and did not display any larger aggregates. To further elucidate the phase transitions observed in these samples, it would be beneficial to obtain AFM images at various temperatures.

Chapter 3: Conclusions & Future Work

3.1 Summary

A variety of water-soluble azobenzenes have been synthesized to further analyze the photo-isomerization process in water. In particular, three main types of azos were synthesized: azos with mild electron influencing groups (azobenzene type), strong electron influencing (amino-azos), and the relatively new ortho-halogenated azos. In these compounds it was evident that the photo-isomerization in water varied significantly for the amino-azobenzene type derivatives. Similar to "push-pull" azos, it was demonstrated here that these azo derivatives have a highly accelerated thermal relaxation process and, additionally, tend to have subtle changes in the absorbance spectra when solvated in water. To observe the photo-isomerization process for these azos more advanced non-linear optical techniques (pump-probe spectroscopy) were needed. Through pump-probe spectroscopy, the half-lives of these derivatives were able to be quantified in water and proved to be significantly faster than in organic solvents. This deems these types of azobenzenes more suitable for applications where fast processing is necessary, and inadequate for applications that require dual functionality based on photo-isomerization. Contrarily, the other azo derivatives were unaffected when introduced into water. The characteristics of the photo-isomerization tend to be similar to that of polar organic solvents, however, there were changes in their UV-Vis spectra. In particular, there was a large red-shift associated with the absorption spectra. Of these, the ortho-fluorinated derivatives displayed particularly promising behaviour, especially with regards to biological applications. This is due to the fact that wavelength of light required to induce

the *trans*-to-*cis* isomerization is quite high and that the *cis* isomer displays a high thermal stability. The lower energy wavelengths required improves the viability for subdermal applications as longer wavelengths typically display better penetration properties. Additionally, the high thermal stability displayed by these derivatives would also enable materials that can act as binary systems, which exist in either the *trans* or *cis* state. However, their relatively low synthetic yield currently hinders their applicability. The two *ortho*-substituted derivatives synthesized in this study were particularly demanding with regards to their synthesis, and therefore, decreased their viability for further studies.

To provide further insight into these experimental findings *ab initio* computational methods were used to analyze these photochromes. First, the geometries of the azo derivatives were optimized for the *trans* and *cis* isomer, to give an idea of the conformational changes that may be occurring the aqueous media. Further transition state calculations also provided insight into the relative activation energies that may be necessary to induce the thermal *cis*-to-*trans* isomerization in water. By scanning the potential conformational isomers that may be occurring in solution, potential transition state structures could be proposed. Then, by implementing the QST3 method theoretical transition state structures could be obtained which could be quantitatively compared to the *cis* and *trans* isomer. This ultimately helped to rationalize the large differences in the half-lives observed between the synthesized derivatives. Furthermore, these studies provide insight on methods to better predict the photodynamics of azobenzene derivatives in water. Specifically, the CAM-B3LYP/6311+G (2d,p) level of theory proved to be more accurate at predicting the excitation energies of these derivatives than the PBEO/cc-pvtz. This aids

in the notion that this functional and basis set should be the preferred theory when analyzing azobenzene derivatives in aqueous systems.

Lastly, based on the promising photo-isomerization characteristics of Azol, this derivative was integrated into a pre-existing supramolecular DNA polymer system. By inserting the azobenzene motif into different positions on the polyA strand, its effect on the self-assembly process was analyzed. Interestingly, it was observed that placing the azo in the middle of the polyA strand inhibited the formation of fibres. However, when placed on the exterior of the strand (on the 5' or 3' end), the fibres were able to form as usual. In fact, the stability of these fibres where typically enhanced when compared to the azo free counterparts. However, for the most part, differences in the placement or quantity of azo motifs in these regions did not significantly alter the fibre morphology, as observed by AFM. The one exception was the situation where the azo motif was placed on the 5' and 3' end of the DNA. In this case, shorter fibres were observed by AFM and the sample appeared to undergo two phase changes when heating from 5°C to 45°C. These findings can be rationalized by the hypothesis that the azo motif is intercalating between adenine base pairs. It is believed that these intercalating units would increase the thermal stability of the fibres, while simultaneously offering opportunities for different aggregation pathways.

3.2 Future Work

Based on the presented work there are still many unanswered questions and opportunities to extend promising work. As noted previously, one of the main types of azobenzene, "push-pull" azobenzenes, were not analyzed in this study, due to the fact that they are hypothesized to possess extremely fast kinetics in water. It would therefore be interesting to extend this work to this class of azos, albeit another optical setup may be necessary. Nevertheless, once quantitative experimental results are obtained the computational methods conducted in this work could also be applied to these systems. In a similar vein, accelerating the *cis*-to-*trans* isomerization rate of the amino-azos through thermal heating would also be very interesting. By analyzing the rate of these azos at different temperatures quantitative values for the thermodynamics of this process, such as the activation energy, could be determined and further verify through computational results. This would aid in the development of novel azos with optimal photodynamics in water.

Of the azos studied the *ortho*-fluorinated derivatives displayed the most intriguing properties for biological systems. However, it should be noted that while classed as "*ortho*-halogenated" azos, these azos could secondarily be classed as "azobenzene-type" azos, due to the fact that they lack strongly influencing substituent groups in the *para* position. For this reason, it would be extremely interesting to apply this study to the isomerization process of other *ortho*-halogenated azobenzenes. For example, *ortho*-fluorinated azos with a strong electron donating or withdrawing group in the *para* position. As noted in this study, these amino-type azobenzenes display a significantly accelerated thermal isomerization when solvated in aqueous systems. However, the *ortho*-halogenation of

azobenzene leads to longer half-lives of the *cis* isomer. As such, in the case of *ortho*-halogenated amino azobenzenes the thermal relaxation may be retarded due to the increased stability of the *cis* isomer afforded by the *ortho* fluorine groups. This could further elucidate the impact of water on the isomerization process as the kinetics of these amino-type azos could be monitored through linear spectroscopic techniques at varying temperatures. Thus, the thermodynamics associated with the reaction could be determined experimentally, a factor that was missing in the preceding work.

By coupling this work again with computational results, a platform can be developed to optimally predict the photodynamics of azo derivatives completely through *in-silico* methods. If used in the same manner as the work presented here, the experimental activation energy of the azos couple be verified by DFT calculations. Through these results, insight into the differences in the mechanism of the thermal relaxation and the energy landscape of each isomer and derivative could be obtained. In a similar vein, TD-DFT calculations could also be conducted as means to accurately predict the required excitation wavelength to induce the isomerization process. Furthermore, as the field of computational chemistry develops there are rising techniques that may be beneficial to further analyze this study and future work. For example, recent work in the field of quantum mechanics/molecular mechanics (QM/MM) has proven to be a successful method to explain the exact mechanism underlying the azobenzene photo-isomerization. 95 With these methods, the exact mechanism of the trans-to-cis or cis-to-trans isomerization can be obtained. Monitoring how a molecule adapts when perturbed by an external energy on the picosecond timescale allows researchers to build reliable movies that display isomerization process. Therefore, applying these methods to aqueous systems could present a promising opportunity to better predict the characteristics of these systems. In particular, how these derivatives are affected by the local environment will have a large impact on further applications. It may be noted that each system is unique in its isomerization process, due to the subtle changes in the local environment.

Lastly, the results acquired from integrating azobenzene into the polyA-cyanuric acid systems were still in the preliminary stages and could be extended further to better understand the system. Firstly, it would be important to conduct experiments to better rationalize the impact of azobenzene on the self-assembly process. Obtaining AFM images of the samples when they are prepared at different temperatures could do this. Furthermore, quantifying the size of the fibres through methods such as dynamic light scattering (DLS) would also provide further insight into the final structures obtained. This technique also has the added advantage that it can be conducted at various temperatures. Once properly analyzed the optimal placement of the azo benzene and ratio of polyA:azo could be determined to have the most significant impact.

Another key aspect to the azo-DNA system presented is that all the samples had a predominately large portion of the *trans* isomer and very little of the *cis*. Indeed, due to the annealing process and the careful procedures to keep the samples in the dark, the percentage of the trans isomer is estimated to be higher than 95%. Interestingly, preliminary studies to isomerize the sample proved unsuccessful, however, this may be due to inadequate irradiation times or insufficient light intensity. The acidity of the system and counter-ions in solution may also be effecting the isomerization. Regardless, how the isomerization process would impact the stability and morphology of the samples is highly intriguing. Further studies to quantify the quantum efficiency of these systems would be

the preliminary steps to move forward in this work. Once the isomerization process is verified, the fibres can be analyzed by the same techniques that were presented in this work.

References

- Avakyan, N. *et al.* Reprogramming the assembly of unmodified DNA with a small molecule. *Nature Chemistry* **8**, 368-376, doi:10.1038/nchem.2451 (2016).
- 2 Pérez-Rigueiro, J., Viney, C., Llorca, J. & Elices, M. Silkworm silk as an engineering material. *Journal of Applied Polymer Science* **70**, 2439-2447, doi:10.1002/(sici)1097-4628(19981219)70:12<2439::Aid-app16>3.0.Co;2-j (1998).
- Deming, T. J. Mussel byssus and biomolecular materials. *Current Opinion in Chemical Biology* **3**, 100-105, doi: https://doi.org/10.1016/S1367-5931(99)80018-0 (1999).
- Berda, E. B., Deravi, L. F., Foster, E. J., Simon, Y. & Thuo, M. M. Virtual Issue: Next-Generation Smart Materials. *Macromolecules* **52**, 6339-6341, doi:10.1021/acs.macromol.9b01402 (2019).
- Tang, J. D., Mura, C. & Lampe, K. J. Stimuli-Responsive, Pentapeptide, Nanofiber Hydrogel for Tissue Engineering. *Journal of the American Chemical Society* **141**, 4886-4899, doi:10.1021/jacs.8b13363 (2019).
- 6 Chen, L.-J. & Yang, H.-B. Construction of Stimuli-Responsive Functional Materials via Hierarchical Self-Assembly Involving Coordination Interactions. *Accounts of Chemical Research* **51**, 2699-2710, doi:10.1021/acs.accounts.8b00317 (2018).
- Warner, P. T. A. J. C. *Green chemistry : theory and practice.* 30 (Oxford University Press, 1998).
- 8 Horváth, I. T. Introduction: Sustainable Chemistry. *Chemical Reviews* **118**, 369-371, doi:10.1021/acs.chemrev.7b00721 (2018).
- 9 Hastings, C. J. in *Handbook of Green Chemistry* 139-168 (2018).
- Szymański, W., Beierle, J. M., Kistemaker, H. A. V., Velema, W. A. & Feringa, B. L. Reversible Photocontrol of Biological Systems by the Incorporation of Molecular Photoswitches. *Chemical Reviews* **113**, 6114-6178, doi:10.1021/cr300179f (2013).
- Hatai, J., Hirschhäuser, C., Niemeyer, J. & Schmuck, C. Multi-Stimuli-Responsive Supramolecular Polymers Based on Noncovalent and Dynamic Covalent Bonds. *ACS Applied Materials & Interfaces* **12**, 2107-2115, doi:10.1021/acsami.9b19279 (2020).

- Raposo, M., Ferreira, Q., Timóteo, A. R. M., Ribeiro, P. A. & Rego, A. M. B. d. Contribution of counterions and degree of ionization for birefringence creation and relaxation kinetics parameters of PAH/PAZO films. *Journal of Applied Physics* **118**, 114504, doi:10.1063/1.4930802 (2015).
- Mahimwalla, Z. *et al.* Azobenzene photomechanics: prospects and potential applications. *Polymer Bulletin* **69**, 967-1006, doi:10.1007/s00289-012-0792-0 (2012).
- Bandara, H. M. D. & Burdette, S. C. Photoisomerization in different classes of azobenzene. *Chemical Society Reviews* **41**, 1809-1825, doi:10.1039/C1CS15179G (2012).
- Schultz, T. *et al.* Mechanism and Dynamics of Azobenzene Photoisomerization. *Journal of the American Chemical Society* **125**, 8098-8099, doi:10.1021/ja021363x (2003).
- Dunn, N. J., Humphries, W. H., Offenbacher, A. R., King, T. L. & Gray, J. A. pH-Dependent cis → trans Isomerization Rates for Azobenzene Dyes in Aqueous Solution. *The Journal of Physical Chemistry A* **113**, 13144-13151, doi:10.1021/jp903102u (2009).
- 17 Schulte-Frohlinde, D. ÜBER DEN MECHANISMUS DER KATALYTISCHEN cis → trans-UMLAGERUNG VON AZOBENZOL. *Justus Liebigs Annalen der Chemie* **612**, 131-138, doi:10.1002/jlac.19586120114 (1958).
- Sanchez, A. M., Barra, M. & de Rossi, R. H. On the Mechanism of the Acid/Base-Catalyzed Thermal Cis-Trans Isomerization of Methyl Orange. *The Journal of Organic Chemistry* **64**, 1604-1609, doi:10.1021/jo982069j (1999).
- Beharry, A. A. & Woolley, G. A. Azobenzene photoswitches for biomolecules. *Chemical Society Reviews* **40**, 4422-4437, doi:10.1039/C1CS15023E (2011).
- Bléger, D., Schwarz, J., Brouwer, A. M. & Hecht, S. o-Fluoroazobenzenes as Readily Synthesized Photoswitches Offering Nearly Quantitative Two-Way Isomerization with Visible Light. *Journal of the American Chemical Society* **134**, 20597-20600, doi:10.1021/ja310323y (2012).
- Bushuyev, O. S., Tomberg, A., Friščić, T. & Barrett, C. J. Shaping Crystals with Light: Crystal-to-Crystal Isomerization and Photomechanical Effect in Fluorinated Azobenzenes. *Journal of the American Chemical Society* **135**, 12556-12559, doi:10.1021/ja4063019 (2013).
- Konrad, D. B. *et al.* Computational Design and Synthesis of a Deeply Red-Shifted and Bistable Azobenzene. *Journal of the American Chemical Society* **142**, 6538-6547, doi:10.1021/jacs.9b10430 (2020).

- Sadovski, O., Beharry, A. A., Zhang, F. & Woolley, G. A. Spectral tuning of azobenzene photoswitches for biological applications. *Angew Chem Int Ed Engl* **48**, 1484-1486, doi:10.1002/anie.200805013 (2009).
- Garcia-Amorós, J. *et al.* Picosecond Switchable Azo Dyes. *Chemistry A European Journal* **25**, 7726-7732, doi:10.1002/chem.201900796 (2019).
- Sanchez, A. & De Rossi, R. H. Strong inhibition of cis-trans isomerization of azo compounds by hydroxide ion. *The Journal of Organic Chemistry* **58**, 2094-2096, doi:10.1021/jo00060a026 (1993).
- Ciccone, S. & Halpern, J. CATALYSIS OF THE CIS-TRANS ISOMERIZATION OF AZOBENZENE BY ACIDS AND CUPRIC SALTS. *Canadian Journal of Chemistry* **37**, 1903-1910, doi:10.1139/v59-278 (1959).
- Ochi, R., Perur, N., Yoshida, K. & Tamaoki, N. Fast thermal cis-trans isomerization depending on pH and metal ions of water-soluble azobenzene derivatives containing a phosphate group. *Tetrahedron* **71**, 3500-3506, doi:https://doi.org/10.1016/j.tet.2015.03.054 (2015).
- Yano, A., Sato, Y., Dachimba, K. & Yano, R. Catalysis of Thermal Isomerization of Methyl Yellow by Salts. *ACS Omega* **5**, 7956-7961, doi:10.1021/acsomega.9b04342 (2020).
- Berthet, J. *et al.* Synthesis and switching properties of new derivatives of azoresveratrol. *Dyes and Pigments* **171**, 107666, doi:https://doi.org/10.1016/j.dyepig.2019.107666 (2019).
- Hong, J.-D., Park, E.-S. & Park, A.-L. Effects of Added Salt on Photochemical Isomerization of Azobenzene in Alternate Multilayer Assemblies: Bipolar Amphiphile–Polyelectrolyte. *Langmuir* **15**, 6515-6521, doi:10.1021/la990265v (1999).
- Leriche, G., Budin, G., Brino, L. & Wagner, A. Optimization of the Azobenzene Scaffold for Reductive Cleavage by Dithionite; Development of an Azobenzene Cleavable Linker for Proteomic Applications. *European Journal of Organic Chemistry* **2010**, 4360-4364, doi:10.1002/ejoc.201000546 (2010).
- Eom, T. & Khan, A. Hypersensitive azobenzenes: facile synthesis of clickable and cleavable azo linkers with tunable and high reducibility. *Organic & Biomolecular Chemistry* **18**, 420-424, doi:10.1039/C90B02515D (2020).
- Zhou, F. *et al.* Hypoxia-Activated PEGylated Conditional Aptamer/Antibody for Cancer Imaging with Improved Specificity. *Journal of the American Chemical Society* **141**, 18421-18427, doi:10.1021/jacs.9b05063 (2019).

- Jacquemin, D. *et al.* Absorption spectra of azobenzenes simulated with time-dependent density functional theory. *International Journal of Quantum Chemistry* **111**, 4224-4240, doi:https://doi.org/10.1002/qua.22910 (2011).
- Adamo, C. & Jacquemin, D. The calculations of excited-state properties with Time-Dependent Density Functional Theory. *Chemical Society Reviews* **42**, 845-856, doi:10.1039/C2CS35394F (2013).
- Panchagnula, V., Jeon, J. & Dobrynin, A. V. Molecular Dynamics Simulations of Electrostatic Layer-by-Layer Self-Assembly. *Physical Review Letters* **93**, 037801, doi:10.1103/PhysRevLett.93.037801 (2004).
- Muždalo, A., Saalfrank, P., Vreede, J. & Santer, M. Cis-to-Trans Isomerization of Azobenzene Derivatives Studied with Transition Path Sampling and Quantum Mechanical/Molecular Mechanical Molecular Dynamics. *Journal of Chemical Theory and Computation* **14**, 2042-2051, doi:10.1021/acs.jctc.7b01120 (2018).
- 38 Crecca, C. R. & Roitberg, A. E. Theoretical Study of the Isomerization Mechanism of Azobenzene and Disubstituted Azobenzene Derivatives. *The Journal of Physical Chemistry A* **110**, 8188-8203, doi:10.1021/jp057413c (2006).
- Peng, C. & Bernhard Schlegel, H. Combining Synchronous Transit and Quasi-Newton Methods to Find Transition States. *Israel Journal of Chemistry* **33**, 449-454, doi:https://doi.org/10.1002/ijch.199300051 (1993).
- Szabo, R., Le, K. N. & Kowalczyk, T. Multifactor theoretical modeling of solar thermal fuels built on azobenzene and norbornadiene scaffolds. *Sustainable Energy & Fuels* **5**, 2335-2346, doi:10.1039/D1SE00041A (2021).
- Cembran, A., Bernardi, F., Garavelli, M., Gagliardi, L. & Orlandi, G. On the Mechanism of the cis-trans Isomerization in the Lowest Electronic States of Azobenzene: S0, S1, and T1. *Journal of the American Chemical Society* **126**, 3234-3243, doi:10.1021/ja038327y (2004).
- Barone, V., Bloino, J., Monti, S., Pedone, A. & Prampolini, G. Fluorescence spectra of organic dyes in solution: a time dependent multilevel approach. *Physical Chemistry Chemical Physics* **13**, 2160-2166, doi:10.1039/C0CP01320J (2011).
- Zuehlsdorff, T. J., Haynes, P. D., Hanke, F., Payne, M. C. & Hine, N. D. M. Solvent Effects on Electronic Excitations of an Organic Chromophore. *Journal of Chemical Theory and Computation* **12**, 1853-1861, doi:10.1021/acs.jctc.5b01014 (2016).

- Seeman, N. C. & Sleiman, H. F. DNA nanotechnology. *Nature Reviews Materials* **3**, 17068, doi:10.1038/natrevmats.2017.68 (2017).
- Rothemund, P. W. K. Folding DNA to create nanoscale shapes and patterns. *Nature* **440**, 297-302, doi:10.1038/nature04586 (2006).
- 46 Dey, S. et al. DNA origami. *Nature Reviews Methods Primers* **1**, 13, doi:10.1038/s43586-020-00009-8 (2021).
- Padroni, G. *et al.* Sequence-Selective Minor Groove Recognition of a DNA Duplex Containing Synthetic Genetic Components. *Journal of the American Chemical Society* **141**, 9555-9563, doi:10.1021/jacs.8b12444 (2019).
- Herrero-Galán, E. *et al.* Mechanical Identities of RNA and DNA Double Helices Unveiled at the Single-Molecule Level. *Journal of the American Chemical Society* **135**, 122-131, doi:10.1021/ja3054755 (2013).
- 49 Yurke, B., Turberfield, A. J., Mills, A. P., Simmel, F. C. & Neumann, J. L. A DNA-fuelled molecular machine made of DNA. *Nature* **406**, 605-608, doi:10.1038/35020524 (2000).
- Kassem, S., Lee, A. T. L., Leigh, D. A., Markevicius, A. & Solà, J. Pick-up, transport and release of a molecular cargo using a small-molecule robotic arm. *Nature Chemistry* **8**, 138-143, doi:10.1038/nchem.2410 (2016).
- Kopperger, E. *et al.* A self-assembled nanoscale robotic arm controlled by electric fields. *Science* **359**, 296, doi:10.1126/science.aao4284 (2018).
- 52 Chen, J. & Seeman, N. C. Synthesis from DNA of a molecule with the connectivity of a cube. *Nature* **350**, 631-633, doi:10.1038/350631a0 (1991).
- Trinh, T. *et al.* "Printing" DNA Strand Patterns on Small Molecules with Control of Valency, Directionality, and Sequence. *Angewandte Chemie International Edition* **58**, 3042-3047, doi:https://doi.org/10.1002/anie.201809251 (2019).
- Greschner, A. A., Toader, V. & Sleiman, H. F. The Role of Organic Linkers in Directing DNA Self-Assembly and Significantly Stabilizing DNA Duplexes. *Journal of the American Chemical Society* **134**, 14382-14389, doi:10.1021/ja3033197 (2012).
- Aldaye, F. A., Palmer, A. L. & Sleiman, H. F. Assembling Materials with DNA as the Guide. *Science* **321**, 1795, doi:10.1126/science.1154533 (2008).
- Aldaye, F. A. *et al.* Modular construction of DNA nanotubes of tunable geometry and single- or double-stranded character. *Nature Nanotechnology* **4**, 349-352, doi:10.1038/nnano.2009.72 (2009).

- Kretschy, N., Sack, M. & Somoza, M. M. Sequence-Dependent Fluorescence of Cy3- and Cy5-Labeled Double-Stranded DNA. *Bioconjugate Chemistry* **27**, 840-848, doi:10.1021/acs.bioconjchem.6b00053 (2016).
- Robinson, M. E. *et al.* Length control of supramolecular polymeric nanofibers based on stacked planar platinum(ii) complexes by seeded-growth. *Chemical Communications* **51**, 15921-15924, doi:10.1039/C5CC06606A (2015).
- Krieg, E., Bastings, M. M. C., Besenius, P. & Rybtchinski, B. Supramolecular Polymers in Aqueous Media. *Chemical Reviews* **116**, 2414-2477, doi:10.1021/acs.chemrev.5b00369 (2016).
- De Greef, T. F. A. *et al.* Supramolecular Polymerization. *Chemical Reviews* **109**, 5687-5754, doi:10.1021/cr900181u (2009).
- Adelizzi, B., Van Zee, N. J., de Windt, L. N. J., Palmans, A. R. A. & Meijer, E. W. Future of Supramolecular Copolymers Unveiled by Reflecting on Covalent Copolymerization. *Journal of the American Chemical Society* **141**, 6110-6121, doi:10.1021/jacs.9b01089 (2019).
- 62 Chandler, D. Interfaces and the driving force of hydrophobic assembly. *Nature* **437**, 640-647, doi:10.1038/nature04162 (2005).
- Korevaar, P. A. *et al.* Pathway complexity in supramolecular polymerization. *Nature* **481**, 492-496, doi:10.1038/nature10720 (2012).
- Kang, J. et al. C5-Symmetric Chiral Corannulenes: Desymmetrization of Bowl Inversion Equilibrium via "Intramolecular" Hydrogen-Bonding Network. *Journal of the American Chemical Society* **136**, 10640-10644, doi:10.1021/ja505941b (2014).
- Song, S. *et al.* Solvent effects leading to a variety of different 2D structures in the self-assembly of a crystalline-coil block copolymer with an amphiphilic corona-forming block. *Chemical Science* **11**, 4631-4643, doi:10.1039/D0SC01453B (2020).
- 66 Chen, J. *et al.* Artificial muscle-like function from hierarchical supramolecular assembly of photoresponsive molecular motors. *Nature Chemistry* **10**, 132-138, doi:10.1038/nchem.2887 (2018).
- Škugor, M. *et al.* Orthogonally Photocontrolled Non-Autonomous DNA Walker. *Angewandte Chemie International Edition* **58**, 6948-6951, doi: https://doi.org/10.1002/anie.201901272 (2019).
- Xu, F. *et al.* From Photoinduced Supramolecular Polymerization to Responsive Organogels. *Journal of the American Chemical Society* **143**, 5990-5997, doi:10.1021/jacs.1c01802 (2021).

- Aida, T., Meijer, E. W. & Stupp, S. I. Functional Supramolecular Polymers. *Science* **335**, 813, doi:10.1126/science.1205962 (2012).
- Langer, R. & Tirrell, D. A. Designing materials for biology and medicine. *Nature* **428**, 487-492, doi:10.1038/nature02388 (2004).
- Fogleman, E. A., Yount, W. C., Xu, J. & Craig, S. L. Modular, Well-Behaved Reversible Polymers from DNA-Based Monomers. *Angewandte Chemie International Edition* **41**, 4026-4028, doi:<a href="https://doi.org/10.1002/1521-3773(20021104)41:21<4026::AID-ANIE4026>3.0.CO;2-E">https://doi.org/10.1002/1521-3773(20021104)41:21<4026::AID-ANIE4026>3.0.CO;2-E (2002).
- Xu, J., Fogleman, E. A. & Craig, S. L. Structure and Properties of DNA-Based Reversible Polymers. *Macromolecules* **37**, 1863-1870, doi:10.1021/ma035546v (2004).
- Jensen, S. A. *et al.* Spherical Nucleic Acid Nanoparticle Conjugates as an RNAi-Based Therapy for Glioblastoma. *Science Translational Medicine* **5**, 209ra152, doi:10.1126/scitranslmed.3006839 (2013).
- Li, H. et al. Molecular spherical nucleic acids. *Proceedings of the National Academy of Sciences* **115**, 4340, doi:10.1073/pnas.1801836115 (2018).
- Dore, M. D. *et al.* Thermosetting supramolecular polymerization of compartmentalized DNA fibers with stereo sequence and length control. *Chem*, doi: https://doi.org/10.1016/j.chempr.2021.05.022 (2021).
- Karinaga, R., Jeong, Y., Shinkai, S., Kaneko, K. & Sakurai, K. Inclusion of DNA into Organic Gelator Fibers Made of Amphipathic Molecules and Its Controlled Release. *Langmuir* **21**, 9398-9401, doi:10.1021/la0515524 (2005).
- Bousmail, D., Chidchob, P. & Sleiman, H. F. Cyanine-Mediated DNA Nanofiber Growth with Controlled Dimensionality. *Journal of the American Chemical Society* **140**, 9518-9530, doi:10.1021/jacs.8b04157 (2018).
- Fakih, H. H., Fakhoury, J. J., Bousmail, D. & Sleiman, H. F. Minimalist Design of a Stimuli-Responsive Spherical Nucleic Acid for Conditional Delivery of Oligonucleotide Therapeutics. *ACS Applied Materials & Interfaces* **11**, 13912-13920, doi:10.1021/acsami.8b18790 (2019).
- Wijnands, S. P. W., Meijer, E. W. & Merkx, M. DNA-Functionalized Supramolecular Polymers: Dynamic Multicomponent Assemblies with Emergent Properties. *Bioconjugate Chemistry* **30**, 1905-1914, doi:10.1021/acs.bioconjchem.9b00095 (2019).
- 80 Alenaizan, A., Fauché, K., Krishnamurthy, R. & Sherrill, C. D. Noncovalent Helicene Structure between Nucleic Acids and Cyanuric Acid. *Chemistry – A*

- *European Journal* **27**, 4043-4052, doi: https://doi.org/10.1002/chem.202004390 (2021).
- Bushuyev, O. S., Aizawa, M., Shishido, A. & Barrett, C. J. Shape-Shifting Azo Dye Polymers: Towards Sunlight-Driven Molecular Devices. *Macromolecular Rapid Communications* **39**, 1700253, doi:https://doi.org/10.1002/marc.201700253 (2018).
- Chang, V. Y., Fedele, C., Priimagi, A., Shishido, A. & Barrett, C. J. Photoreversible Soft Azo Dye Materials: Toward Optical Control of Bio-Interfaces. *Advanced Optical Materials* **7**, 1900091, doi:https://doi.org/10.1002/adom.201900091 (2019).
- Landry, M. J. *et al.* Tunable Engineered Extracellular Matrix Materials: Polyelectrolyte Multilayers Promote Improved Neural Cell Growth and Survival. *Macromolecular Bioscience* **19**, 1900036, doi:https://doi.org/10.1002/mabi.201900036 (2019).
- Asanuma, H., Ito, T., Yoshida, T., Liang, X. & Komiyama, M. Photoregulation of the Formation and Dissociation of a DNA Duplex by Using the cis–trans Isomerization of Azobenzene. *Angewandte Chemie International Edition* **38**, 2393-2395, doi:https://doi.org/10.1002/(SICI)1521-3773(19990816)38:16<2393::AID-ANIE2393>3.0.CO;2-7 (1999).
- Lubbe, A. S., Szymanski, W. & Feringa, B. L. Recent developments in reversible photoregulation of oligonucleotide structure and function. *Chemical Society Reviews* **46**, 1052-1079, doi:10.1039/C6CS00461J (2017).
- Asanuma, H. *et al.* Enantioselective Incorporation of Azobenzenes into Oligodeoxyribonucleotide for Effective Photoregulation of Duplex Formation. *Angewandte Chemie International Edition* **40**, 2671-2673, doi:https://doi.org/10.1002/1521-3773(20010716)40:14<2671::AID-ANIE2671>3.0.CO;2-Z (2001).
- Biswas, M. & Burghardt, I. Azobenzene Photoisomerization-Induced Destabilization of B-DNA. *Biophysical Journal* **107**, 932-940, doi:10.1016/j.bpj.2014.06.044 (2014).
- Samai, S., Bradley, D. J., Choi, T. L. Y., Yan, Y. & Ginger, D. S. Temperature-Dependent Photoisomerization Quantum Yields for Azobenzene-Modified DNA. *The Journal of Physical Chemistry C* **121**, 6997-7004, doi:10.1021/acs.jpcc.6b12241 (2017).
- 89 Wu, L., Koumoto, K. & Sugimoto, N. Reversible stability switching of a hairpin DNAvia a photo-responsive linker unit. *Chemical Communications*, 1915-1917, doi:10.1039/B819643E (2009).

- 90 Wu, L. *et al.* Photoswitching properties of hairpin ODNs with azobenzene derivatives at the loop position. *MedChemComm* **6**, 461-468, doi:10.1039/C4MD00378K (2015).
- 91 Hammill, M. L., Isaacs-Trépanier, C. & Desaulniers, J.-P. siRNAzos: A New Class of Azobenzene-Containing siRNAs that Can Photochemically Regulate Gene Expression. *ChemistrySelect* **2**, 9810-9814, doi:https://doi.org/10.1002/slct.201702322 (2017).
- Hammill, M. L., Islam, G. & Desaulniers, J.-P. Synthesis, Derivatization and Photochemical Control of ortho-Functionalized Tetrachlorinated Azobenzene-Modified siRNAs. *ChemBioChem* **21**, 2367-2372, doi:https://doi.org/10.1002/cbic.202000188 (2020).
- 93 Merino, E. Synthesis of azobenzenes: the coloured pieces of molecular materials. *Chemical Society Reviews* **40**, 3835-3853, doi:10.1039/C0CS00183J (2011).
- Antoine John, A. & Lin, Q. Synthesis of Azobenzenes Using N-Chlorosuccinimide and 1,8-Diazabicyclo[5.4.0]undec-7-ene (DBU). *The Journal of Organic Chemistry* **82**, 9873-9876, doi:10.1021/acs.joc.7b01530 (2017).
- Pirone, D. *et al.* Contrasting Photo-Switching Rates in Azobenzene Derivatives: How the Nature of the Substituent Plays a Role. *Polymers* **12**, doi:10.3390/polym12051019 (2020).
- Corchado, J. C. *et al.* Theoretical Study of Solvent Effects on the Ground and Low-Lying Excited Free Energy Surfaces of a Push–Pull Substituted Azobenzene. *The Journal of Physical Chemistry B* **118**, 12518-12530, doi:10.1021/jp506876v (2014).
- Knie, C. *et al.* ortho-Fluoroazobenzenes: Visible Light Switches with Very Long-Lived Z Isomers. *Chemistry – A European Journal* **20**, 16492-16501, doi:https://doi.org/10.1002/chem.201404649 (2014).
- Norio, N. *et al.* Thermal Cis-to-Trans Isomerization of Substituted Azobenzenes II. Substituent and Solvent Effects. *Bulletin of the Chemical Society of Japan* **49**, 1381-1387, doi:10.1246/bcsj.49.1381 (1976).
- 99 Simeth, N. A., Bellisario, A., Crespi, S., Fagnoni, M. & König, B. Substituent Effects on 3-Arylazoindole Photoswitches. *The Journal of Organic Chemistry* **84**, 6565-6575, doi:10.1021/acs.joc.8b02973 (2019).
- Heindl, A. H., Becker, J. & Wegner, H. A. Selective switching of multiple azobenzenes. *Chemical Science* **10**, 7418-7425, doi:10.1039/C9SC02347J (2019).

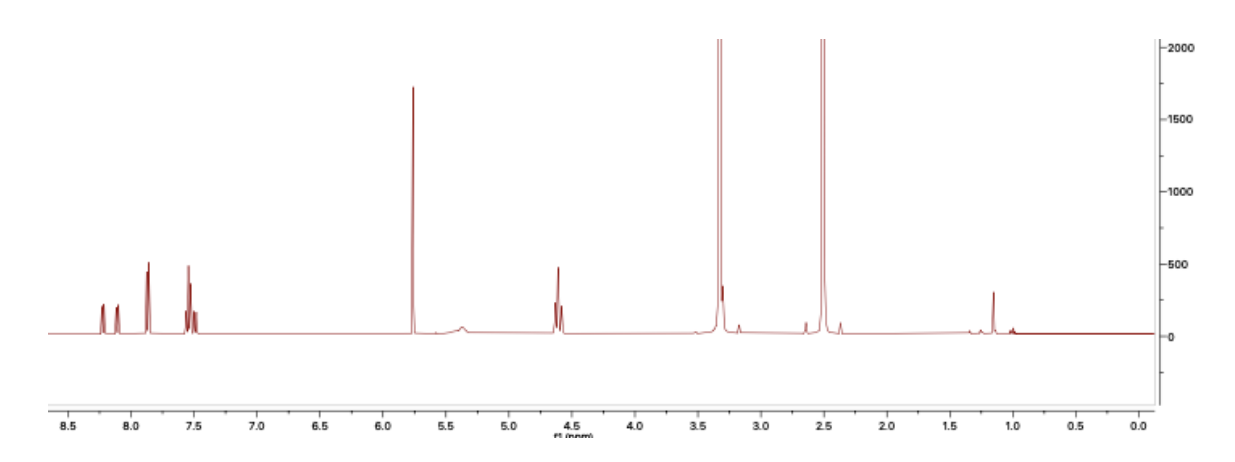
- Sun, J. S. *et al.* Sequence-specific intercalating agents: intercalation at specific sequences on duplex DNA via major groove recognition by oligonucleotide-intercalator conjugates. *Proc Natl Acad Sci U S A* **86**, 9198-9202, doi:10.1073/pnas.86.23.9198 (1989).
- Johnson, C. A. *et al.* Effect of intercalator substituent and nucleotide sequence on the stability of DNA- and RNA-naphthalimide complexes. *Bioorganic & Medicinal Chemistry* **23**, 3586-3591, doi:https://doi.org/10.1016/j.bmc.2015.04.030 (2015).

Appendix

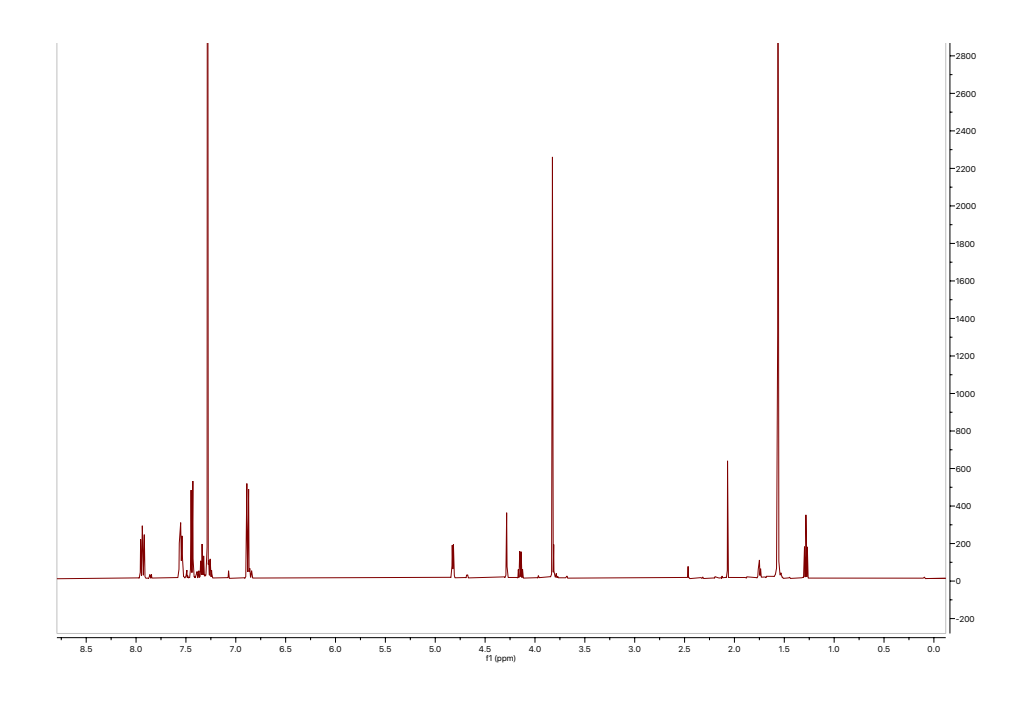
The following NMR data is presented as a means to assist future students in their work. For simplicity, only the ¹H data is presented as these served as adequate means to identify the synthesized compounds. The references stated throughout the methods section would also be helpful in this regard, however, they typically do not show the full NMR spectra.

¹H NMR Data

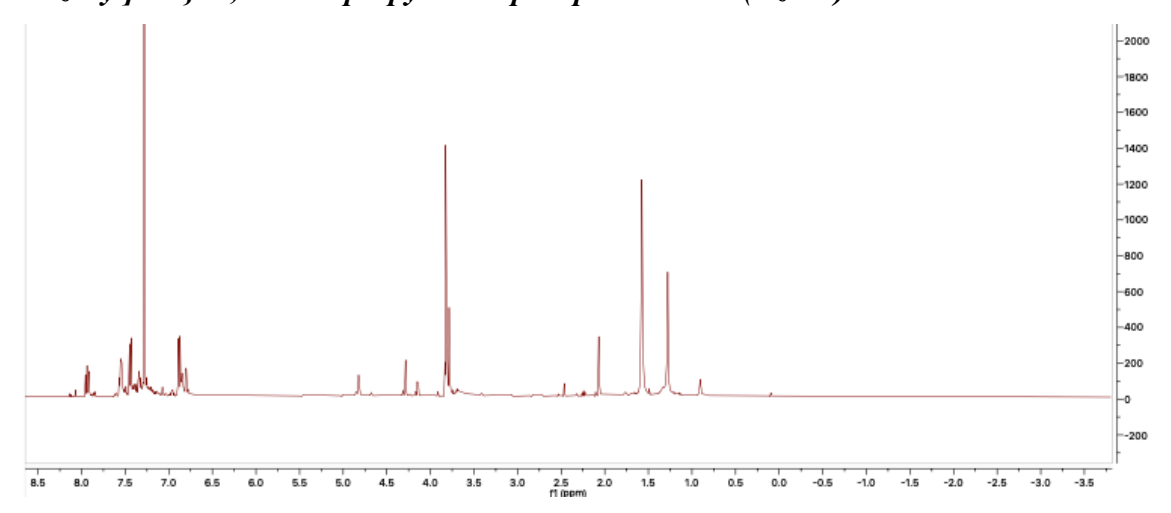
Bis(hydroxymethyl)azobenzene (Azo1)



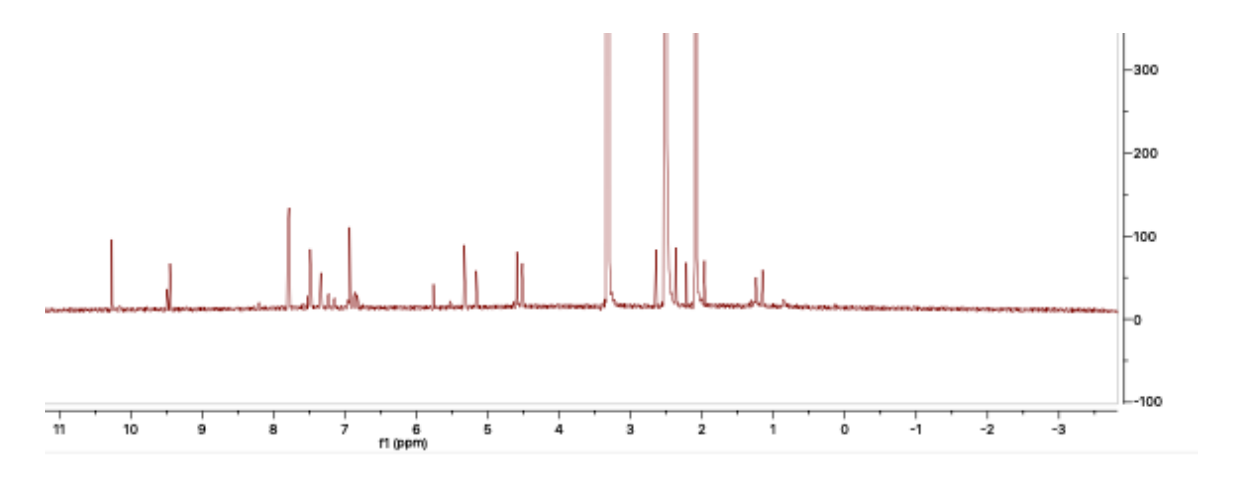
4-hydroxymethyl-4'-O-(4,4'-dimethoxytrityl)-azobenzene (Azo1a)



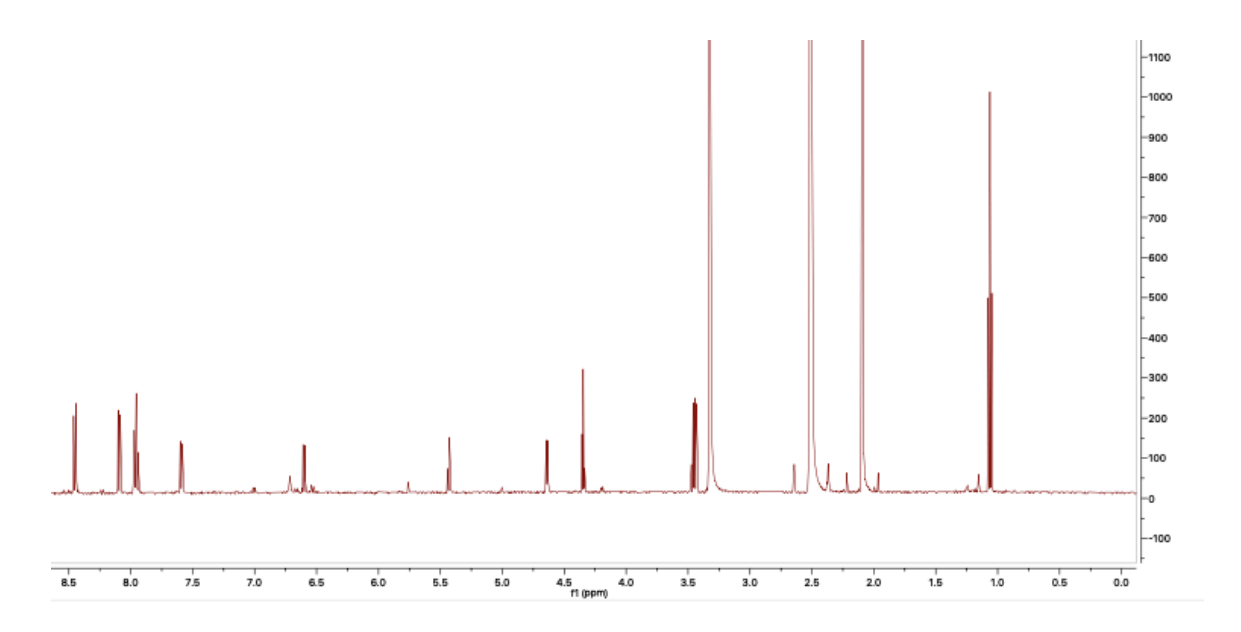
 $2-Cyanoethyl-4-O-\{[4-hydroxymethyl-4'-O-(4,4'dimethoxytrityl)-O-methyl-diazenyl]kon\}-N,N'-diisopropylaminophosphoramidite~(Azo1b)$



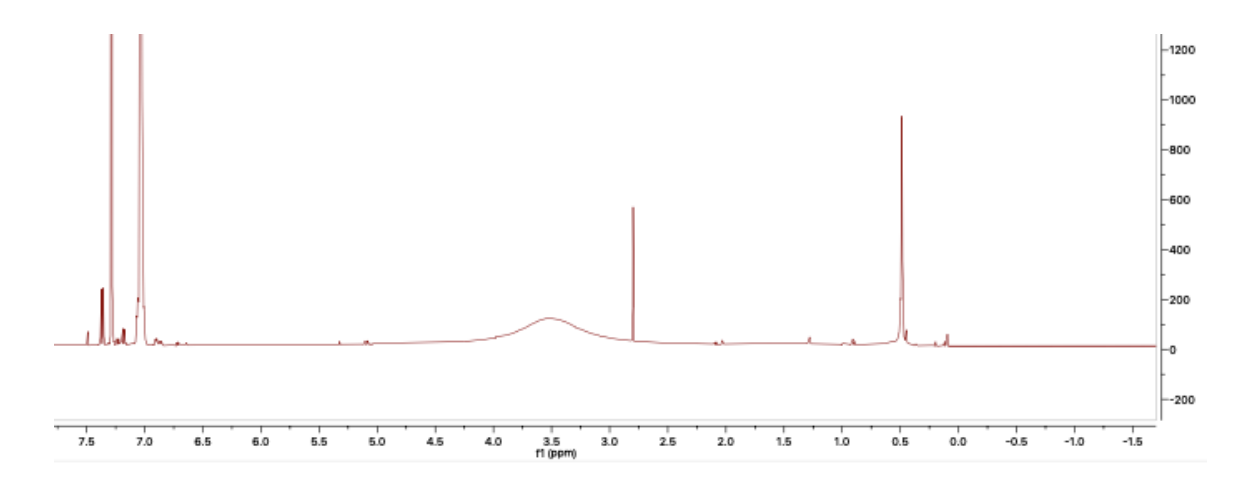
4-hydroxy-4'-hydroxymethylazobenzene (Azo2)

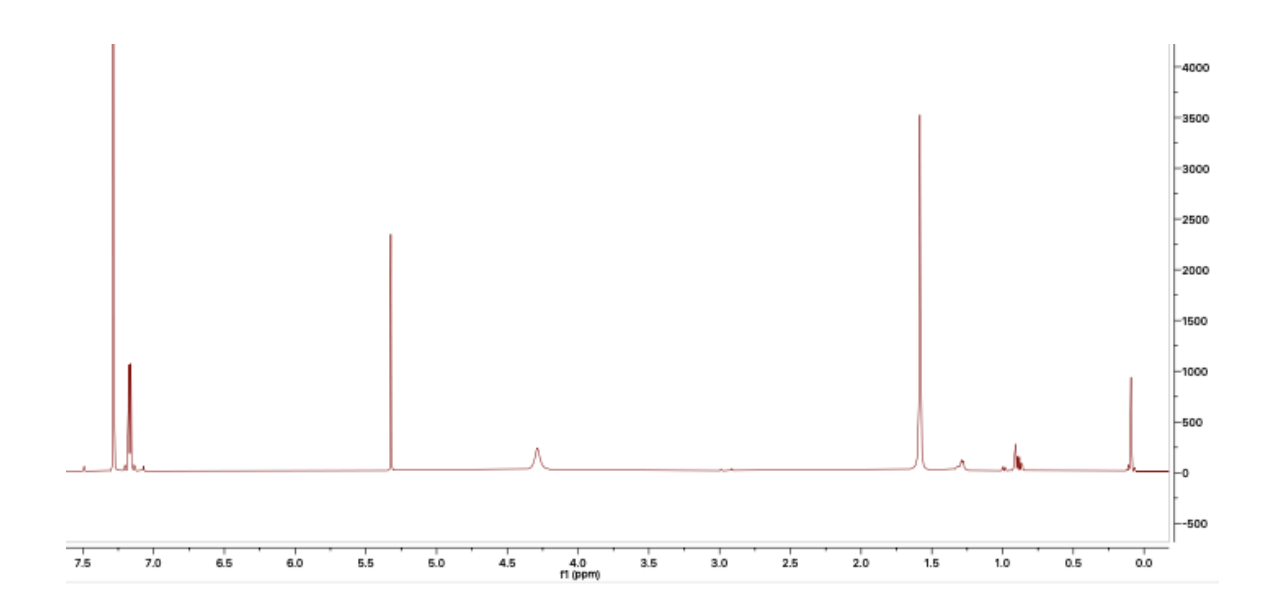


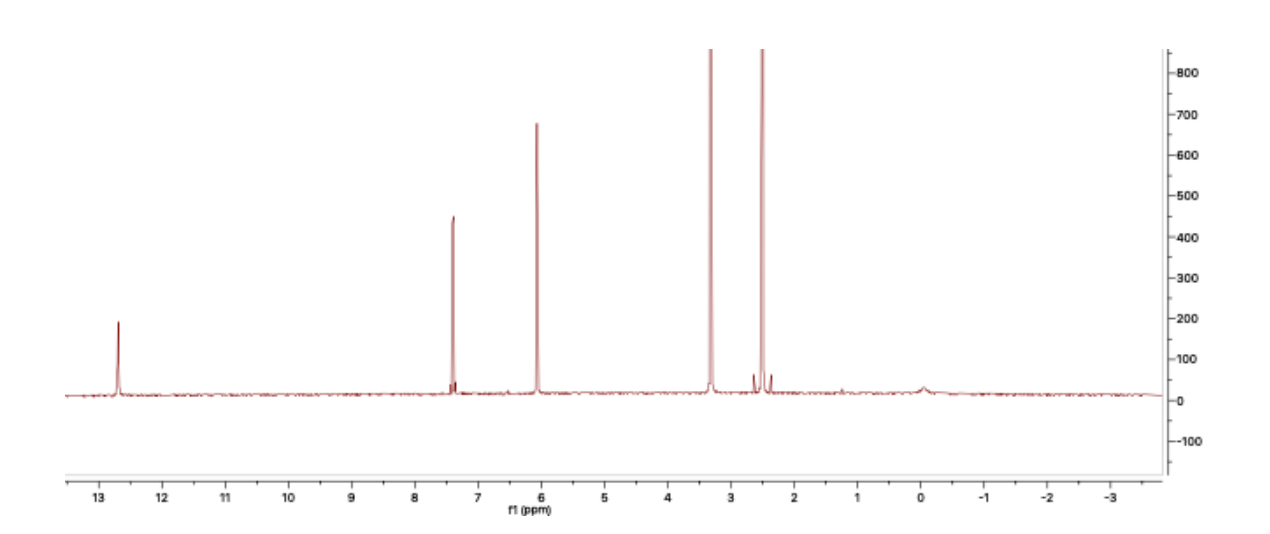
4-hydroxymethyl-4'-nitro-azobenzene (Azo3)



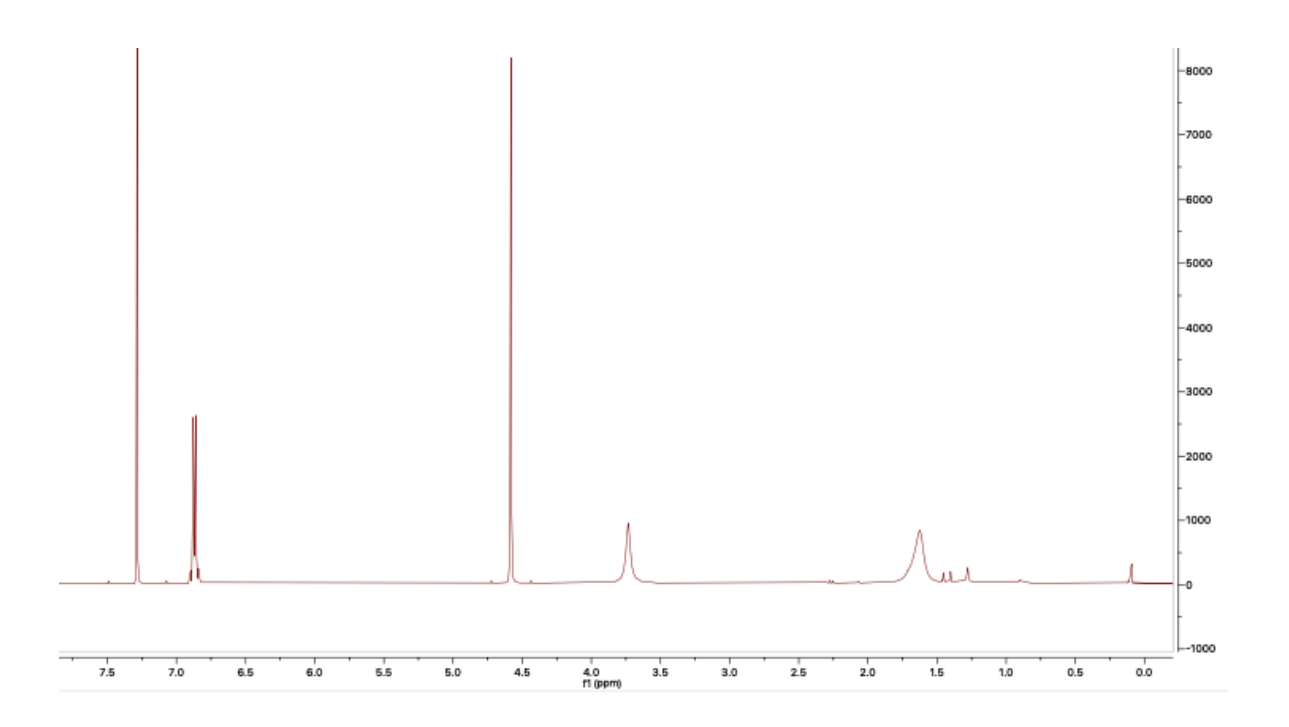
4-amino-3,5-difluorobenzoic acid (4a-4c, in order)

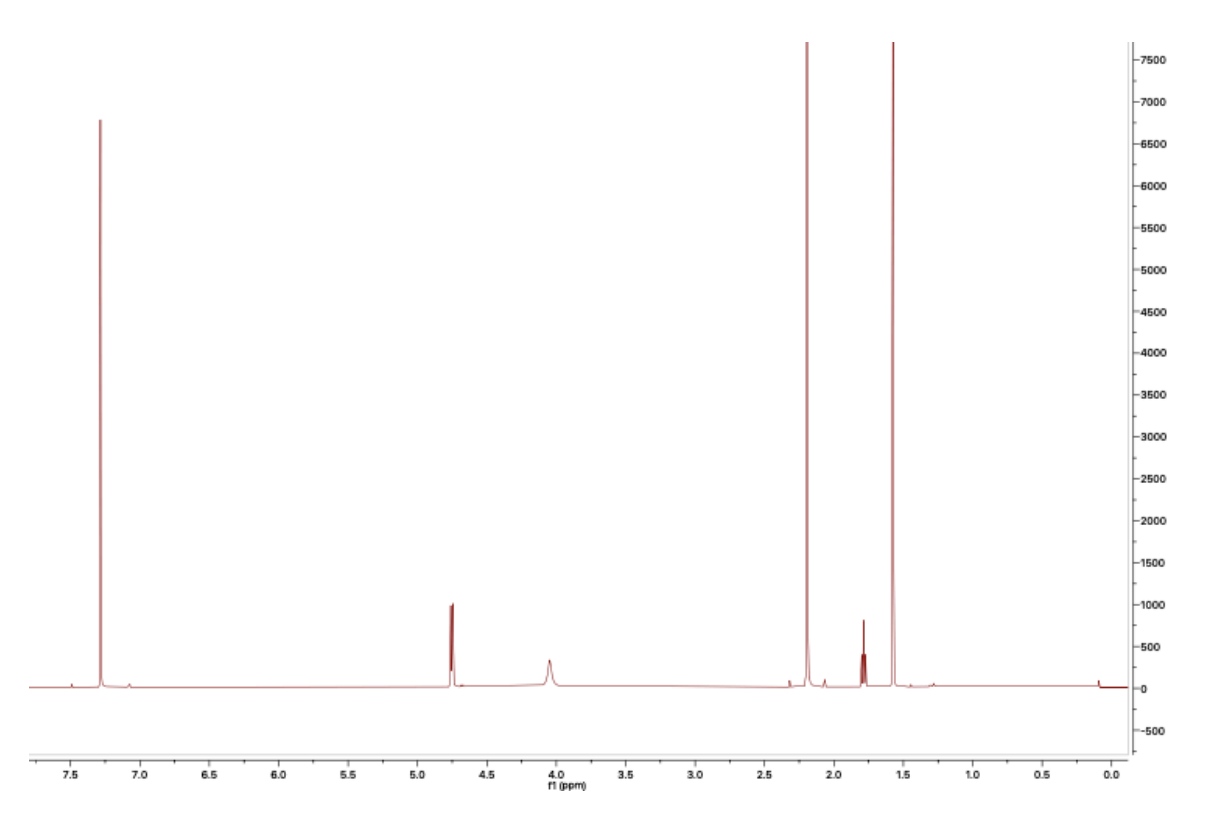




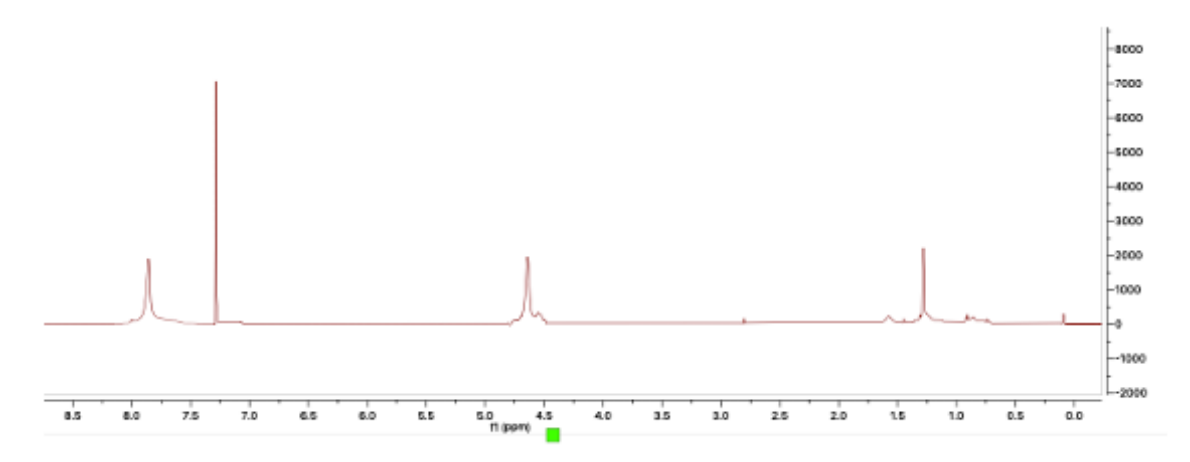


4-amino-3,5-difluorobenzyl alcohol & 4-amino-2,3,5,6-tetrafluorobenzyl alcohol (4d & 5a, in order)





bis(2,6-difluoro-4-hydroxymethyl)diazene (Azo4)



bis(2,3,5,6-tetrafluoro-4-hydroxymethyl) diazene (Azo5)

